UNIVERSITÄT PADERBORN
Die Universität der Informationsgesellschaft

Continuous Flow Investigation of Organocatalyzed Reactions using Gel-Bound Catalysts inside Microfluidic Reactors

Dissertation

Zur Erlangung des akademischen Grades des
Doktor rerum naturalium
(Dr. rer. nat.)

vorgelegt
der Fakultät für Naturwissenschaften
Universität Paderborn

eingereicht von
Carsten Janis Schmiegel M.Sc.
geboren am 07.11.1991 in Herford

Paderborn 2021

Gutachter: Prof. Dr. Dirk Kuckling
Prof. Dr. Jan Paradies

Eingereicht am: 03.05.2021
Datum der Verteidigung: 14.06.2021

Diese Arbeit wurde in einem Zeitraum vom 01. April 2018 bis zum 31. März 2021 im Fachbereich organische und makromolekulare Chemie der Universität Paderborn unter der Leitung von Prof. Dr. Dirk Kuckling angefertigt.

Abstract

One of the greatest challenges of today is to provide satisfactory and at the same time fair access to resources and to make the use of existing primary materials as efficient as possible. Approaches for a more efficient usage of resources within chemical industries are based on the utilization of catalysts. However, the manufacturing process of many commercially significant catalysts is often time-consuming, costly and in many cases linked to environmental pollution. Hence, research to efficiently use and at best to fully recover catalysts is of immense importance. One possible way to address this challenge is the immobilization of catalysts on various carrier materials. A large area within this research field is the immobilization of catalysts on polymer-based carrier materials.

The aim of the present work was to determine the potential and possibilities, but also possible challenges, of using polymer networks (gels) as carriers for organocatalysts in various reactions. Organocatalysts immobilized within polymer networks were introduced into a microfluidic reactor. The advantages of such a microfluidic reactor are primarily the minimized amount of chemicals required and the continuous operation of the reactor. These principles lead to safer reaction management and increased efficiency due to the higher local catalyst concentration inside of the reaction chamber. Since the size of the microfluidic reactor is invariable, the dimensions of the network structures obtained were specifically adapted to the conditions and requirements within the reactor. The systems adjusted in this way were then built into the reactor and examined by performing various organocatalyzed reactions. In the present work different L-proline based organocatalysts could be produced and successfully immobilized. The swelling behavior of the resulting catalytically active gel structures was analyzed in detail and the catalyst containing gels were used successfully for the implementation and in-depth analysis of the asymmetric aldol reaction as well as a reductive dimerization reaction of nitroso arenes. In this context, various relationships between the gel composition and the photopolymerization were investigated and adjusted. Using the reactor optimized in this way, numerous different derivatives could be produced for both, the asymmetric aldol reaction as well as the dimerization reaction.

Kurzzusammenfassung

Eine der größten Herausforderungen der Gegenwart besteht darin, einen zufriedenstellenden und gleichzeitig angemessenen Zugang zu Ressourcen zu gewährleisten und die Nutzung vorhandener Primärmaterialien so effizient wie möglich zu gestalten. Ansätze für eine effizientere Ressourcennutzung innerhalb der chemischen Industrie basieren auf der Nutzung von Katalysatoren. Die Herstellung vieler kommerziell bedeutender Katalysatoren ist jedoch oft zeitaufwändig, kostspielig und in vielen Fällen mit Umweltverschmutzung verbunden. Daher ist die Erforschung der effizienten Verwendung und bestenfalls der vollständigen Rückgewinnung von Katalysatoren von immenser Bedeutung. Ein möglicher Weg, um diesen Herausforderungen zu begegnen, ist die Immobilisierung von Katalysatoren auf verschiedenen Trägermaterialien. Ein großes Gebiet in diesem Forschungsbereich ist die Immobilisierung von Katalysatoren auf polymerbasierten Trägermaterialien.

Ziel der vorliegenden Arbeit war es, das Potenzial und die Möglichkeiten, aber auch mögliche Herausforderungen der Verwendung von Polymernetzwerken (Gelen) als Träger für Organokatalysatoren in verschiedenen Reaktionen zu bestimmen. Innerhalb von Gelen immobilisierte Organokatalysatoren wurden in einen mikrofluidischen Reaktor eingeführt. Die Vorteile eines mikrofluidischen Reaktors sind in erster Linie die minimierte Menge an erforderlichen Chemikalien und der kontinuierliche Betrieb eines solchen Reaktors. Diese Prinzipien führen zu einem sichereren Reaktionsmanagement und einer erhöhten Effizienz aufgrund der höheren lokalen Katalysatorkonzentration innerhalb der Reaktionskammer. Da die Größe des mikrofluidischen Reaktors unveränderlich ist, wurden die Dimensionen der erhaltenen Netzwerkstrukturen speziell an die Bedingungen und Anforderungen innerhalb des Reaktors angepasst. Die auf diese Weise eingestellten Systeme wurden nachfolgend in den Reaktor eingebaut und die Leistungsfähigkeit anschließend für verschiedene organokatalysierte Reaktionen untersucht. In der vorliegenden Arbeit konnten verschiedene Organokatalysatoren auf L-Prolin-Basis hergestellt und erfolgreich immobilisiert werden. Das Quellverhalten der resultierenden katalytisch aktiven Gelstrukturen konnte detailliert analysiert werden und die katalysatorhaltigen Gele wurden erfolgreich zur Durchführung und eingehenden Analyse der asymmetrischen Aldolreaktion sowie einer reduktiven Dimerisierungsreaktion von Nitrosoaromaten eingesetzt. In diesem Kontext wurden verschiedene Zusammenhänge zwischen der Gelzusammensetzung und der Photopolymerisation untersucht und adjustiert. Unter Verwendung des auf diese Weise optimierten Reaktors konnten sowohl im Falle der asymmetrischen Aldolreaktion als auch der Dimerisierungsreaktion zahlreiche verschiedene Derivate hergestellt werden.

Eidesstaatliche Erklärung

Hiermit versichere ich, die vorliegende Arbeit selbständig angefertigt und keine anderen als die von mir angegebenen Hilfsmittel verwendet zu haben. Wörtliche und sinngemäße Zitate wurden als solche gekennzeichnet und die Genehmigungen zur Veröffentlichung der urheberrechtlich geschützten Publikationen wurden eingeholt.

Paderborn, 03.05.2021

Carsten Janis Schmiegel

Anerkennung der Promotionsordnung

Hiermit erkenne ich, Carsten Schmiegel, die Promotionsordnung der Fakultät für Naturwissenschaften der Universität Paderborn, welche am 12. November 2012 von der Universität erlassen wurde und durch die Satzung vom 20. Februar 2020 zuletzt geändert wurde, an. Bisher wurde weder an der Universität Paderborn noch an einer anderen Hochschule im In- oder Ausland ein Promotionsversuch unternommen.

Paderborn, 03.05.2021

Carsten Janis Schmiegel

Danksagung

An dieser Stelle möchte ich meinen persönlichen Dank an all jene Menschen zum Ausdruck bringen, die mir bei der Durchführung der praktischen Arbeiten und der Anfertigung dieser Arbeit in ganz unterschiedlicher Form geholfen haben.

Mein besonderer Dank gilt Herrn Prof. Dr. Dirk Kuckling für das interessante Thema, das stete Interesse am Fortgang der Arbeit und die vielen Anregungen und Diskussionen.

Herrn Prof. Dr. Jan Paradies danke ich für die Übernahme des Zweitgutachtens sowie die Anregungen zur Synthese.

Ferner möchte ich mich bei allen bedanken, die an der Erstellung dieser Arbeit beteiligt waren: Für die zahlreichen NMR-Untersuchungen sowie die permanente Hilfsbereitschaft und die wertvollen Hinweise bei der NMR-Analytik danke ich Herrn PD Dr. Hans Egold sowie Frau Karin Stolte. Für die Einkristallanalyse – Dr. Roland Schoch. Für die massenspektrometrischen Analysen Dr. Adam Neuba und Christiane Gloger.

Dr. Dietmar Appelhans und Dr. Franziska Obst vom *Leibniz Institut für Polymerforschung Dresden* möchte ich für die Unterstützung bei Fragen der technischen Umsetzung des Reaktordesigns danken.

Den Studenten R. Baier und J. Bartenbach danke ich für die Durchführung wichtiger Synthesen im Rahmen von Bachelorarbeiten, Vertiefungspraktika und SHK-Stellen.

Bei meinen Arbeitskollegen/innen möchte ich mich für die wunderbare Arbeitsatmosphäre während der Zeit bedanken. Besonderer Dank gilt in diesem Zusammenhang: Rafael Methling, Dimitri Jung, Maksim Rodin, Tarik Rust, Matthias van der Linde, Dr. Jingjiang Sun und Dr. Xiaoqian Yu sowie Dr. Artjom Herberg und Annette Lefarth. All diese Personen sorgten für einige unterhaltsame und interessante Kaffeepausen und Unterhaltungen.

Meinen engen Freunden Dr. Patrik Berg, Dr. Marie-Theres Berg und Dr. Yannik Vukadinovic danke ich nicht nur für die Hilfestellung während der Erstellung dieser Arbeit, sondern auch für die vielfältigen mehr oder weniger fachlichen und fachfremden Diskussionen und die Ablenkung über ganze Abende.

Zu guter Letzt möchte ich mich bei meiner Familie und insbesondere meiner Freundin Sophie bedanken, die während des gesamten Studiums und auch in der Zeit der Promotion so viel Geduld und Verständnis aufbrachten und mich verschiedentlich unterstützt haben.

Table of Contents

1 Introduction

One of the greatest challenges of today is to provide satisfactory and at the same time fair access to resources and to make the use of existing resources as efficient as possible. A basic concept was established around 20 years ago, which on the one hand is gaining in importance due to increasing environmental awareness and on the other hand appears self-evident on closer inspection. The underlying concept encompasses the almost omnipresent term of "Green Chemistry" and refers to a large number of different aspects.[1] Some of the finest examples encompass the reduction of the quantities of chemicals used, the avoidance of waste and the prevention of dangers within the laboratories. However, the concept also includes other aspects such as the maximization of conversion with a view to maximum yield with a given quantity of resources. In this context, two areas of investigations are of particular interest: Research on efficient, continuously operable reactor systems and catalysis research. As these key points allow various aspects of "Green Chemistry" to be effectively combined. Continuously operated flow reactors could represent a possibility for an actual implementation of the mentioned aspects in everyday laboratory work. Such a closed reactor system minimizes possible risks for the user[2,3] and it also conceals the option of online analysis of reaction parameters such as conversion.[4] This allows adaptations to be made to the reactor during operation and thus to maximize the reaction conversion.

As early as the mid-1970s, the basis for flow reactors was laid which included automatic conversion determination and product extraction.[5] With regard to catalysis research, many industrial synthesis processes include metal-based heterogeneous catalysts.[6] In contrast, many different biochemical processes are essentially catalyzed by protein structures and thus by organic compounds, namely enzymes.[7] As a result, general knowledge about the capabilities and relationships of catalysis by organic compounds has been around for more than a century. However, it was not until the 1990s that this type of catalysis found acceptance as an important part of catalysis research.[8] It even took until the year 2000 that the pioneering work of LIST et al. made the use of amino acids and thus organic catalysts in asymmetric reactions accessible to a wide audience.[9] The corresponding work precisely addresses the different concepts of how chemists would typically realize reactions[10] and the way reactions take place in biological systems.[9] Enzymatically catalyzed reactions in biological systems are often performed by highly complex and highly specialized enzyme structures. Although it is possible to use these for synthetic purposes, the complex and sensitive protein structure makes them susceptible to undesired denaturation and thus to a loss of catalytic activity.[11] However, if one takes a closer look at the basic chemical processes that underlie the reactions of enzymes, one can gain useful ideas of potential practicable implementations. One example is class I aldolase. This enzyme breaks down fructose-1,6-bisphosphate into the isomers dihydroxyacetone phosphate (DHAP) and glyceraldehyde-3-phosphate (GAP) using an enamine-based mechanism.[12] Such findings allow a transcription of the complex reaction principles of biological catalysis into simple, low molecular weight catalyst structures which enable a targeted use in synthetic laboratories.[9]

In this context, the combination of continuously operated flow reactors and catalysts is of particular interest. Immobilizing the catalyst within continuously operated reactors would prevent the loss of the catalytically active structure and, at the same time, opens up the possibility of continuous product synthesis. The combination of these two concepts appears to be an interesting challenge against the background of current topics.

1.1 Problem Statement

A well-known challenge in the usage of organocatalysts is their relatively low turnover efficiency compared to metal-based catalysts.[13] Consequently, it is essential for a targeted application of organocatalysts to establish efficient variants for avoiding the loss of the catalyst structure. In order to address this problem, there is enormous interest in the efficient recovery and immobilization of catalysts. Polymers are particularly suitable as a potential carrier material for the catalytically active structure.[14] Numerous examples of the immobilization of biologically inspired catalysts, particularly proline, can be found in the known literature. For example, these have already been immobilized on the surface of solid particles[15–17], within nanoparticles consisting of a single chain[18], or as part of block copolymer structures in micellar catalysis.[19,20] Most of these approaches have the disadvantage that the immobilization leaves a volume which is inaccessible for the actual catalysis due to the properties of the carrier material used. The use of swellable, flexible carrier materials such as gels thus appears to be an interesting approach.

The vast majority of previous approaches to immobilizing catalysts relate to an application within classic stirred tank reactors. Although these are characterized by their simplicity, in terms of the efficient use of catalysts they do not come close to continuous flow reactors. This is essentially because in the case of the batch reactor the catalyst used is distributed over the entire reactor volume. Consequently, the spatially resolved catalyst concentration in flow reactors, which can only contain the catalyst within the specified dimensions of the reactor chamber, is significantly higher.

1.2 Objective and Scope of the Presented Work

To compensate for the disadvantages of lower turnover efficiency and at the same time combine with the advantages of locally increased catalyst concentrations, it is advisable to choose the immobilized amount of catalyst as high as possible. Furthermore, it seems worth striving to establish a reactor size that is practicable on a laboratory scale and that allows efficient access to the immobilized catalyst centers. In this context, the use of microfluidic reactors (MFRs) also appears to be particularly attractive with regard to "Green Chemistry". The combination of a continuously operated microfluidic reactor with swellable polymer-networks (gels) as a carrier material for efficient organocatalysts appears to be a promising approach to avoid some of the well-known difficulties of catalyst immobilization, as shown in Figure 1.

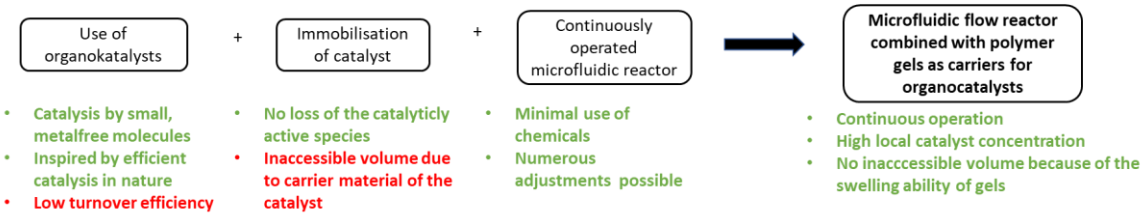

Figure 1: The combination of a continuously operated reactor with swellable polymer gels as a carrier material.

Gels allow the diffusion of educt molecules into the gel structure and the diffusion of formed product out of it. If such a gel consists of a catalytically active monomer in addition to other components, the catalytically usable area shifts from a square-surface-relationship to a cubic-volume-relationship. The same amount of catalyst can therefore be made available more efficiently and bundled in a smaller reactor chamber, which in turn increases the local catalyst concentration again at the same time. Due to the combination of the different components outlined, it is feasible to compensate the possible weaknesses or disadvantages of one of the components by the advantages of another and in this way to build up a powerful combination system of different components.

The basic functionality of polymer gels as carrier materials for organocatalysts and especially enzymes has already been successfully demonstrated.[21] Based on this, Knoevenagel reactions with a wide range of derivatives could already be carried out in continuous flow, catalyzed by an immobilized tertiary amine.[22,23]

In contrast to the previous work[22], the present work aims to build a network consisting of methacrylate-based components. The reason for this change lies in the profound literature on methacrylate-based structures of organocatalysts. The catalyst structure is then to be introduced within this network and immobilized on a glass slide using photolithography. This offers two advantages: On the one hand, the shape of the polymer gel can be adapted to the shape of the reactor chamber on the other hand, the polymerization through lithography enables a high spatial resolution. Using the model system to be subsequently established, various organocatalysts are then to be immobilized. Thus, different reactions for this type of reaction management are made accessible. Based on this, the various parameters of both the polymer structure and the respective reactions are to be varied and analyzed accordingly. In relation to the polymer gels, the degree of swelling in the respective reaction medium needs to be adjusted for efficient use of the reactor chamber. Furthermore, it is to be examined whether a temperature control can be established and to what extent the high local catalyst concentration affects the necessary reaction times within the microfluidic reactor compared to conventional approaches. Since the previous work has primarily focused on the analysis of conversion using various methods such as NMR and UV-Vis[22,23], the actual yield within this work is also of great interest.

2 Theoretical Background

Some content of the following chapter has already been published.[24,25]

2.1 Polymers

The term "polymer" basically describes a high-molecular chemical compound which is also known as a macromolecule. This in turn is made up of repeating units, the monomers.[26] Polymers, as a great generic term, can be classified in many different ways and based on a variety of properties. A classification based on the physicochemical properties subdivides polymers into three subcategories: Thermoplastics, duromers and elastomers. There is also the possibility of differentiation based on the origin of the polymer into synthetic polymers, natural polymers and modified natural polymers. Another possible classification differentiates between the origin of the raw materials which form the basis of the polymers. This distinguishes between polymers from renewable sources and from non-renewable or fossil sources. Furthermore, a differentiation can also be made on the basis of the degradation properties, on the one hand into biodegradable polymers and non-biodegradable polymer structures on the other hand.[26]

2.2 Polymer Networks

In addition to the above-mentioned classification of polymers based on different properties, polymers can also be differentiated on the basis of their structural properties. Such a classification provides five subcategories for the generic term polymer: Linear, branched, star-shaped, ring-shaped and crosslinked polymers.[26] The latter crosslinked polymers are of particular interest for the present work. Crosslinked polymers can also be referred to as polymer networks and represent a particularly interesting group of polymers. This is due to the possibility of making targeted changes and adjustments to the macroscopic properties by combining them with other components.

The transition from linear or branched polymer chains to polymer networks is generally based on various interactions between the polymer chains and is based on the three-dimensional linkage of the polymers. These interactions can be of distinct types but are mostly of physical or chemical nature.

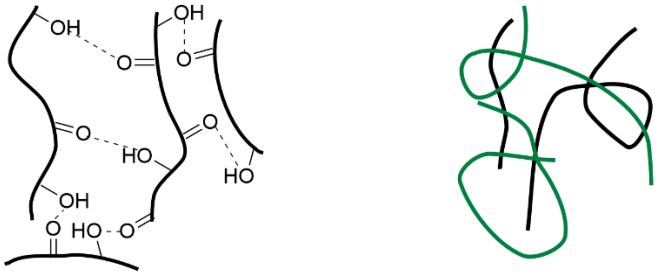

Figure 2: Physical networking within polymer networks based on polar interactions (left) and mechanical interactions (right). Own illustration according to [27].

The basis of physical networks are often polar interactions of different functional groups within the polymer structure or mechanical effects such as entanglements (Figure 2). The heterogeneity of physical interactions also harbors a wide range of strengths in networking. Polar interactions of different functional groups, such as hydrogen bonds, are commonly classified as weak to medium interactions, whereas ionic interactions are classified as strong.[27]

Regarding possible applications, the use of physical interactions is of particular interest if the aim is not permanent but reversible networking. Specifically, this behavior can be modeled analogously to enzymes and is used, among other things, as part of sensor systems.[28] Furthermore, by choosing different ion pairs, the interactions can be coordinated in such a precise manner that both reversible and irreversible crosslinks can be achieved.[29] A further possible property that is of particular research interest is the possible use of physically crosslinked polymers with regard to self-healing systems. This concept is based on the reversible crosslinking properties as there is the possibility of dividing polymer workpieces and simply connecting them again through subsequent contact with the cut edges.[29,30]

In contrast to physical crosslinking, chemical crosslinking is based on covalent bonds that are built up between the individual polymer chains. The process on which chemical crosslinking is based is fundamentally identical (Figure 3). The first step is the formation of a large number of linear and branched polymer chains of different lengths which are still soluble. This stage of the chemical crosslinking process is referred as sol. Above a certain expansion and concentration, the chemical crosslinking, that takes place, reaches a tipping point, the so-called gel point. The result is a three-dimensional crosslinked polymer chain, a gel which on the one hand spans the entire solution, but which on the other hand is still present in a mixture of individual chains and branched chains. This transition is also known as the sol-gel transition. As a result of the ongoing crosslinking, the built-up gel is no longer soluble in the original solvent but rather surrounds it just like the smaller chains. Both smaller chains and the original solvent are absorbed into the gel and swell it.[27]

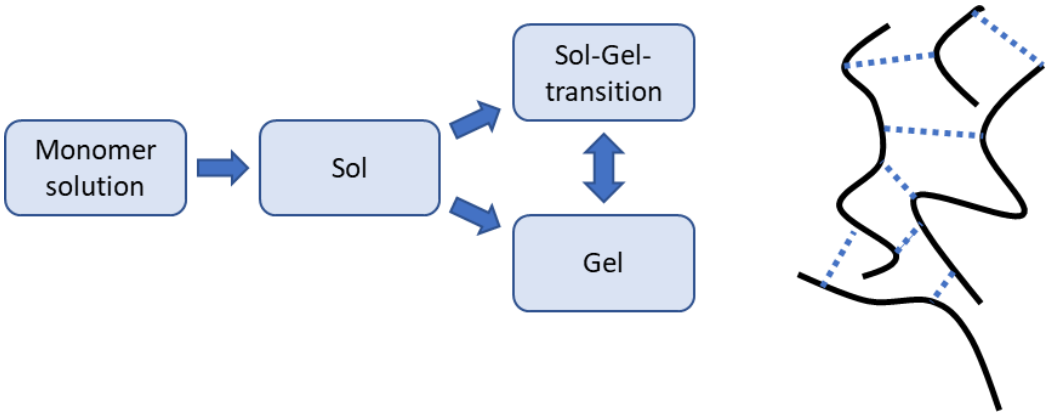

Figure 3: Schematic representation of the chemical crosslinking process (left) and chemical crosslinking of polymer chains through covalent bonds between the chains (right). Own illustration according to [27].

Various options are available to produce chemically crosslinked polymers. Two of the most common variants are crosslinking following the actual polymerization reaction and crosslinking using multifunctional monomers as part of a one-pot synthesis. In the case of crosslinking following the polymer building reaction,

multifunctional monomers are used which, however, do not crosslink during the actual polymerization. This takes place in a second step following the polymer build-up reaction. A multi-step procedure is particularly advantageous if further processing is required before networking. The variant of the one-step synthesis, however, is based on the use of multifunctional monomers which enter a network during the polymer synthesis reaction at the same time. Widespread synthesis variants for building polymer networks are, for example, free radical polymerization[31], polycondensation[32] or, alternatively, controlled mechanisms such as Atom Transfer Radical Polymerization (ATRP)[33]. Depending on the intended application, the possible synthesis sequences of a polymer network have individual advantages and disadvantages. Variants which initially build up a polymer structure in order to crosslink it in a second step are common methods (Figure 4). The crosslinking of the polymers formed can be achieved, for example, photochemically or thermally. A prominent example of such a procedure is the use of monomers based on maleimide. After the polymerization, this functional group can be crosslinked both thermally and photochemically, using UV-irradiation.[34]

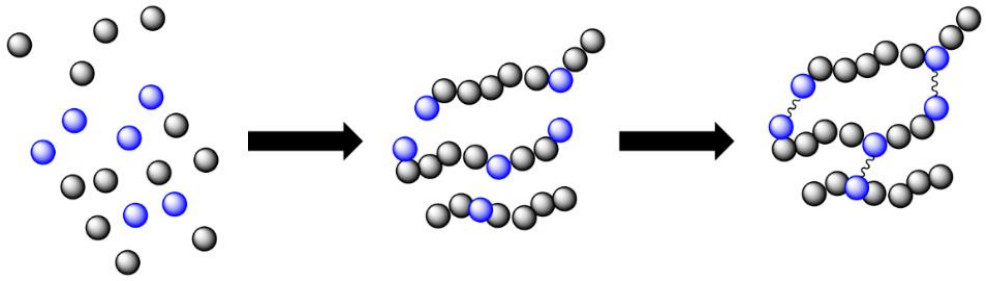

Figure 4: Two-stage synthesis of a polymer network by crosslinking functional groups following a polymer building reaction.

This approach is used by applying a polymer solution in the form of thin layers with the help of a spin coater on a surface which can then be crosslinked. Under certain circumstances it can also be advantageous to introduce the cross linkable functionality after the polymer build-up reaction (Figure 5). This multi-step approach may be necessary for crosslinkers that are difficult to polymerize. An example of such difficulties is the maleimide-based monomer, which tends to crosslink non-selectively at different temperatures.[35] One possible solution to this problem is the incorporation of azlactone-based monomers in order to introduce the crosslinker after the polymer build-up reaction.[36]

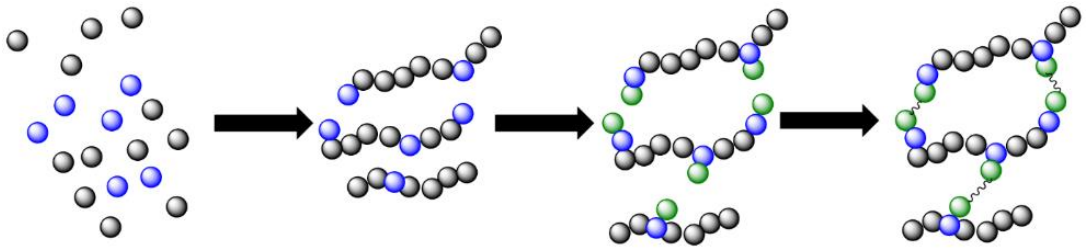

Figure 5: Three-stage synthesis of a polymer network through a polymer-analogous connection of a crosslinkable structural unit following a polymer building reaction.

The simplest variant for building polymer networks, which was also applied in the present work, is undoubtedly the one-pot synthesis (Figure 6). In this type of synthesis, the polymer network is obtained directly from the low molecular weight composition of monomers, initiators and crosslinkers which makes the synthesis extremely simple.

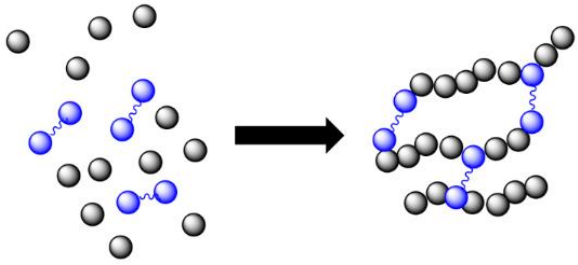

Figure 6: One-pot synthesis of a polymer network using a multifunctional monomer.

2.3 Gels

Such polymer networks are referred to as gels which take up a further component, a solvent for instance. Compared to uncrosslinked polymers in solution, their macroscopic properties can undergo significant changes. Consequently, they are of particular interest and importance for the presented work. Within the microfluidic reactor (MFR), the gels are used as the carrier material for the catalyst structure. The term gel can be defined very differently based on the relevant literature. Different definitions have been drawn up based on the mechanical properties or the macroscopic properties.[37] In addition to many differences, all these different definitions have some central, common points:[38,39] Basically, gels are considered to be soft and brittle three-dimensionally linked polymers, which are composed of at least two different materials. One of these two components is the so-called matrix (polymer network) which in turn can accommodate other components such as solvents. The crosslinking of the gel can be covalent (chemical crosslinking) or non-covalent (physical crosslinking).

2.3.1 Physical Properties of Gels

The remarkable properties of gels become particularly clear when comparing crosslinked and uncrosslinked polymers. Some physical properties, such as polarity or the influence of individual functional groups, remain comparable in the case of crosslinked polymers as well as non-crosslinked polymers. In contrast, other properties change fundamentally. This can be illustrated using the example of polymer samples based on the well-studied monomer *N*-isopropylacrylamide (NIPAAm). Linear NIPAAm-based polymers show pronounced thermoresponsive behavior in water.[40] Basically, this is the Lower Critical Solution Temperature (LCST), a phase transition. A very similar behavior can also be observed with networked NIPAAm-based gels.[41] From a macroscopic point of view, however, differences between crosslinked and uncrosslinked polymers can be determined taking into account the physical condition. These different behaviors are based on the different concentrations of the polymer chains and the associated different interactions between the polymer chains. The basis of the behavioral differences can be traced back to different interactions in polymer solutions and polymer networks. In polymer solutions of different concentrations, high levels of

interactions such as overlaps between the polymer chains occur which are highly dynamic and therefore short-lived. Nevertheless, those interactions mean that the individual polymer chains can no longer be viewed as isolated. In addition to highly concentrated solutions, these effects also occur in diluted and semi-diluted polymer solutions. In polymer networks, there are permanent, less dynamic interactions between the chain segments.[42] This becomes particularly clear when a solvent is added. Since polymer networks consist of three-dimensionally linked polymer chains, they are no longer soluble. Rather, the solvent leads to a swelling process, often with significant volume expansion.[39]

Typically, a liquid is used as a solvent and the gel obtained is then referred to as a lyogel.[43] Lyogels can be divided into further subcategories. If the swelling process takes place in water, the resulting gel is called a hydrogel. The use of organic solvents results in an organogel.[44] If a gas rather than a liquid is used as the solvent, the result is an aerogel. The swelling process in the respective solvent can result in enormous weight increases with an uptake of the solvent of several thousand times its own weight.[45] The resulting increase in volume or weight can be quantified via the degree of volume or mass swelling. This is defined as:

$$d = \frac{V_{swollen}}{V_{dry}} \qquad (1)$$

d = Degree of volume swelling [-]

$V_{swollen}$ = Volume of swollen gel [mm³]

V_{dry} = Volume of dry gel [mm³]

In addition to Equation 1 the degree of mass swelling can also be used to quantify a swelling process (Eq 2).

$$d_w = \frac{m_{swollen}}{m_{dry}} \qquad (2)$$

d_w = Degree of weight swelling [-]

$m_{swollen}$ = Mass of swollen gel [g]

m_{dry} = Mass of dry gel [g]

According to Equations 1 and 2, the degree of swelling of a gel depends on the composition of the gel, the solvent and the swelling time. There are basically two different types of swelling. The isotropic swelling describes an uninfluenced swelling in all three spatial directions. Anisotropic swelling, however, denotes hindered swelling. In the context of the present work, this type of influenced swelling is of particular interest as the gels under consideration are surface-bound within the MRF and, consequently, do not swell freely. An approximation of the swelling behavior of such gels suggests an increased swelling of the gels along the z direction.[46]

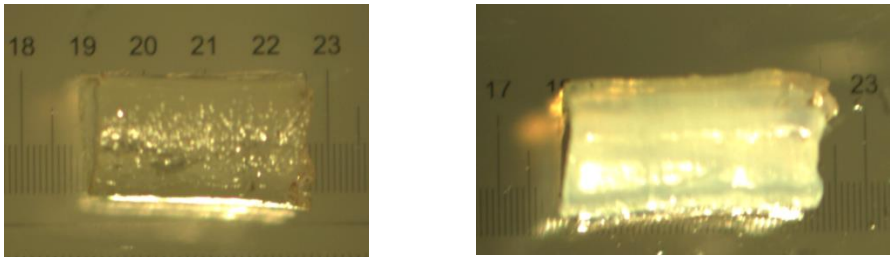

Figure 7: Image taken with a light microscope of a gel in the freshly prepared state (left) and the likewise cylindrical shape of the swollen gel in dimethylsulfoxide (DMSO) (right).

Furthermore, the mechanical properties are changed in comparison to dissolved uncrosslinked polymer chains. For highly concentrated solutions of linear polymer chains it can be observed that these become increasingly viscous.[42] In particular, covalently crosslinked gels tend to behave more like solids. This is particularly evident from the fact that they essentially retain their original shape. (Figure 7).[37,39] The respective properties of the gel in terms of mechanical stability[47] and the degree of swelling[48] can be influenced by the degree of crosslinking or the number of crosslinking points. The degree of crosslinking is simply dependent on the amount of crosslinker used during the synthesis. In principle, the mechanical properties can be influenced in a variety of ways during the synthesis. For example, the addition of synthetic clay minerals is known from the literature which results in nanocomposite gels with improved mechanical properties.[49] Another possibility for influencing the mechanical stability is to carry out the gel synthesis at low temperatures. The resulting cryogels are also characterized by increased mechanical stability.[50] Aside from these singular influences on gel synthesis, it is also possible to combine several different methods.[51] If an attempt is made to positively influence a certain parameter such as mechanical stability during the synthesis, it should be noted that this is often done on the basis of changes in the overall polymer composition. This means that various other properties may also be influenced simultaneously.[52] In addition to the polymer composition, both the degree of swelling and the associated mechanical stability depend on the amount of solvent absorbed. A more pronounced swelling capacity and a larger quantity of absorbed solvent lead to lower mechanical stability.[53] Besides this, their optical properties such as the refractive index are commonly used properties to describe the physical behavior of gels. The change of refractive index due to the swelling process can for example be used to determine the thickness of thin layers by surface plasmon resonance spectroscopy (SPR).[54] Another possible method to determine the refractive index is ellipsometry which can also provide information about the layer thickness.[55] Based on these parameters, it is even possible to make statements about the degree of networking.[56]

2.3.2 Application of Gels

Due to their physical properties, gels are promising candidates for a large number of applications, such as a high level of research interest in the field of biotechnology.[57] This interest is based on the soft and elastic properties which are similar to human tissue. Based on the comparable properties, there is the possibility of using gels based on polyvinyl alcohol as heart valve stents. These could be advantageous in the long term as conventional bioprostheses often require repeated surgical interventions due to material fatigue.[58] Further applications of gels are as promising materials in the optical industry[59], as drug delivery systems[60] or for

the targeted removal of mercury ions from aqueous media.[61] Probably the most prominent application of gels is the "Eversense sensor" from "Senseonics". This sensor was developed in 2014 and enables the long-term determination of blood sugar levels.[62]

In addition to the areas of application of gels already mentioned, there is a wide field of application for crosslinked polymer structures. A particularly far-reaching example of the improvement of mechanical properties through crosslinking was the discovery of the vulcanization of rubber.[63] In addition, the use of polymers as carrier material for catalysts, which makes them easier to reuse, is known from the literature.[14] Due to their swelling behavior, this application can also be adopted for gels and is therefore enjoying great interest.[14,23,64] It has already been demonstrated that, in addition to polymers, gels can also serve as carrier materials for catalysts and can also be successfully recycled without their effectiveness being excessively reduced.[65] After the reaction has taken place, the gel particles can be recovered, for example by filtration.

Another step on the way to more efficient catalytic processes could be the combination of gel-immobilized catalysts with continuously operated flow reactors. The history of this approach goes back to the mid-1970s, when a fully automated flow reactor was established for the regeneration of nicotine diamide as part of an enzymatic reaction.[5] In this case, an aluminum bed served as the carrier material. In the period that followed, however, various crosslinked carrier materials for catalysts have been established. Sometimes these materials hardly swell which means that only the surface is available as a catalytically accessible space. As a result, the amount of catalyst depends on the square of the diameter of the particles used. In order to increase the catalyst performance in a reactor chamber of given dimensions, there are only two options available. On the one hand, the amount of catalyst used can be increased, on the other hand, a more powerful catalyst could be used.[23] One possible solution approach could be the use of gels as a matrix. It has already been shown successfully that gels can serve as a cage structure in enzyme-catalyzed reactions.[21] In the underlying work, the gels are produced in a one-pot reaction from the monomers and the respective biocatalysts. It has already been shown that diffusion into the gel structures within the reactor is possible. Since the biocatalyst is present within the gels, successful diffusion is of the utmost importance. Due to the swelling process of the gels, the amount of catalyst no longer depends on the surface but on the volume of the gels. Another successful example of this approach is performing a variety of Knoevenagel reactions using a tertiary amine as a catalyst.[22,23] In this example too, the local amount of catalyst inside the reactor chamber is increased which means that more efficient catalysis can be established.
On the basis of the above-mentioned examples and interrelationships it becomes clear that a gel is a complex interplay of various influencing factors and characteristics which must be coordinated with one another and with regard to possible application ideas.

2.4 Lithography

An established method for the selective microstructuring of surfaces is lithography. Within lithography, different types are differentiated based on the structuring methods.[66]

Among the mechanical methods, a distinction is made between soft lithography and dip-pen lithography. The field of radiation-based methods for lithography composes of electron beam lithography and ion beam lithography. The variants that are most frequently used, are mechanical structuring and using electromagnetic radiation. Further distinguishing features are the resolution and the speed of structuring.

In addition to the already mentioned lithographic methods, photolithography in particular stands out as a powerful and versatile method of microstructuring.[66] The structuring is often implemented using UV radiation[67,68] or radiation within the visible wavelength range.[69] Using this method, structures of very different sizes can be produced. Examples of poly(ethyleneglycol) hydrogel structures which have a diameter of 7 - 500 µm and heights between 3 and 12 µm, are known from the literature. The reaction times required for this are very short at 0.5 seconds.[67] Furthermore, significantly smaller diameters of only 1.5 µm[70] and layer thicknesses of nanometers are known.[68] Using additional aids, such as lenses to improve the optical resolution, structures with a width of 180 nm and a depth of 35 nm can be produced at a speed of 6 $\frac{m}{s}$.[71] For achieving resolutions in the nanometer range, it is advisable to use a focused point source.[71] When using a surface spotlight instead, it is important to equip the photomask with the appropriate resolution and to suppress undesired scattered radiation. Contrary to the previously discussed generation of positive structures on the substrate surface, the production of negative structures using photolithography is also possible.[23,72] The difference between the preservation of positive and negative structures is that in the case of positive structures the exposed layer becomes soluble, whereas in the case of negative structures it becomes insoluble Figure 8).

However, a specific and already established application area for photolithography is semiconductor technology. Inside this, a temporary protective layer is applied by means of photolithography which serves as a shape for the actual semiconductor.[73]

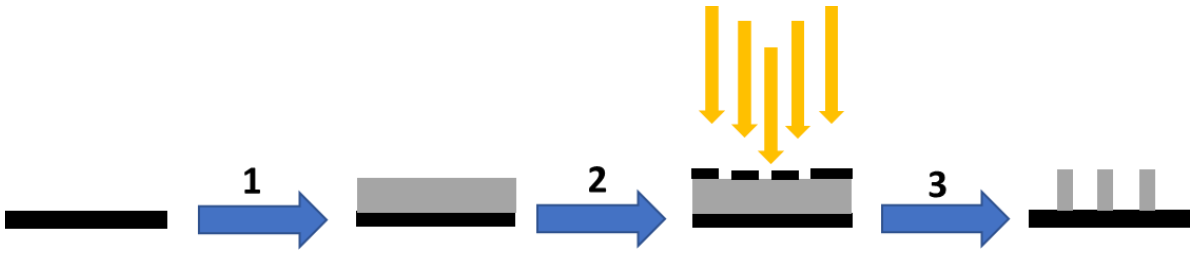

Figure 8: Schematic representation of the process of photolithography. A substrate optionally modified with an adhesion promoter (1) is coated with a photoresist (2) and then irradiated with UV light through a mask (3), the exposed areas hardening and the desired structures can be obtained after cleaning. Own illustration according to [66].

The process to be followed to obtain both positive and negative structures consists of three successive manufacturing steps.[74] In the first step, a substrate is coated with a photoresist (Figure 8, (1)). If the photoresist is not able to adhere directly to the substrate, a further step is interposed with the application of an adhesion promoter to the substrate. Then, in the second step, irradiation is carried out through a shaping photomask (Figure 8, (2)). After the irradiation is completed, the mask is removed and excess photoresists is washed off, the desired structures are obtained (Figure 8, (3)). The method of photolithography is an efficient, versatile and powerful process to build structures of very different sizes. This process has already been used successfully several times for the micro structuring of MFR, whereby both acrylate and acrylamide-based monomers could be used successfully.[21–23,74]

2.5 Catalysis

In general, catalysts increase the speed of a chemical reaction. Due to the Arrhenius equation, a catalyst must lower the activation energy of the reaction to increase the reaction rate constant. This is possible in two different ways: On the one hand the energy of the transition state can be reduced, on the other hand the energy of the educts can be increased.[75,76] In the following, some exposed variants of catalysts are presented as examples. Metal catalysts are particularly important for industrial processes. Additionally, biocatalysts and organocatalysts should also be emphasized.

2.5.1 Metal based Catalysts

Powerful metal-based catalysts are at the center of many large-scale technical and industrial processes. The basis of the catalysts is usually a transition metal which is used as a complex with various ligands. Several heavy metals such as Co, Ni, Zn or Ce are used that unfortunately are hardly environmentally friendly due to their toxicity. Furthermore, metals such as Fe, Pt, Ir and Pd are also used which can be viewed as environmentally friendly to a limited extent.[77] As already mentioned, these metals are used in the vast majority of applications combined with various complexes and thus in their oxidized form. The choice of a suitable ligand also enables control of the stereo information of the reaction carried out.[78]

Depending on the transition metal used and the inherent extraction costs as well as the productivity of the extraction sites, these metals turn out to be expensive catalysts. Furthermore, the ligand synthesis, which must be adapted to the intended use, is often complex. Nonetheless, matched metal-based catalyst systems

are extremely effective.[79] The turnover number (TON) and the turnover frequency (TOF) are key figures which enable the comparison of different catalyst systems.

$$TON = \frac{n_{Product}}{n_{Catalyst}} \quad (3)$$

TON = Turnover Number [-]

$n_{Product}$ = Amount of product $\left[\frac{mol}{l}\right]$

$n_{Catalyst}$ = Amount of catalyst $\left[\frac{mol}{l}\right]$

Taking into account a corresponding time component, it follows:

$$TOF = \frac{n_{Product}}{n_{Catalyst} \cdot t} \quad (4)$$

TOF = Turnover Frequency $\left[\frac{1}{h}\right]$

t = Time $[h]$

Known TOFs of metal complexes can be in the order of tens of several ten thousands per second.[80] Due to their high performance, for example in the production of polyolefins, such a large number of catalytic cycles are run through that the catalyst used can remain in the product and does not need to be separated.[81] Further examples of large-scale processes that use metal catalysts are the "Wacker"[82] or the "Cativa"[83] process. Beyond the large-scale industrial area of application, they are also used in various syntheses on a laboratory scale, whereby they are typically only used in a few mole percent due to their high performance.

2.5.2 Biocatalysts

Based on natural processes, enzymes can be used as catalysts for various reactions. Due to the high complexity of the enzyme structure, the products of the corresponding reactions are typically characterized by excellent stereoselectivity.[84] The selectivity is the result of the build-up of the protein structure. Proteins exist in a specific spatial structure and interact with the substrate within the binding pocket according to the key-lock principle.[85] In addition to the high selectivity, a major advantage is the environmental compatibility of enzymes which in contrast to metal catalysts is in line with the aspects of "Green chemistry". Problems in the large-scale use of enzymes are essentially their production. This is extremely complex and has to be carried out using biological processes and sources which increases the price and thus limits the possible use. The enzyme activity is used to enable comparisons to be made in the same way as metal catalysts.[7]

$$a = \frac{U}{m} \qquad (5)$$

a = Enzyme activity $\left[\frac{\mu mol}{s \cdot mg}\right]$

U = Conversion rate of the enzyme for a substrate $\left[\frac{\mu mol}{s}\right]$

m = Amount of enzyme $[mg]$

Another problem using enzymes is their high sensitivity to external influencing factors. Such factors can be the existing pH value, the temperature or the solvent itself.[86] Typical values for enzyme activity are in the range of a few micromoles per hour.[86,87] By building a highly selective binding pocket and shielding reactive groups from unwanted reactions, enzymes are characterized by remarkable reactivity and selectivity.[75]

2.5.3 Organocatalysts

The basic idea behind metal-based catalysts is the availability of labile coordination sites that can carry chiral ligands. At the same time, the coordination sites allow the substrates to interact with one another in a chiral environment created by chiral ligands for instance.[75] A subsequent dissociation of the product allows the catalysis process to proceed. At the beginning of the 21st century, various chemists around the world realized that metals are not necessarily required for high enantioselectivities in catalytic reactions. For instance, in the form of amines there are numerous chiral and enantiomerically pure molecules which are also able to interact reversibly with substrates. A prominent advocate of this approach is David MacMillan, who developed the catalyst of the same name.[75,88] The corresponding catalyzed reaction is the catalytic enantioselective conjugate addition of, for example, aldehydes with cyclic secondary amines. Furthermore, the imidazolidinone-based organocatalyst (Figure 9) is able to catalyze a large number of asymmetric reactions. For example, the first highly enatioselective organocatalyzed Diels-Alder reaction (Figure 10) which was published in 2000. The iminium ion obtained by condensation of the chiral secondary amine of the catalyst and an unsaturated aldehyde reacts in this case with various agents to provide the [4 + 2]-cycloadducts in outstanding yields and enantioselectivities.[88]

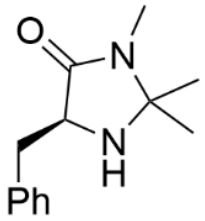

Figure 9: Chiral secondary amine catalyst.

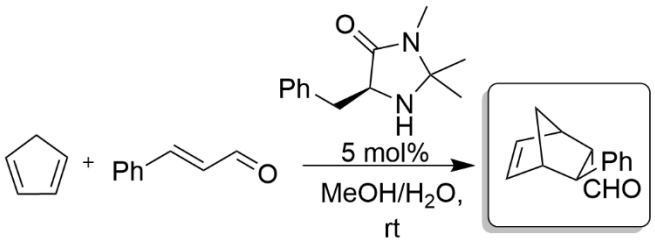

Figure 10: Example for metal-free asymmetric catalysis. Own illustration according to [88].

Further organocatalyzed reactions using the MacMillan imidazolidinone organocatalyst are 1,3-dipolar cycloadditions[89], Friedel-Crafts alkylations[90], α-chlorinations[91], α-fluorinations[92] and intramolecular Michael reactions[93]. All these reactions proceed highly enantioselective.

Organocatalysts are characterized by the fact that they are small organic molecules which can carry out catalytic asymmetric reactions. With the conversions listed, it becomes clear that the catalyst does not have to be used in such large quantities as a chiral auxiliary. At the same time, however, it is also clear that organocatalysts have to be used in significantly larger amounts (up to 20 mol%) than the most powerful metal catalysts.[75] A reliable and robust synthesis route to the desired catalyst structure is therefore crucial. In the case of the catalyst structure discussed, this takes place by condensation of a derivative of L-phenylalanine, its *N*-methyl amide, with an equivalent of acetone.[75]

Analogous to this example, amino acids of natural origin are often used in the synthesis of organocatalysts. All three primary, secondary and tertiary amines are catalytically active. In addition to the catalytically active nitrogen centers[94], organocatalysts with phosphorus[95] or carbene centers[96] are also known. However, due to the range of organocatalysts, only nitrogen-based organocatalysts are dealt with in this study.

Organocatalysts based on catalytically active nitrogen centers can develop a catalytic effect in various ways. On the one hand, mechanisms of action can be run through as a classic base or with imine or enamine intermediates.[97] On the basis of these versatile reaction possibilities, in addition to the reactions already mentioned, for example aza-Michael-[98] Mannich-[99], Aldol-[100] or Knoevenagel reactions[101], a wide variety of other catalysis can be achieved. The most established examples of organocatalysts based on primary amines are again based on natural amino acids, for example L-Alanine or L-Valine.[102] In addition to this structure, numerous other organocatalysts derived from primary amines are known.[103]

Among the secondary amine catalysts, L-proline deserves special mention. L-proline and its derivatives are particularly diverse and changeable organocatalysts as there are many possibilities for modification.[104] In addition to various proline derivatives, various catalysts are also used which can be traced back to the basic structural elements of proline (Figure 11).[105]

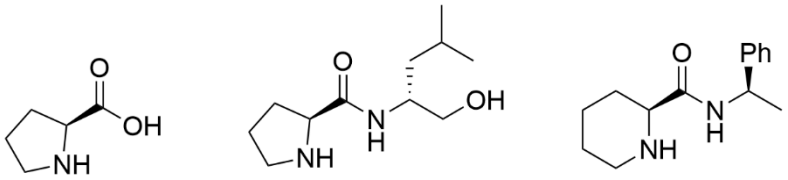

Figure 11: Secondary amine based organocatalysts.

Besides primary and secondary amine-based catalysts, organocatalysts based on tertiary amines are also known. The nucleophilic catalyst 4-*N*,*N*-(dimethylamino)pyridine and 1,8-diazabicyclo[5.4.0]undec-7-ene are particularly prominent in this context (Figure 12).

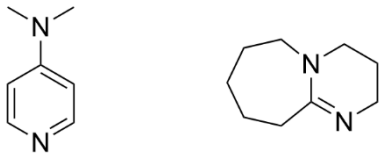

*Figure 12: Structural examples for organocatalysts based on tertiary amines. 4-*N*, N-(dimethylamino)pyridine (left) and 1,8-diazabicyclo[5.4.0]undec-7-ene (right).*

Due to the diverse structural features, a large number of modifications can be made to organocatalysts.[106] These can be used, for example, to optimize the catalyst properties for the desired application. The better the prepared catalyst structure is adapted to the intended use, and the more complex the synthesis on which it is based, the more important it is to efficiently recover or immobilize the catalyst. The immobilization itself is based on minor structural modifications which ideally have hardly any influence on the catalytic activity, but, at the same time, enable an effective connection to carrier materials. In the case of metal-based catalysts, polymerizable ligands must be attached to the metal center[107] or, alternatively, the metal based catalyst can be introduced into the polymer via subsequent post modification.[108] In the case of organic catalysts, however, there are various options. There are possibilities of immobilization on the surface of solid particles[16,17,109], single chain nanoparticles[18] or as part of block copolymers, in micellar catalysis.[19,20]

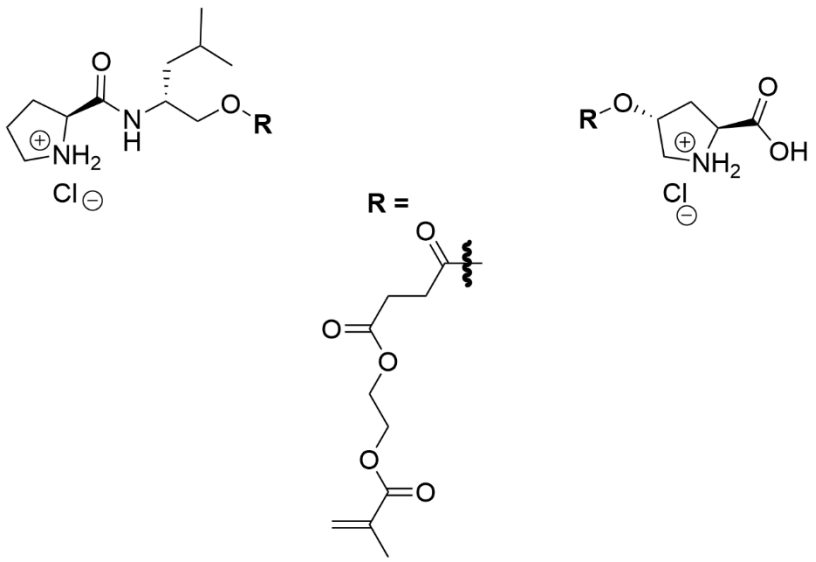

Figure 13: Structural formulas of L-Proline based organocatalysts.

As part of this work, different catalyst structures based on an L-proline backbone were made available for use within the MFR (Figure 13). Immobilization takes place through simultaneous polymerization of the vinyl group of the methacrylate unit with other methacrylate-based monomers. Using proline-based monomers inside the MFR, it is possible to catalyze various types of reactions.

2.6 Aldol Reaction

In general, the reaction of an enol or enolate of a carbonyl compound, which takes the role of the nucleophile with an aldehyde or ketone, which functions as an electrophile, is referred to as an aldol reaction (Figure 14). The resulting primary product is an β-hydroxycarbonyl compound which, under suitable conditions, undergoes dehydration and ultimately yields the corresponding α,β-unsaturated carbonyl product.[75]

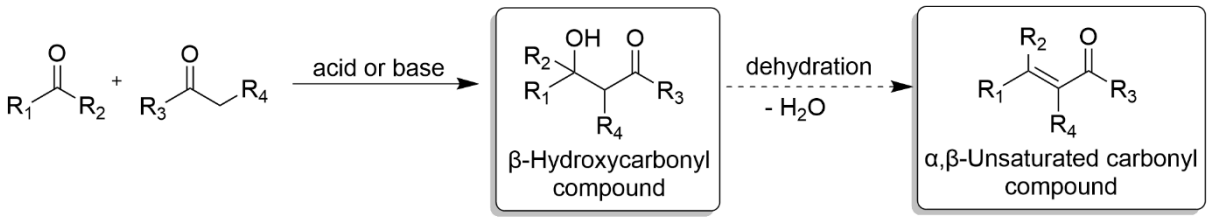

Figure 14: Classical aldol reaction, leading to α,β-hydroxycarbonyl compound. Own illustration according to [101].

The original type of aldol reaction was based on the use of Brønsted acid or base as catalysts. Under these reaction conditions, however, undesirable side reactions, such as self-condensation, polycondensation and dehydration followed by Michael addition, often occur.[75,101] The solution to this problem lies in the formation of preformed enolates. The most widespread enolates are based on lithium, boron, titanium and silyl enol ethers. Enolate formation can take place in a highly regionally and stereoselective manner. The aldol reaction connected to enolate formation takes place in a highly diastereoselective fashion. Thus, *(E)*-enolates generally provide the anti product while *(Z)*-enolates lead to the formation of the syn product as the dominant diastereomer (Figure 15).[101]

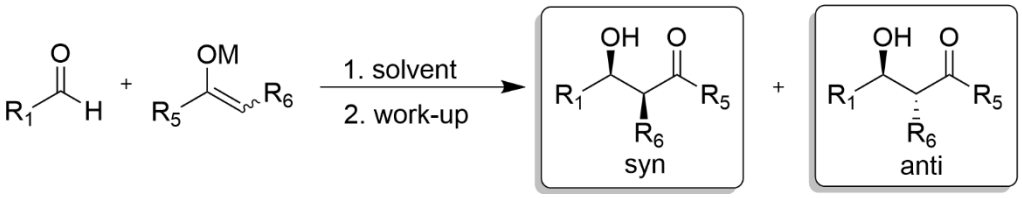

Figure 15: Aldol reaction using preformed enolate. Own illustration according to [101].

Control of absolute stereochemistry can be achieved in a number of ways. On the one hand, enantiomerically pure starting materials can be used, which is generally referred to as reagent control, on the other hand, asymmetric catalysis can also be carried out. Reagent control can be achieved, for example, by using chiral auxiliaries or by using chiral ligands on the boron enolates.[101] Another possibility is the use of chiral aldehydes. In addition, the direct asymmetric aldol reaction represents a particularly elegant variant of the reaction process which can also be accessed in different ways. First, there is the option of biochemical catalysis using enzymes or catalytically active antibodies. In addition, chiral metal complexes can be used or organocatalytically, using small organic molecules.[75,101]

Mechanistically, in the case of the classical aldol reaction, a large number of equilibrium steps are run through and the formation of the product is also reversible. Therefore, only the aldol reaction using preformed enolates and the direct asymmetric variant will be discussed in the following.[101]

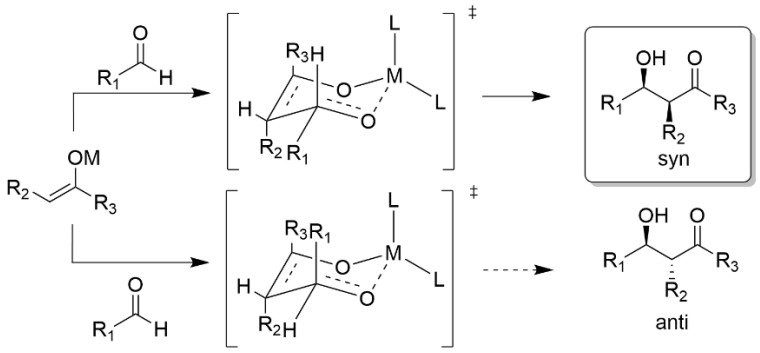

Figure 16: Zimmerman-Traxler model for (Z)-enolate. Own illustration according to [101].

A characteristic feature of the aldol reaction with preformed enolates is the product synthesis with high diastereoselectivity. (*Z*)-enolates supply the *syn* product (Figure 16), whereas (*E*)-enolates supply the *anti*-product as the main product (Figure 17). These relationships can be understood using the Zimmermann-Traxler model. According to this model, the reaction goes through a six-limb chairlike transition state. Based on this, the controlling factor is the avoidance of the destabilizing 1,3-diaxial interaction within the cyclic transition state.[75]

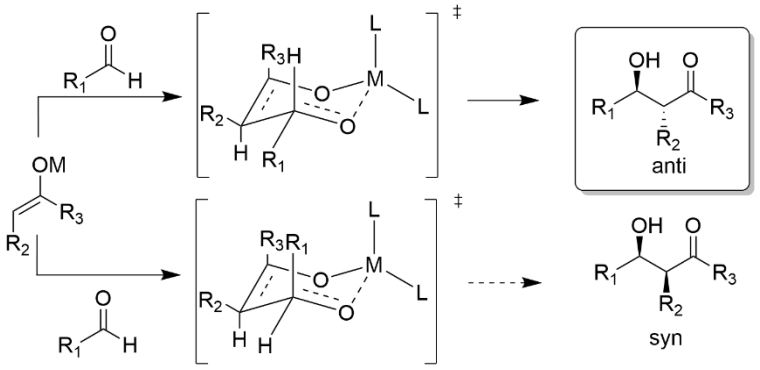

Figure 17: Zimmerman-Traxler model for (E)-enolate. Own illustration according to [101].

According to the postulated mechanism by LIST et al.[9] (Figure 18), a nucleophilic attack of the amine function on the carbonyl carbon takes place as a first step, whereby the intermediate (I) is formed. With elimination of water, the carboxylic acid of the proline acting as Brønstedt acid, an immonium ion (II) is formed which is then converted into the enamine (III). If this enamine attacks an aldehyde species, a preferred conformation can be adopted in the transition state (IV). This is promoted by the hydrogen bond between the carbonyl oxygen of the aldehyde and the carboxylic acid functionality of the proline and therefore leads to the stereoselectivity shown in the formation of species (V).[110] The imminium ion (V) is then converted again into the amine by the addition of water and proline is recovered by the subsequent elimination.[111,112]

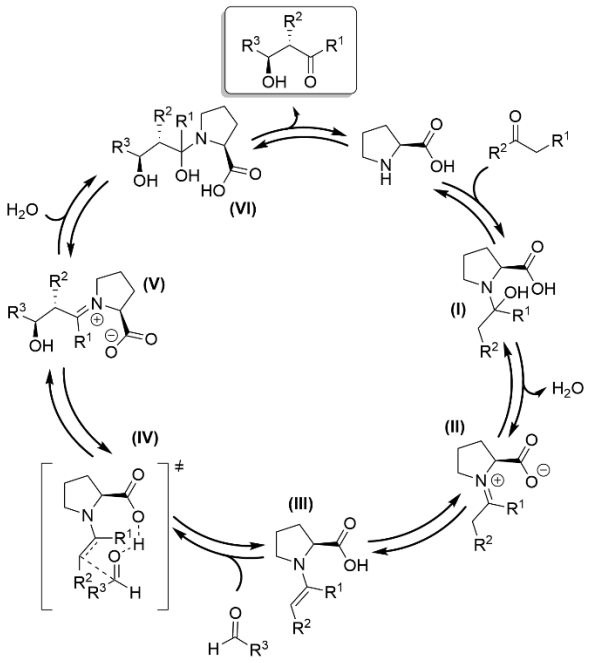

Figure 18: Mechanism of the L-Proline catalyzed asymmetric aldol reaction. Own illustration according to [9].

From the mechanism, it can be seen that proline acts as both a Lewis base and a Brønstedt acid. Therefore it is treated as a bifunctional catalyst.[111] This bifunctionality is linked directly to a stereocenter. Thus, the enantioselectivity of the proline-catalyzed reaction is dictated by the conformation within the proline itself.[110,111] In the literature, the use and immobilization of proline and derivatives derived from it have received a great deal of attention. There are examples for the immobilization on the surface of solid particles[16,17,109], single chain nanoparticles[18] or, as part of block copolymers in micellar catalysis.[19,20] Based on the results known from literature, a wide range of different aldol products is known. In the overwhelming majority of cases, relatively long reaction times are necessary which can hardly be achieved within the MFR. For precisely this problem, however, the high local catalyst concentration within the reactor chamber could prove to be advantageous for effectively reducing the reaction times.

2.7 Azoxyarenes

Azoxyarenes are valuable building blocks carrying an uncommon oxygen-nitrogen-nitrogen 1,3-dipolar moiety (Figure 19). Overall, this group of compounds is one of the azobenzenes. In recent years the interest in preparing azoxybenzene compounds increased drastically due to their versatile properties in applications to liquid crystals[113], polymer materials, stabilizers and analytical reagents.[114]

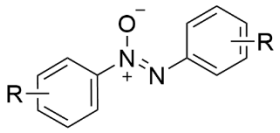

Figure 19: General structure of azoxyarenes.

Additional attractive properties of azoxybenzenes, especially for medical as well as synthetic chemists, are the retinoidal activities[115] and the opportunity to act as *o*-directing group in C-H-functionalizations of arenes.[116] Furthermore, the azoxy functionality can be seen as a bioisoster for amide and alkene functions and thus shows promising anti-cancer activities as the corresponding bioactive amides and alkenes.[117]

Usually, the preparation of azoxybenzenes proceeds via condensation of aryl nitroso compounds with aryl hydroxylamines.[118] Consequently, this synthesis strategy involves the oxidation of anilines or the reduction of nitroaromatics, respectively, to obtain the two constituents of the subsequent condensation. Exemplary for this approach, the conversion of aniline to azoxybenzene with H_2O_2 as oxidant was demonstrated[119], while the use of a Rh(I)-catalyst for a transfer hydrogenation with alcohols and nitrosobenzene as hydrogen acceptor to form aldehydes and also to generate azoxybenzene was also investigated.[120] Another work used isopropanol both as reducing agent and as solvent.[121] More recently, the synthesis of azoxybenzenes from nitrobenzenes by light irradiation under continuous flow conditions was reported.[122] Difficulties in these approaches are the harsh reaction conditions, over-reduction or oxidation of the educts and in competition reactions which include in particular the condensation of anilines with nitrosoarenes to generate diazo compounds. Consequently, there is a great interest in efficient and simplified synthetic strategies for the selective preparation of these valuable compounds.

2.8 Chemical Reactors

The following chapter is a brief summary of previous work on the basic interrelationships of chemical reactors.[23] In general terms, a division can be made into two types of chemical reactors. The discontinuously operated batch reactors (BR) and the continuously operated flow reactors (FR).[123] Both reactor variants are characterized by various advantages and disadvantages. The greatest advantage of a BR is its ease of implementation. In contrast to this, FR are characterized by increased complexity in the structure, but at the same time increased economic efficiency and easier scale-up as well as consistent product quality.[124]

2.8.1 Discontinuously operated Reactors

The basic feature of the BR is the discontinuous or batch mode of operation. First, the reactor is loaded with reactants which then are mingled. This is followed by the actual reaction and, in the third step, the emptying of the reactor and further processing of the product. As an example, the conversion can be defined by the reaction rate constant (k) for any chemical reaction that is carried out in the BR. The following example illustrates this connection:[76]

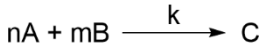

Figure 20: Reaction equation of an example reaction of n reactants A with m reactants B to form product C.

A kinetic analysis based on an example reaction is of interest for a comparative analysis of different reactor types. Based on the example reaction shown in Figure 20, the reaction rate is calculated according to:[76]

$$v = k \cdot [A]^n \cdot [B]^m \quad (6)$$

v = Reaction rate $\left[\frac{mol}{l \cdot s}\right]$

k = reaction rate constant $\left[\left(\frac{1}{mol}\right)^{n+m-1} \cdot \frac{1}{s}\right]$

$[A]$ = Concentration reactant A $\left[\frac{mol}{l}\right]$

$[B]$ = Concentration reactant B $\left[\frac{mol}{l}\right]$

n, m = stoichiometric factors

Following Formula 6, the reaction rate is defined as the decrease in the concentration of reactant A over time. The reaction rate can therefore also be expressed as a change in the concentration of A:[76]

$$v = -\frac{d[A]}{dt} = k \cdot [A]^n \cdot [B]^m \quad (7)$$

t = Time $[s]$

The result is:

$$-\frac{d[A]}{dt} = k \cdot [A]^2 \quad (8)$$

Assuming equal initial concentrations of [A] and [B] and a stoichiometric reaction.[76] The concentration of reactant A at time t can then be concluded from Equation 8:[76]

$$[A]_t = \frac{[A]_0}{1 + k \cdot t \cdot [A]_0} \quad (9)$$

$[A]_0$ = Concentration reactant A at time t = 0 $\left[\frac{mol}{l}\right]$

$[A]_t$ = Concentration reactant A at time t $\left[\frac{mol}{l}\right]$

For the operation of a BR this means that the concentration of the product [C] increases in a reaction of the second order over time and tends towards a maximum. The reactor system has reached its maximum conversion after a certain period of time and must then be emptied and filled with fresh reaction mixture.

A decisive factor for the economic efficiency of a BR is the reaction time component, according to Equation 9. In addition, the available volume of the reactor is of particular importance. Typically, round-bottom flasks with volumes in the range from milliliters to a few liters are used. In addition, a cooler, agitator and a heating source are required. In principle, this basic structure can be applied to industrial standards with volumes ranging from liters to cubic meters (Figure 21). The particular advantage of this type of reactor design is the flexibility of its application since no adaptation to individual reactions has to be made. However, disadvantageous, the achievable yield is limited based on the underlying parameters. Another problem is the need for constant process control and active influence on the reactor structure. A specific application of this type of reactor is therefore primarily in the area of specialized chemicals.[125]

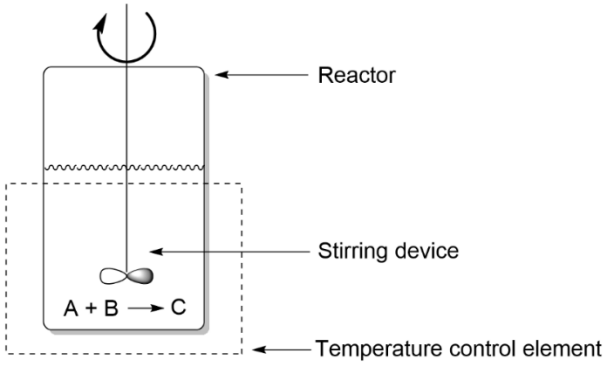

Figure 21: Schematic representation of a BR for the reaction of reactants A and B to form C. Own illustration according to [125].

Another disadvantage associated with BR is the transfer of reactor volume from laboratory scale (milliliters to a few liters) to industrial scale (liters to cubic meters) due to various additional elements that must be considered.[126] Within such a scaling process, the entirety of the running processes must be traced. The heat energy within the BR can be formulated as the sum of all heat input and output. Due to the changed surface-to-volume ratio, the thermal energy inside the reactor is no longer defined solely by the energy released by exothermic processes or external heat input, in contrast to the laboratory scale.[126] Rather, it is important to consider other energy contributions such as the stirrer in the overall constellation.

$$q_{ac} = q_r + q_{ex} + q_{fd} + q_s + q_{loss} \qquad (10)$$

q_{ac} = Total thermal energy $[J]$

q_r = Thermal energy of the reaction $[J]$

q_{ex} = Thermal energy through exchange with heating or cooling element $[J]$

q_{fd} = Thermal energy of reactant solution $[J]$

q_s = Thermal energy generated by stirring $[J]$

q_{loss} = Thermal energy loss through exchange with environment $[J]$

A comparison of the relevant energy contributions from BR on a laboratory or industrial scale shows that, on a laboratory scale, only the amount of heat of the reaction and that of the exchange with the heating and cooling source have to be taken into account. It is therefore obvious that in an enlarged BR no observation comparable to the laboratory scale can take place. The conversion of the reaction is determined by the diffusion as well as by locally occurring conversion rates. The key parameter for both aspects is mixing within the reactor. In most cases, the conversion of an intermixed BR is higher than that of a non-intermixed one, which is why, consequently, the conversion depends on the quality of the mingling.[127]

For the successful operation of a BR, two key points are of great importance: On the one hand, permanent good mixing must be guaranteed within the reactor as this has a significant impact on conversion.[127] On the other hand, sufficient heat supply and heat dissipation must be ensured via the outer sheath of the reactor. Inadequate mixing and the associated temperature control of the reaction mass can, according to the heat balance in Equation 10, result in the reaction failing or the reactor system overheating, which can result in economic losses, but can also lead to extremely dangerous incidents and accidents. Because of this, a reactor, which is run in batches, has a high potential for errors and dangers, particularly when it comes to loading.

Numerous examples of such accidents are known in the literature. As an example, reference is made to an incident from 1971.[126] When loading a BR with chloronitrobenzene to produce nitroaniline, the temperature of the reactor got out of control due to overloading which resulted in the destruction of the reactor.[128] In a more precise statistical evaluation of 65 such accidents, a little over 50 % (33) could be traced back to the reaction temperature.[129] Due to the simplicity of this type of reactor and the great economic importance associated with it, the safety and controlled management of BR is still a challenge and is constantly being investigated and improved.[126,130] The first results were, for example, separate scientific journals such as “Process Safety Progress” (1982 Wiley VCH) or “Loss Prevention” (1999 Elsevier).

Vice versa, semi-batch reactors (sBR) can be operated more reliably than BR. This is also evident from an evaluation of the number of accidents.[126] The number of incidents could be reduced from 13 to 1 if an sBR was used instead of a BR.[129] The crucial difference lies in the charging step of the reactor. In the case of an sBR, not both reactants are completely present in the reactor at the time $t = 0$, but only one reactant is introduced, and the others are metered in sequentially. Through the sequential addition of reactants, the reaction can initially subside before further educt is added. This procedure allows the temperature of the entire reaction mixture to be controlled and, if necessary, reduced by stopping the supply of reactants. In addition to large-scale industrial processes, this approach is also known from laboratory practice. With less reactive syntheses, the BR is very popular, with highly reactive reactions, nonetheless, the sBR should be preferred. The better control of the reaction achieved as a result, however, is accompanied by a more complex kinetic view of the reaction. The increased complexity of the kinetic analysis is due to the fact that the conversion of the reactant A also depends on the addition of the reactant B.

Assuming an equimolar reaction, the following relationship arises:[125]

$$-\frac{d[A]_t}{dt} = \frac{\dot{V}[A]_t}{V_0 + \dot{V}\,t} + k\,[A]_t^2 + k[A]_t\left(\frac{\dot{V}[B]_F\,t - [A]_0\,V_0}{V_0 + \dot{V}\,t}\right) \tag{11}$$

$$\frac{d[B]_t}{dt} = \frac{\dot{V}([B]_F - [B]_t)}{V_0 + \dot{V}\,t} - k[A]_t^2 + k[B]_t\left(\frac{\dot{V}[B]_F\,t - [A]_0\,V_0}{V_0 + \dot{V}\,t}\right) \tag{12}$$

$\dot{V}$ = Speed of influx $\left[\frac{m}{s}\right]$

$[B]_F$ = Concentration of reactant B in volume flow $\left[\frac{mol}{l}\right]$

V_0 = Volume of the submitted reactant solution A $[l]$

Based on the above argued relationships, it becomes clear how effective control of the reaction can be achieved by adding component B in sequence and furthermore, it becomes clear that, for an effective control a detailed analysis of the possible combinations of the charging of the reactor must be carried out. To obtain the best possible results, the order in which the reactor is charged with the various reactants is crucial. For instance, it can be shown on the basis of theoretical calculations that the achievable conversion in case of the free radical polymerization of styrene is determined by two different factors. On the one hand side it is determined by the reactivity of the added solution and consequently on the other hand by the order in which it is charged. Depending on the order in which it is charged (first present the initiator, then add the monomer continuously or vice versa), fundamentally different results are obtained.[131]

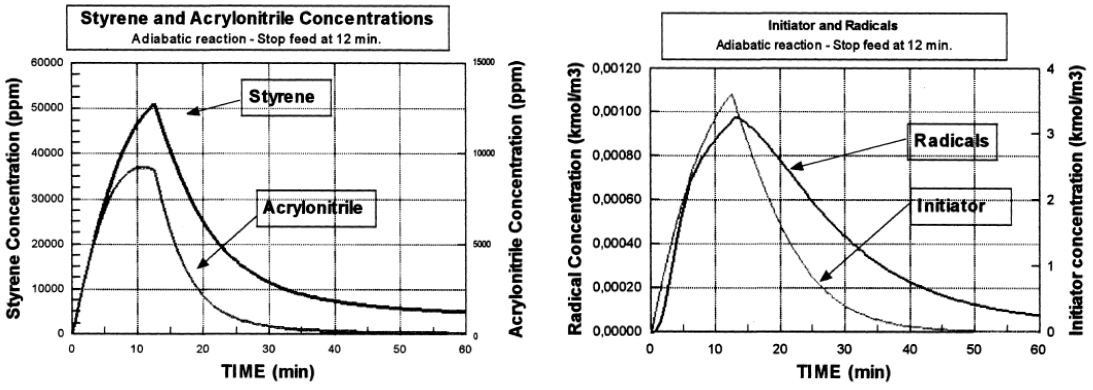

Figure 22: Concentration-time diagram of the free radical reaction of styrene and acrylonitrile carried out in a semi-batch reactor (left). Concentration-time diagram of the corresponding initiator and radicals (right).[132] Reprinted from Catalysis Today, 52, Gianni Donati and Renato Paludetto, Batch and semibatch catalytic reactors (from theory to practice), 183 – 195, Copyright 1999, with permission from Elsevier.

Another specific example is the free radical copolymerization of styrene and acrylonitrile (Figure 22), in which the reactor is equipped with one educt, followed by the second educt, added over a period of 12 minutes. It can be observed that the educt concentration initially rises up to a reaction time of around 12 minutes. Then, as soon as the addition of the second reactant is stopped, i.e. from around minute 12, the

concentration decreases as a result of the increasing conversion of the reaction.[132] Using this example, it can be shown that the turnover of an sBR is rather low at the beginning as the reactor continues to be continuously charged with reactant. As a result, there is initially only a small conversion of the reactants present in low concentrations.[125,132] Due to the differences in the way the reactions are conducted, the conversion trends of the BR and the sBR differ significantly.

2.8.2 Continuously operated Reactors

Continuously operated reactors can be viewed as an alternative to batch reactors. These are characterized by a permanent influx of reactants and an outflow of product. The continuous operation results in a high level of economic efficiency, and thus a continuously operated form of the reactor, the Continuous Stirred Tank Reactor (CSTR), is particularly popular in industrial processes. The structure of such a reactor is outlined in the following (Figure 23).[125]

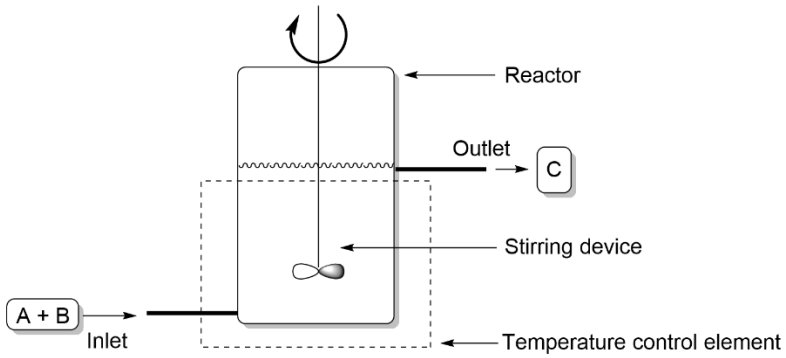

Figure 23: Schematic representation of a CSTR in which reactants A and B are continuously added and product C is continuously removed. Own illustration according to [125].

Basically, a CSTR can be viewed as a BR after an infinitely long reaction time which results in a steady state. For the operation of a CSTR, homogeneous mixing is assumed which results in an identical concentration distribution and temperature in the entire reactor volume. On the basis of the steady state, the mass balance of reactants supplied and products removed is zero, so that the reactant and product concentrations as well as the conversion within the reactor are also constant. By extending the reaction time, a BR achieves an almost complete conversion of the reactants. Consequently, from a certain reaction time onwards, there are only infinitesimal changes in the product and educt concentrations as well as in the conversion.[133]

In case of BR and sBR, the reaction is terminated when the steady state is reached, and the reactors are emptied. In contrast, a characteristic of the CSTR is the maintenance of the steady state of the reaction. The decisive factor here is the continuous supply and removal of reactants and the product formed. The product flow of a CSTR is characterized by the fact that it reflects the conditions within the reactor and consequently has a high product concentration with a low reactant concentration. Contrary, the reactant inflow has a high reactant concentration with a low product concentration and is clearly different from the concentration ratios within the CSTR. When the reactant inflow reaches the reactor chamber, these differences are abruptly adjusted and the stationary reactor state is consequently not influenced.[125,133] This process management means that the reactant solution is quickly and heavily diluted when it enters the reactor volume which only

leads to a low level of heat development within the solution. The risk of overheating of the reactor system and other risks, as already discussed, is thus minimized during the entire operating time.

Based on these fundamental relationships within a CSTR, it becomes clear that complete conversion can never be achieved within this type of reactor. This makes it all the more important to achieve an optimal ratio between feed speed and conversion. The residence time of the reactants within the reactor is decisive for this ratio.

$$\tau = \frac{V_{Reactor}}{\dot{V}} \qquad (13)$$

$\dot{V}$ = Volume influx $\left[\frac{l}{s}\right]$

$V_{Reactor}$ = Reactor volume $[l]$

τ = Residence time $[s]$

As can be seen in Equation 13, the dwell time is influenced by the volume flow $\dot{V}$. This is defined by Equation 14.

$$\dot{V} = \frac{V}{t} \qquad (14)$$

V = Volume conveyed $[l]$

The analogies between BR and CSTR can also be continued regarding residence time. The residence time in a CSTR is equivalent to the reaction time of a discontinuous reactor. Even in discontinuous reactor systems, the reaction time is decisive for conversion. Since full conversion cannot be reached within a CSTR, it is neither possible to determine a terminal point for the entire process.[134] Nonetheless, the constant conversion over the entire term results in the high economic efficiency of this type of reactor. After the reactor has started up, the desired product can be produced for any length of time with constant turnover and consistent quality. For a further optimization of the turnover and thus the reactor output, it is possible to operate several CSTRs connected in series.[135] Using Equation 14, it becomes clear that conversion depends on the reactor volume. In addition to the total volume of all reactors connected in series, the sequence of the reactors for optimizing conversion is sacrosanct. If two successive reactors are almost equal in volume, a minimum in conversion results, whereas the conversion is maximized if a smaller first reactor is followed by a larger second one.[136]

In addition to the modifications of reactors already discussed, the Flow Reactor (FR) is another type of reactor that operates continuously. In the simplest case, this is a tubular reactor. A FR is therefore fundamentally different from BR, sBR or CSTR, as all these reactors are essentially based on a stirred tank. The basic principle in this case is the continuous supply of reactants on one side of the reactor and the continuous

removal of the resulting product on the other side. Taking another look at the example reaction from the educts A and B to the product C, as shown in Figure 24, it becomes apparent that the reactants are continuously fed to the FR, while the product formed is continuously discharged. A further differentiation of FR is possible on the basis of an important characteristic: The inside diameter (iD). In the range of a few millimeters up to 500 µm, systems are named minifluidic. Reactors with an iD of 500 - 10 µm are called microfluidic reactors.[137] Special advantages of MFR lie in an increased surface-volume ratio which can reach values of 50 000 $\frac{m^2}{m^3}$.[137] The obvious advantages of this are the excellent heat exchange via the outer shell of the reactor.[138]

Figure 24: Schematic representation of a tubular FR in which a reaction of the reactants A and B takes place with the formation of product C. Own illustration according to [125].

Analogous to the example reaction of the second order, a conversion analysis can also be carried out in the case of the FR. The reaction time within the reactor is equivalent to a location coordinate as the continuous flow drives the entire reaction solution in the reactor. Contrary to the reactors considered so far (BR, sBR and CSTR), there is no intermixing inside of a FR. As a result, a considered volume increment within the reactor is constant in its composition and temperature and so the conditions within any such volume increment are comparable to the conditions within a CSTR. Hence, a cascade of an infinite number of CSTRs is comparable in its behavior to a FR.[139,140] Without any back mixing and under constant conditions in the respective volume increment, the reactor is called Plug Flow Reactor (PFR). This state corresponds to the idealized case which, due to diffusion processes, cannot be reached but can only be approximated.

$$RD = \frac{D}{F \cdot L} \qquad (15)$$

RD = Reaction dispersion number $[/]$

D = Dispersion coefficient $\left[\frac{1}{s}\right]$

F = Flow rate $\left[\frac{m}{s}\right]$

L = Length of the reactor $[m]$

One way of expressing the difference between the ideal and the real reactor is the degree of back-mixing that occurs within the FR. This can be represented concretely as a reactor dispersion number which, with zero or infinity and one, corresponds to an ideal PFR without back-mixing and a completely back-mixed reactor.[141] The back-mixing of a reactor is inversely related to the volume flow, a higher volume flow

consequently results in less back-mixing.[142] This behavior results from the relationship between the reactor dispersion number and the volume flow.

$$F = \frac{\dot{V}}{A} \tag{16}$$

A = Cross sectional area $[m^2]$

In addition to the back-mixing along the length of the reactor, which has already been illuminated, mixing over the cross-sectional area of the reactor is also important for the most homogeneous reaction solution possible. The Reynolds number, which is dependent on the flow velocity, can be used for a corresponding analysis.[140]

$$Re = \frac{\rho \cdot F \cdot d}{\eta} \tag{17}$$

Re = Reynolds number $[/]$

ρ = Density of solvent $\left[\frac{kg}{l}\right]$

η = Viscosity $\left[\frac{kg}{m \cdot s}\right]$

d = Reactor diameter $[m]$

When considering this key figure, an increase in the Reynolds number is associated with behavior that is increasingly like the PFR and therefore increasingly ideal. The main informative value of this figure relates to the transition from laminar to turbulent flow which for a simple tubular reactor is reached at about 2300. Above this, the flow profile is constant over the entire reactor diameter, which can be assumed to be a homogeneous composition of the reaction solution over the entire cross-sectional area.[140] Such statements are only valid for tubular reactors; other reactor geometries require the critical Reynolds number to be determined separately. Based on Equations 16 and 17, it becomes clear that, with a constant volume flow and simultaneous minimization of the reactor diameter, increasingly ideal reactor conditions can be achieved. A consistently high Reynolds number is only achieved with small diameters or high volume flows. If, apart from that, the Reynolds number is low and the flow is more laminar, the mixing is almost exclusively determined by diffusion. In addition to the cross-sectional area of the molecules, diffusion also depends on the distance covered and consequently enables no efficient mixing.[143] One possible solution to this problem is the use of microfluidic flow reactors (MFR). The smaller volumes of this type of reactor lead to a reduced distance to be covered by diffusion. As a result, homogeneous mixing along the cross-sectional area can also be achieved more easily by diffusion. In addition to the restriction to diffusion, mixers can still be used.[144] These prove to be extremely efficient for the homogeneous mixing of two components in a small space.[145]

A large number of options are available for the manufacture of microfluidic reactor systems. A frequently used approach is based on casting a negative mold with polydimethylsiloxane (PDMS). Due to the shaping process, this material can be brought into almost any shape which allows extremely flexible use.[146] Furthermore, PDMS is chemically inert and hardly swells in organic solvents.[147] If there is no negative mold available, it is possible to manufacture the reactor mold from 3D printing materials. This also enables automated production of the reactor forms.[148] In addition to the examples mentioned, there is also the possibility of manufacturing microfluidic systems using high-performance milling cutters.[149] Interesting materials for this variant would be, for example, polytetrafluoroethylene (PTFE) which is also chemically inert but at the same time more durable and therefore less prone to failure than PDMS. Based on the various manufacturing processes, very different shapes can be manufactured. These can be in the form of simple tubular reactors, meandering structures or chamber-shaped reactors.[150] Choosing a chamber reactor offers the advantage that the flow profile within the actual reactor chamber can be adjusted by adapting the geometry.[151] In addition, the chamber surface can be modified in various ways in a spatially resolved manner.[152] Therefore, it is possible to carry out several successive reactions or domino reactions.[153] Considering these numerous aspects, an MFR represents a potent and versatile foundation for the connection of continuously operated reactors and reuse of catalysts.

2.8.3 Combination of Organocatalysts and Continuous Reactors

Due to the above mentioned many interesting properties and advantages of continuously operated reactors, they appear to be a versatile and promising opportunity to address aspects of modern organic and continuous chemistry as well as "Green Chemistry", particularly in combination with organocatalysts.[154] These aspects concern an increased safety as well as an increased efficiency and thus lower use of chemicals. One example of improved safety aspects in continuous reactors is the ozonolysis of alkenes. The system is based on hoses made of semipermeable membranes which are brought into contact with the reactive and toxic ozone within a closed chamber. In addition to the reduced user risks, this process is also characterized by high yields.[2] In other examples, reaction times could be shortened and side reactions suppressed at the same time.[24,25,155] Furthermore, a variety of reactions are accessible in this way. Examples range from the α-amonoxylation[156] of aldehydes to synthetically extremely valuable cyclopropanation reactions[157] to classic aldol reactions.[25,158] The operation of continuous reactors is particularly advantageous if the catalyst used is efficiently recovered or in immobilized form.[159] By means of such procedures, the required amount of catalyst can be significantly reduced and a significant increase in efficiency can be achieved compared with reactors operated batchwise.[23,160]

3 Experimental Part

This section lists all chemicals and auxiliary materials used as well as analysis methods. The syntheses carried out are also described and the products obtained from them are characterized. Some content of the following chapter has already been published.[24,25]

3.1 Chemicals and Materials

Table 1: Overview of all chemicals and materials used as well as their purity, manufacturers and special comments.

Reagent	Manufacturer	Purity	Remark
Acetone	Sigma-Aldrich	>99 %	
2-aminobenzonitrile	TCI	>98 %	
3-aminobenzonitrile	TCI	>99 %	
Ammonia		Technical grade	25 % solution in water
Argon	Wöhning Gas	5.0	
2-bromoaniline	TCI	>98 %	
3-bromoaniline	TCI	>98 %	
4-bromoaniline	TCI	>99 %	
2-butanone	Alfa Aesar	99 %	
4-chloroaniline	TCI	>99 %	
Chloroforme-d_1	Deutero	99.8 %	
Cyclohexanone	Sigma-Aldrich	99.8 %	
Deuterated water	Deutero	99.9 %	
Dichloromethane		Technical grade	

Dicyclohexylcarbodiimide	Sigma-Aldrich	99 %	
Diethyl ether		Technical grade	
Diiodomethane	Sigma-Aldrich	99 %	ReagentPlus
Diisopropylethylamine	Sigma-Aldrich	>99 %	
4-Dimethylaminopyridine	Fluka	>99 %	
Dimethylphenylphosphonite	Sigma-Aldrich	98 %	
Dimethylsulfoxide	Grüssing	>99 %	
Dimethylsulfoxide-d_6	Deutero	99.8 %	
1,4-Dioxane	Grüssing	99.5 %	
Di-*tert*-butyldicarbonate	Alfa Aesar	97+ %	
Ethanol		Technical grade	
Ethyl acetate		Technical grade	
4-ethylaniline	TCI	>99 %	
Ethylene glycol dimethacrylate	Sigma-Aldrich	98 %	
4 N HCl in 1,4-Dioxane	TCI		
1-hydroxybenzotriazole hydrate	Sigma-Aldrich	97 %	wetted with not less than 20 wt. % water, 97%
Isopropanol	Sigma-Aldrich	99.5 %	HPLC grade

L-Leucinol	TCI	>96 %	
L-Proline	TCI	>99 %	
Lithium bromide	Fluka	>98 %	
Methanol		Technical grade	
Mono-2-(methacryloyloxy)ethyl succinate	Sigma-Aldrich	>95 %	
Methyl-3-aminobenzoate	TCI	>98 %	
Methyl-4-aminobenzoate	TCI	>98 %	
Methyl methacrylate	Sigma-Aldrich	99 %	
2-nitrobenzaldehyde	TCI	>99 %	
3-nitrobenzaldehyde	TCI	>98 %	
4-nitrobenzaldehyde	Sigma-Aldrich	98 %	
Nitrosobenzene	TCI	>98 %	
2-nitrosotoluene	Sigma-Aldrich	98 %	
N-(3-Dimethylaminopropyl)-*N*'-ethylcarbodiimidhydrochloride (EDC·HCL)	TCI	>98 %	
N,*N*-Dimethylformamide	Carl Roth	>99 %	
N,*N*-Dimethyl-4-nitrosoaniline	Sigma-Aldrich	97 %	
N-(*tert.*-Butoxycarbonyl)-L-prolin	TCI	>99 %	
n-Hexane		Technical grade	

n-Heptan	Carl Roth	>99 %	HPLC grade
Object slides	Carl Roth		72 x 26 mm
Oxone®	TCI		
Tetrahydrofuran		Technical Grade	
Thionyl chloride	Sigma-Aldrich	97 %	
trans-4-Hydroxy-L-proline	TCI	>99 %	
3-(trichlorsilyl)propylmethacrylate	Sigma-Aldrich	≥90 %	
Triethylamine	Acros Organics	99 % pure	
Trifluoroacetic acid	Carl Roth	>99 %	
2,4,6-trimethylbenzoylchloride	Alfa Aesar	98+ %	
Water	Carl Roth	Rotisolv HPLC Gradient	

3.2 Methods of Characterization

In this section, the devices used for analysis and the software used for evaluation are named. Associated specifications, such as temperatures and relevant hardware, are also listed.

Nuclear Magnetic Resonance (NMR)

An "Avance 500" spectrometer from "Bruker" was available for nuclear magnetic resonance spectroscopy. Unless otherwise stated, the ^{1}H and ^{13}C-NMR standard measurements were carried out with the "Avance 500" spectrometer. To determine the conversion of the various MFR experiments, the ^{1}H-NMR spectra were recorded with an "Ascent 700" spectrometer from "Bruker". The software "Topspin 4.0.6" from

"Bruker" was used to analyze the spectra. When using the solvents listed, the following lock signals were used:

Table 2: Lock-signals of the NMR solvents used.

Solvent	**^{1}H-NMR-spectrum**	**^{13}C-NMR-spectrum**
$CDCl_3$	7.26 ppm	77.16 ppm
DMSO-d_6	2.50 ppm	39.52 ppm
D_2O	4.75 ppm	-

Electrospray Ionization Mass Spectrometry (ESI-MS)

The samples were analyzed by means of electrospray ionization mass spectrometry (ESI-MS) using a "Synapt-G2 HDMS" mass spectrometer from "Waters", together with a quadrupole time-of-flight analyzer. The samples were ionized using electrospray ionization (ESI) in the positive measurement mode.

Table 3: Device parameters used for recording the ESI mass spectra.

Capillary voltage	130 kV
Sampling cone	120 V
Extraction cone	3 V

Electron Impact Ionization Mass Spectrometry (EI-MS)

Electron impact ionization (EI) is used to record mass spectra. This measurement method was recorded with a high-resolution sector field mass spectrometer (DFS) from "Thermo Scientific".

Table 4: Device parameters used for recording the EI mass spectra.

R	1200
Voltage	70 eV
Temperature	200 °C

Confocal Microscopy

A "VK-9700" confocal microscope from "Keyence" was used to determine the height of the gel structures on microscope slides. The recordings of the structures were taken with the "VK Viewer 2.4.0.1" program and visualized and processed with the "VK Analyzer 3.4.0.1" program.

Melting point (MP)

The melting point of the synthesized solids was determined using a "Melting Point B-545" device from "Büchi". A gradient of 1 $\frac{°C}{min}$ was used.

Contact Angle Measurement

The contact angle measurements were performed using a "Drop Shape Analyzer-DSA25" from "Krüss".

High Performance Liquid Chromatography (HPLC)

For analytical HPLC a chiral stationary phase for the determination of enantiomeric excess (ee) a "VARIAN 920-LC" was used with the following capillary columns: "CHIRALCEL" IA and IC.

3.3 Batch Synthesis

In this chapter, all syntheses of the low molecular weight compounds as well as the characterization of the products obtained from batch reactions are described.

3.3.1 Synthesis of lithium phenyl-2,4,6-trimethylbenzoylphosphinate (LAP)

The synthesis was carried out according to known literature protocols.[161,162] Dimethylphenylphosphonite (1.56 g, 11.3 mmol) was placed in a baked out 50 ml round bottom flask. Afterwards 2,4,6-trimethylbenzoyl chloride (1.65 g, 1.8 ml, 9.0 mmol) was slowly added dropwise via a syringe. The reaction was stirred for 24 h with the exclusion of light. A solution of lithium bromide (3.2 g, 36.9 mmol) in 2-butanone (50 ml) of was then added. The solution was heated to 50 °C for 10 min before stirring for 4 h at RT, again with the exclusion of light. The precipitated colorless solid is filtered off and washed twice with 2-butanone (100 ml). 1.76 g (5.9 mmol, 65 %) of the colorless solid were obtained.

Characterization:

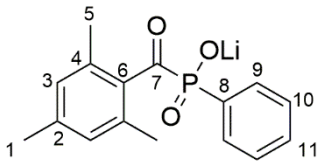

^{1}H-NMR (500 MHz, D_2O):

δ (ppm) = 1.99 (s; 6H; $^{5}CH_3$); 2.12 (s; 3H; $^{1}CH_3$); 6.76 (s; 2H; ^{3}CH); 7.39 (t; $^{3}J_{HH}$ = 7.3 Hz; 2H; ^{10}CH); 7.46 (t; $^{3}J_{HH}$ = 7.1 Hz; 1H; ^{11}CH); 7.71 (pt; $^{3}J_{PH}$ = 11.2 Hz; $^{3}J_{HH}$ = 7.1 Hz; 2H; ^{9}CH)

^{13}C-NMR (125 MHz, D_2O):

δ (ppm) = 18.5 ($^{5}CH_3$); 20.2 ($^{1}CH_3$); 128.1 (^{3}CH); 128.3/128.4 (^{10}CH); 132.0 (^{11}CH); 132.2/132.3 (^{9}CH); 132.4/133.2 (^{8}CP); 133.7 (^{2}Cq); 137.8/138.1 (^{6}Cq); 139.8 (^{4}Cq); 228.1/228.8 (^{7}CO)

^{31}P-NMR (202 MHz, D_2O):

δ (ppm) = 12.31 (s; 1P; P-O^-)

ESI-MS; m/z:

Calculated for $[C_{16}O_3PH_{16}]^+$ 287.2702 found 287.0846

3.3.2 Synthesis of 2-methacryloyloxyethylsuccinicacidchloride

The synthesis was carried out according to known literature protocols.[163] Mono-2-(methacryloyloxy)ethyl succinate (17.84 g, 15.0 ml, 77.5 mmol, containing 750 ppm MEHQ) was added to neat $SOCl_2$ (49.25 g,

30.0 ml, 414 mmol), and the mixture stirred at room temperature for 30 min and at 50 °C for 1 h. The excess $SOCl_2$ was evaporated under reduced pressure to give 2-methacryloyloxyethylsuccinoylchloride as a near colorless yellowish oil.

The product obtained was used for the synthesis in chapter 3.3.3 without additional purification. A conversion of 99 % could be determined by ^{1}H NMR spectroscopy.

Characterization:

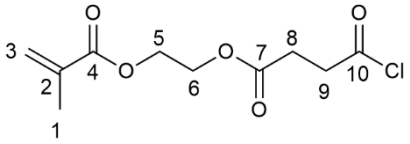

^{1}H-NMR (500 MHz, $CDCl_3$-d_1):

δ (ppm) = 1.86 (s; 3H; $^1CH_3$); 2.46 (t; $^3J_{HH}$ = 6.5 Hz; 2H; $^8CH_2$); 3.15 (t; $^3J_{HH}$ = 6.4 Hz; 2H; $^9CH_2$); 4.24 – 4.32 (m; 4H; $^{5+6}CH_2$); 5.50 – 5.54 (m; 1H; $^3CH_2$); 6.02 – 6.06 (m; 1H; $^3CH_2$)

^{13}C-NMR (125 MHz, $CDCl_3$-d_1):

δ (ppm) = 17.87 ($^1CH_3$); 28.96 ($^5CH_2$); 41.43 ($^6CH_2$); 61.94 ($^8CH_2$); 62.47 ($^9CH_2$); 125.67 ($^3CH_2$); 135.67 (^2C); 166.61 (^7CH); 170.37 (^4CH); 172.59 (^{10}CH)

3.3.3 Synthesis of *O*-(2-methacryloyloxyethylsuccinoyl)-*trans*-4-hydroxy-L-prolin (MAOESLP)

The synthesis was carried out according to known literature protocols.[163] A 250 ml round bottom flask was charged with CF_3CO_2H (25.0 ml), containing a spatula tip of hydroquinone and *trans*-4-hydroxy-L-proline (5.13 g, 39.2 mmol) was added under vigorous stirring. The mixture was stirred for 10 min, the crude product of 3.3.2 was added under ice cooling and the reaction mixture was stirred at room temperature for 2 h to give a clear, nearly colorless solution. The solution was cooled in an ice/water bath and Et_2O (150 ml) was added under vigorous stirring. A syrupy precipitate forms, stirring was discontinued and the precipitate was allowed to settle by gravity for 1 h. The reaction flask was removed from the ice/water bath, the supernatant was decanted and Et_2O (120 ml) was added. The syrupy crystals were left overnight in a refrigerator to solidify. The colorless solid was then dried at room temperature over night to give *O*-(2-methacryloyloxyethylsuccinoyl)-*trans*-4-hydroxy-L-proline hydrochloride. 10.78 g (31.3 mmol, 72 %) of the colorless solid were obtained.

Characterization:

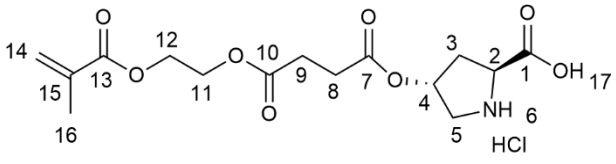

^{1}H-NMR (500 MHz, DMSO-d$_6$):

δ (ppm) = 1.88 (s; 3H; $^{16}CH_3$); 2.27 – 2.40 (m; 2H; $^{3}CH_2$); 2.54 – 2.68 (m; 4H; $^{8+9}CH_2$); 3.21 – 3.29 (m; 1H; $^{5}CH_2$); 3.49 – 3.66 (m; 1H; $^{5}CH_2$); 4.25 – 4.30 (m; 4H; $^{11+12}CH_2$); 4.39 – 4.45 (m; 1H; ^{2}CH); 5.24 – 5.35 (m; 1H; ^{4}CH); 5.70 (d; $^{2}J_{HH}$ = 1.6 Hz; 1H; $^{14}CH_2$); 6.03 (d; $^{2}J_{HH}$ = 1.6 Hz; 1H; $^{14}CH_2$); 9.06 (s; br.; 1H; ^{6}NH); 10.32 (s; br.; 1H; $^{17}COOH$)

^{13}C-NMR (125 MHz, DMSO-d$_6$):

δ (ppm) = 17.69 ($^{16}CH_3$); 28.19/28.51 ($^{8/9}CH_2$); 33.83 ($^{3}CH_2$); 45.22 ($^{5}CH_2$); 57.38 (^{2}CH); 61.85/62.16 ($^{11/12}CH_2$); 72.22 (^{4}CH); 125.93 ($^{14}CH_2$); 135.40 (^{15}CH); 166.19 (^{13}C); 169.24 (^{7}C); 171.07/171.65 (^{10}C); 173.03 (^{1}C)

ESI-MS; m/z:

Calculated for $[C_{15}H_{20}NO_8]^-$ 342.1189 found 342.1189

3.3.4 Synthesis of *N*-(*tert*-butoxycarbonyl)-L-proline

The synthesis was carried out according to known literature protocols.[164] In a 500 ml round bottom flask, L-proline (20.0 g, 170 mmol) was submitted in aqueous 10 % $NaHCO_3$ (200 ml) solution. Di-*tert*-butyl dicarbonate (44.5 g, 210 mmol) dissolved in 1,4-dioxane (150 ml) were slowly added to this solution. With vigorous evolution of gas, the mixture was stirred at room temperature overnight, a white solid precipitated. The pH of the liquid phase was then adjusted to 7 with a sat. citric acid solution as a result of which the precipitate went into solution. Sat. NaCl solution was added and the mixture was extracted with ethyl acetate (100 ml) three times. The combined organic layers were dried using a hydrophobic filter. The solvent was removed and the crude product was subsequently dried in a fine vacuum. 37.3 g (169.5 mmol, 99 %) of the colorless solid were obtained.

Characterization:

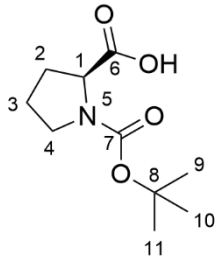

^{1}H-NMR (700 MHz, DMSO-d$_6$):

δ (ppm) = 1.36 (s; br.; 9H; $^{9-11}CH_3$); 1.70 – 1.81 (m; 2H; $^{2}CH_2$); 1.81 – 1.86 (m; 1H; $^{3}CH_2$); 2.10 – 2.16 (m; 1H; $^{3}CH_2$); 3.22 – 3.34 (m; 2H; $^{4}CH_2$); 4.00 – 4.06 (m; 1H; ^{1}CH)

^{13}C-NMR (176 MHz, DMSO-d_6):

δ (ppm) = 23.1 ($^{2}CH_2$); 28.0 ($^{9-11}CH_3$); 30.4 ($^{3}CH_2$); 46.1 ($^{4}CH_2$); 59.2 (^{1}C); 78.3 (^{8}C); 153.5 (^{7}C); 174.7 (^{6}C)

3.3.5 Synthesis of *tert*-butyl (S)-2-(((*R*)-1-hydroxy-4-methylpentan-2-yl)carbamoyl)pyrrolidine-1-carboxylate

The synthesis was carried out according to known literature protocols.[19] *N*-(*tert*-Butoxycarbonyl)-L-proline (10.09 g, 46.9 mmol) with EDC·HCl (9.84 g, 51.3 mmol) and HOBt (6.47 g, 47.9 mmol) were placed in a 250 ml round bottom flask in DCM (150 ml). The solution was stirred for 15 min. Then DIPEA (10.39 g, 82.3 mmol) and L-leucinol (5.69 g, 48.5 mmol) were added dropwise. The mixture was stirred overnight under an argon atmosphere at room temperature. The reaction solution was then washed with water (100 ml). The washing process was totaled with $NaHCO_3$ solution (100 ml), sat. citric acid solution (100 ml) and sat. NaCl solution (100 ml). The washed organic phase was dried using a hydrophobic filter and the solvent was removed. The colorless crude product was dried in fine vacuum. For further work-up, the crude product was purified by column chromatography on silica using a mixture of ethylacetate : MeOH (9 : 1) as the mobile phase (R_f = 0.83). After purification, 11.49 g (38.5 mmol, 82 %) of a colorless solid were isolated.

Characterization:

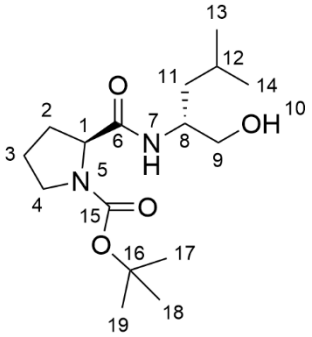

^{1}H-NMR (700 MHz, DMSO-d_6):

δ (ppm) = 0.86 (m; 6H; $^{13+14}CH_3$); 1.30 (dd; $^{3}J_{HH}$ = 7.16 Hz; 2H; $^{11}CH_2$); 1.36 (s; br.; 9H; $^{17-19}CH_3$); 1.57 – 1.66 (m; 1H; ^{12}CH); 1.68 – 2.13 (m; 4H; $^{2+3}CH_2$); 3.18 – 3.27 (m; 2H; $^{9}CH_2$); 3.29 – 3.40 (m; 2H; $^{4}CH_2$); 3.74 – 3.81 (m; 1H; ^{8}CH); 4.04 (d; $^{3}J_{HH}$ = 4.27 Hz; 1H; ^{1}CH); 4.55 (m; 1H; ^{10}OH); 7.41 (d; $^{3}J_{HH}$ = 8.69 Hz; 1H; ^{7}NH)

^{13}C-NMR (176 MHz, DMSO-d_6):

δ (ppm) = 21.7 / 23.5 ($^{13/14}CH_3$); 24.1 (^{12}CH); 28.0 ($^{17-19}CH_3$); 29.9 ($^{2}CH_2$); 31.4 ($^{3}CH_2$); 40.0 ($^{11}CH_2$); 46.5 ($^{9}CH_2$); 46.7 ($^{4}CH_2$); 48.6 (^{8}CH); 59.7 (^{1}CH); 78.3 (^{16}CH); 153.4 (^{15}C); 172.1 (^{6}C)

ESI-MS; m/z:

Calculated for $[C_{16}H_{30}N_2ONa]^+$ 337.2103 found 337.2114.

3.3.6 Synthesis of (S)-*N*-((R)-1-hydroxy-4-methylpentan-2-yl)pyrrolidine-2-carboxamide

(S)-*N*-((R)-1-hydroxy-4-methylpentan-2-yl)pyrrolidine-2-carboxamide (0.3 g, 0.95 mmol) were placed in a 50 ml round bottom flask and dissolved in 4 N HCl in 1,4-dioxane (1.86 ml) with vigorous stirring. The mixture was stirred at room temperature for 3 h. After 3 h, the colorless precipitate formed was filtered off, dissolved in DCM and brought to pH 8 with sat. sodium hydrogen carbonate solution. After subsequent extraction with ethyl acetate, removal of the solvent and subsequent drying in a fine vacuum, 0.18 g (0.84 mmol, 88 %) of a highly viscous yellowish oil were isolated.

Characterization:

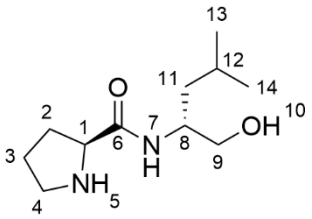

^{1}H-NMR (500 MHz, $CDCl_3$-d_1):

δ (ppm) = 0.85 – 0.98 (m; 6H; $^{13+14}CH_3$); 1.19 – 1.46 (m; 3H; $^{11+12}CH$); 1.53 – 1.78 (m; 2H; $^{3}CH_2$); 1.86 – 1.97 (m; 1H; $^{2}CH_2$); 2.10 – 2.25 (m; 1H; $^{2}CH_2$); 2.86 – 3.15 (m; 3H; $^{4}CH_2$; ^{10}OH); 3.44 – 3.72 (m; 2H; $^{9}CH_2$); 3.77 – 3.88 (m; 1H; ^{1}CH); 3.89 – 4.14 (m; 1H; ^{8}CH); 7.38 – 8.17 (s; 1H; ^{5}NH)

^{13}C-NMR (176 MHz, DMSO-d_6):

δ (ppm) = 21.8 ($^{13/14}CH_3$); 23.3 ($^{13/14}CH_3$); 23.6 ($^{2}CH_2$); 24.2 (^{12}CH); 30.0 ($^{3}CH_2$); 39.7 ($^{11}CH_2$); 45.5 ($^{4}CH_2$); 49.5 (^{8}CH); 58.7 (^{1}CH); 63.5 ($^{9}CH_2$); 167.8 (^{6}C)

ESI-MS; m/z:

Calculated for $[C_{11}H_{22}N_2O_2]^+$ 215.1754 found 215.1760

3.3.7 Synthesis of (*R*)-2-((*S*)-1-(*tert* -butoxycarbonyl)pyrrolidine-2-carboxamido)-4-methylpentyl (2 -(methacryloyloxy)ethyl)succinate

The synthesis was carried out according to known literature protocols.[165] *Tert*-butyl(S)-2-(((*R*)-1-hydroxy-4-methylpentan-2-yl)carbamoyl)pyrrolidine-1-carboxylate (7.25 g, 24.1 mmol) together with DCC (9.96 g, 48.2 mmol) and DMAP (130 mg, 1.1 mmol) in DCM (150 ml) were placed in a 250 ml round bottom flask. To the mixture, *O*-(2-methacryloyloxyethyl)succinic acid (5.75 g, 25.0 mmol) was added. The mixture was stirred for 48 h under an argon atmosphere at room temperature. The precipitated colorless solid was filtered off, washed with DCM and then discarded. After removal of the solvent, the crude product was first purified by column chromatography with silica as the stationary phase. A solvent gradient from *n*-hexane : ethyl acetate (10 : 1) to n-hexane : ethyl acetate (1 : 9) was used. The product phase had an R_f value of 0.95 in *n*-hexane : ethyl acetate (1 : 9). Afterwards the product was purified again by column chromatography using

neutral aluminum oxide as the stationary phase. The same mobile phase was used as in the previous column chromatography. After purification, 11.30 g (21.4 mmol, 89 %) of a viscous, slightly yellowish oil were isolated.

Characterization:

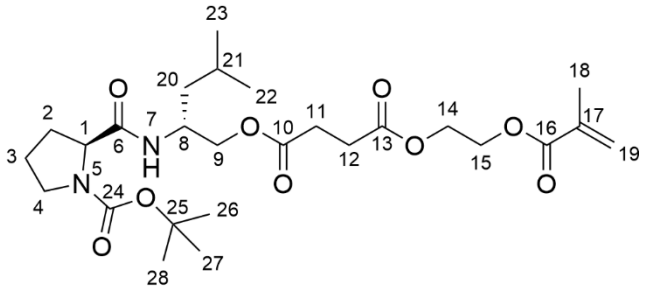

^{1}H-NMR (700 MHz, DMSO-d$_6$):

δ (ppm) = 0.71 – 0.93 (m; 6H; $^{22+23}CH_3$); 1.29 – 1.46 (m; 9H; $^{26-28}CH_3$); 1.51 – 1.63 (m; 3H; $^{3+20+21}CH_2$); 1.87 (s; 3H; $^{18}CH_3$); 2.05 – 2.15 (m; 3H; $^{2+3}CH_2$); 2.51 – 2.60 (m; 4H; $^{11+12}CH_2$); 3.22 – 3.28 (m; 1H; $^{4}CH_2$); 3.34 – 3.41 (m; 1H; $^{4}CH_2$); 3.78 – 3.98 (m; 2H; $^{9}CH_2$); 3.99 – 4.06 (m; 2H; ^{1+8}CH); 4.23 – 4.31 (m; 4H; $^{14+15}CH_2$); 5.69 (s; 1H; $^{19}CH_2$); 6.03 (s; 1H; $^{19}CH_2$); 7.65 (m; 1H; ^{7}NH)

^{13}C-NMR (176 MHz, DMSO-d$_6$):

δ (ppm) = 17.9 ($^{18}CH_3$); 21.4 ($^{22/23}CH_3$); 22.8 ($^{20}CH_2$); 23.2 ($^{22/23}CH_3$); 24.0 (^{21}CH); 28.0 ($^{26\,-\,28}CH_3$); 28.5 ($^{11/12}CH_2$); 28.6 ($^{11/12}CH_2$); 31.3 ($^{3}CH_2$); 34.5 ($^{2}CH_2$); 45.5 ($^{9}CH_2$); 46.4 ($^{4}CH_2$); 59.6 (^{8}CH); 62.0 ($^{14/15}CH_2$); 62.4 ($^{14/15}CH_2$); 66.2 (^{1}CH); 78.3 (^{25}C); 126.1 (^{17}C); 135.6 ($^{19}CH_2$); 153.4 (^{24}C); 166.4 (^{16}C); 168.3 (^{10}C); 171.7 (^{13}C); 172.1 (^{6}C)

ESI-MS; m/z:

Calculated for $[C_{26}H_{42}N_2O_9Na]^+$ 549.2890 found 549.2774

3.3.8 Deprotection of (*R*)-2-((*S*)-1-(*tert*-butoxycarbonyl)pyrrolidine-2-carboxamido)-4-methylpentyl(2-(methacryloyloxy)ethyl)succinate

The synthesis was done according to known literature protocols.[166] (*R*)-2-((*S*)-1-(*tert*-butoxycarbonyl)pyrrolidine-2-carboxamido)-4-methylpentyl(2-(methacryloyloxy)ethyl)-succinate (11.30 g, 21.5 mmol) were placed in a 500 ml round bottom flask and dissolved in 4 N HCl in 1,4-dioxane (100 ml) with vigorous stirring. The mixture was stirred at room temperature overnight. After removal of the solvent and subsequent drying in a fine vacuum, 9.60 g (20.9 mmol, 97 %) of a highly viscous yellowish oil were isolated.

Characterization:

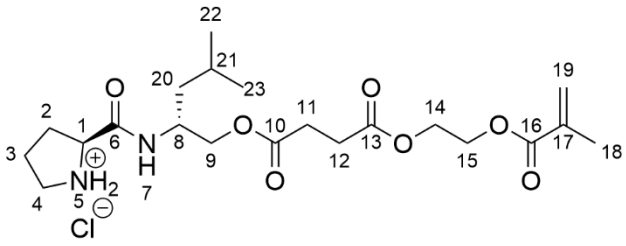

^{1}H-NMR (700 MHz, DMSO-d$_6$):

δ (ppm) = 0.81 – 0.92 (m; 6H; $^{22+23}CH_3$); 1.58 – 1.63 (m; 1H; ^{21}CH); 1.70 – 1.90 (m; 9H; $^{2+3+20}CH_2$; $^{18}CH_3$); 2.52 – 2.58 (m; 4H; $^{11+12}CH_2$); 3.13 – 3.27 (m; 2H; $^{4}CH_2$); 3.80 – 3.88 (m; 1H; $^{9}CH_2$); 4.0 – 4.17 (m; 1H; $^{9}CH_2$); 4.23 – 4.30 (m; 4H; $^{14+15}CH_2$); 5.69 (s; 1H; $^{19}CH_2$); 6.03 (s; 1H; $^{19}CH_2$); 8.44 – 8.61 (m; br.; 2H; NH); 9.89 – 10.11 (s; br.; 1H; NH)

^{13}C-NMR (176 MHz, DMSO-d$_6$):

δ (ppm) = 17.9 ($^{18}CH_3$); 21.6 ($^{22/23}CH_3$); 22.8 ($^{20}CH_2$); 23.0 ($^{22/23}CH_3$); 23.5 ($^{2}CH_2$); 24.0 (^{21}CH); 28.5 ($^{11/12}CH_2$); 28.6 ($^{11/12}CH_2$); 29.8 ($^{3}CH_2$); 45.5 ($^{4}CH_2$); 46.3 ($^{9}CH_2$); 58.7 (^{1}CH); 60.0 (^{8}CH); 62.0 ($^{14/15}CH_2$); 62.4 ($^{14/15}CH_2$); 126.1 ($^{19}CH_2$); 135.6 (^{17}C); 166.4 (^{16}C); 168.1 (^{6}C); 171.7 (^{10}C); 171.8 (^{13}C)

ESI-MS; m/z:

Calculated for $[C_{21}H_{35}N_2O_7]^+$ 427.5148 found 427.2479

3.3.9 Synthesis of Racemic Aldol Products

Different nitro benzaldehydes (4.0 mmol) and the respective ketones (20 mmol) were suspended in water (4 ml) and placed in a 50 ml round bottom flask. 25 % aqueous ammonia solution (0.5 ml) were added dropwise to this solution via a septum. The reaction mixture was then heated to 60 °C and stirred for 24 h. The mixture was then allowed to cool off and sat. NaCl solution (25 ml) were added. It was extracted with ethyl acetate (15 ml) three times and the organic phase was dried using a hydrophobic filter. The solvent was removed and the crude product was purified via column chromatography using silica as the stationary phase and different mixture of *n*-hexane : ethyl acetate as the mobile phase.

2-[-hydroxy(4-nitrophenyl)methyl]-cyclohexanone

Characterization:

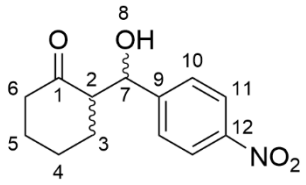

^{1}H-NMR (500 MHz, DMSO-d_6):

δ (ppm) = 1.12 – 1.24 (m; 1H; $^{4}CH_2$); 1.46 – 1.87 (m; 5H; $^{3\text{-}5}CH_2$); 2.20 – 2.39 (m; 2H; $^{6}CH_2$); 2.63 – 2.68 (m; 1H; ^{2}CH; syn); 2.69 – 2.74 (m; 1H; ^{2}CH; anti); 5.09 (dd; $^{3}J_{HH}$ = 7.20 Hz; $^{3}J_{HH}$ = 4.56 Hz; 1H; ^{7}CH; anti); 5.23 (t; $^{3}J_{HH}$ = 4.47 Hz; 1H; ^{7}CH; syn); 5.47 (d; $^{3}J_{HH}$ = 4.73 Hz; 1H; ^{8}OH; syn); 5.54 (d; $^{3}J_{HH}$ = 4.56 Hz; 1H; ^{8}OH; anti); 7.61 (d; $^{3}J_{HH}$ = 8,67 Hz; 2H; ^{10}CH); 8.17 (d; $^{3}J_{HH}$ = 8.5 Hz; 2H; ^{11}CH)

Chiral HPLC: Chiralpack IA, *n*-Heptan : 2-Propanol (85 : 15), 0.8 $\frac{ml}{min}$, T = 15 °C, λ = 254 nm, t_{R1} = 21.2 min, t_{R2} = 24.9 min, t_{R3} = 26.5 min, t_{R4} = 36.1 min

ESI-MS; m/z:

Calculated for $[C_{13}H_{15}NO_4Na]^+$ 272.0899 found 272.0883

2-[hydroxy(3-nitrophenyl)methyl]cyclohexan-1-one

Characterization:

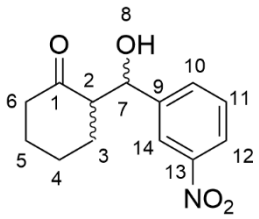

^{1}H-NMR (500 MHz, $CDCl_3$-d_1):

δ (ppm) = 1.45 – 1.88 (m; 6H; $^{3\text{-}5}CH_2$); 2.28 – 2.35 (m; 2H; $^{6}CH_2$); 2.52 – 2.67 (m; 2H; ^{2}CH; anti; syn); 4.45 – 5.01 (m; 2H; ^{7}CH; anti; syn); 7.47 – 7.56 (m; 1H; ^{11}CH); 7.63 – 7.71 (m; 1H; ^{10}CH); 8.07 – 8.26 (m; 2H; $^{12+14}$CH)

Chiral HPLC: Chiralpack IA, *n*-Heptan : 2-Propanol (95 : 5), 0.8 $\frac{ml}{min}$, T = 15 °C, λ = 254 nm, t_{R1} = 25.4 min, t_{R2} = 27.5 min, t_{R3} = 30.1 min, t_{R4} = 38.9 min

ESI-MS; m/z:

Calculated for $[C_{13}H_{15}NO_4Na]^+$ 272.0899 found 272.0893

2-[hydroxy(2-nitrophenyl)methyl]cyclohexan-1-one

Characterization:

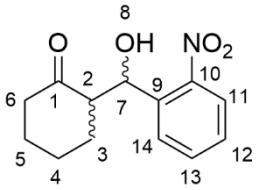

^{1}H-NMR (500 MHz, $CDCl_3$-d_1):

δ (ppm) = 1.49 – 1.89 (m; 6H; $^{3\text{-}5}CH_2$); 2.27 – 2.48 (m; 2H; $^{6}CH_2$); 2.70 – 2.93 (m; 2H; ^{2}CH; anti; syn); 5.07 (d; $^{3}J_{HH}$ = 9.1 Hz; 1H; ^{7}CH; anti); 5.38 – 5.46 (m; 1H; ^{7}CH; syn); 7.39 – 7.44 (m; 1H; ^{12}CH); 7.65 – 7.68 (m; 1H; ^{13}CH); 7.82 – 7.85 (m; 1H; ^{14}CH); 7.97 – 8.02 (m; 1H; ^{11}CH)

Chiral HPLC: Chiralpack IA, *n*-Heptan : 2-Propanol (95 : 5), 0.8 $\frac{ml}{min}$, T = 15 °C, λ = 254 nm, t_{R1} = 18.6 min, t_{R2} = 20.2 min, t_{R3} = 29.4 min, t_{R4} = 32.0 min

ESI-MS; m/z:

Calculated for $[C_{13}H_{15}NO_4Na]^+$ 272.0899 found 272.0869

2-[hydroxy(4-nitrophenyl)methyl]cyclopentan-1-one

Characterization:

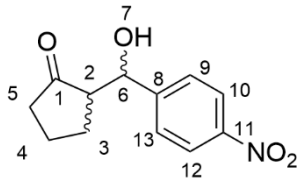

^{1}H-NMR (500 MHz, $CDCl_3$-d_1):

δ (ppm) = 1.58 – 1.81 (m; 3H; $^{3+4}CH_2$); 1.90 – 2.21 (m; 3H; $^{3\text{-}5}CH_2$); 2.33 – 2.53 (m; 2H; ^{2}CH; anti; syn); 4.84 (d; $^{3}J_{HH}$ = 9.2 Hz; 1H; ^{6}CH; anti); 5.43 (m; 1H; ^{6}CH; syn); 7.49 – 7.56 (m; 2H; $^{9+13}$CH); 8.19 – 8.24 (m; 2H; $^{10+12}$CH)

Chiral HPLC: Chiralpack IA, *n*-Heptan : 2-Propanol (95 : 5), 0.8 $\frac{ml}{min}$, T = 15 °C, λ = 254 nm, t_{R1} = 39.2 min, t_{R2} = 54.4 min, t_{R3} = 62.6 min, t_{R4} = 66.9 min

ESI-MS; m/z:

Calculated for $[C_{12}H_{13}NO_4Na]^+$ 258.0845 found 258.0735

2-[hydroxy(3-nitrophenyl)methyl]cyclopentan-1-one

Characterization:

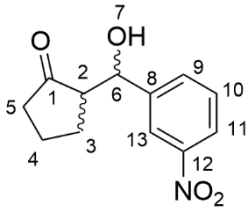

^{1}H-NMR (500 MHz, $CDCl_3$-d_1):

δ (ppm) = 1.65 – 1.80 (m; 2H; $^{3+4}CH_2$); 1.93 – 2.43 (m; 4H; $^{3-5}CH_2$); 2.47 – 2.54 (m; 2H; ^{2}CH; anti; syn); 4.83 (d; $^{3}J_{HH}$ = 9.1 Hz; 1H; ^{6}CH; anti); 5.38 – 5.46 (m; 1H; ^{6}CH; syn); 7.49 – 7.55 (m; 1H; ^{10}CH); 7.65 – 7.71 (m; 1H; ^{9}CH); 8.09 – 8.26 (m; 2H; $^{11+13}$CH)

Chiral HPLC: Chiralpack IA, *n*-Heptan : 2-Propanol (95 : 5), 0.5 $\frac{ml}{min}$, T = 15 °C, λ = 254 nm, t_{R1} = 27.4 min, t_{R2} = 39.6 min, t_{R3} = 42.7 min, t_{R4} = 48.8 min

ESI-MS; m/z:

Calculated for $[C_{12}H_{13}NO_4Na]^+$ 258.0845 found 258.0744

2-[hydroxy(2-nitrophenyl)methyl]cyclopentan-1-one

Characterization:

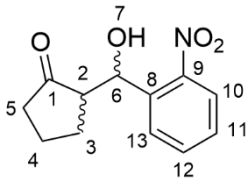

^{1}H-NMR (500 MHz, $CDCl_3$-d_1):

δ (ppm) = 1.65 – 1.78 (m; 2H; $^{3+4}CH_2$); 1.93 – 2.23 (m; 3H; $^{3-5}CH_2$); 2.35 – 2.42 (m; 1H; $^{5}CH_2$); 2.67 – 2.92 (m; 2H; ^{2}CH; anti; syn); 5.88 – 5.92 (m; 2H; ^{6}CH; anti; syn); 7.39 – 7.56 (m; 1H; ^{11}CH); 7.63 – 7.69 (m; 1H; ^{12}CH); 7.86 – 7.90 (m; 1H; ^{13}CH); 7.96 – 8.01 (m; 1H; ^{10}CH)

Chiral HPLC: Chiralpack IA, *n*-Heptan : 2-Propanol (95 : 5), 0.5 $\frac{ml}{min}$, T = 15 °C, λ = 254 nm, t_{R1} = 28.9 min, t_{R2} = 32.4 min, t_{R3} = 38.1min, t_{R4} = 39.9 min

ESI-MS; m/z :

Calculated for $[C_{12}H_{13}NO_4Na]^+$ 258.0845 found 258.0738

4-(4-nitrophenyl)-4-hydroxy-4-butan-2-one

Characterization:

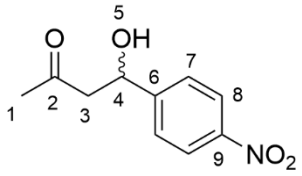

^{1}H-NMR (500 MHz, DMSO-d_6):

δ (ppm) = 2.13 (s; 3H; $^{1}CH_3$); 2.75 (d; $^{3}J_{HH}$ = 6.65 Hz; 2H; $^{3}CH_2$); 5.11 – 5.18 (m; 1H; ^{4}CH); 5.69 – 5.74 (m; 1H; ^{5}OH); 7.64 (d; $^{3}J_{HH}$ = 8.61 Hz; 2H; ^{7}CH); 8.19 (d; $^{3}J_{HH}$ = 8.74 Hz; 2H; ^{8}CH)

Chiral HPLC: Chiralpack IC, *n*-Heptan : 2-Propanol (90 : 10), 0.7 $\frac{ml}{min}$, T = 15 °C, λ = 254 nm, t_{R1} = 23.9 min, t_{R2} = 25.4 min

EI-MS; m/z:
Calculated for $[C_{10}H_{11}NO_4Na]^+$ 209.0688 found 272.0691

3.3.10 Synthesis of 4-nitrosobenzonitrile

The synthesis was based on known literature protocols.[167] 4-aminobenzonitrile (2.5 g, 21.15 mmol) was dissolved in DCM (125 ml). To this solution Oxone® (26 g, 42.3 mmol) dissolved in water (250 ml) was added. The solution was stirred under nitrogen at room temperature until TLC monitoring indicated complete consumption of the starting material (3 h). After separation of the layers, the aqueous layer was extracted with DCM twice. The combined organic layers were washed with 1N HCl, sat. sodium bicarbonate solution, water, brine and the two phases were separated using a hydrophobic filter. Removal of the solvent in vacuo yielded 2.74 g (20.7 mmol, 96 %) of the crude product as an amber solid with a purity of ≥ 95 % as determined by ^{1}H-NMR spectroscopy. Column chromatography on silica gel (pentane : ethyl acetate 100 : 1) resulted in partial decomposition. R_f = 0.77 (DCM).

Characterization:

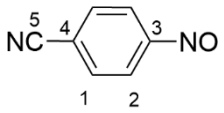

^{1}H-NMR (500 MHz, $CDCl_3$-d_1):

δ (ppm) = 7.95 – 8.01 (m; 4H; $^{1+2}CH_2$)

^{13}C-NMR (125 MHz, $CDCl_3$-d_1):

δ (ppm) = 117.63 (^{4}C); 118.59 (^{5}C); 120.98 (^{2}CH); 134.19 (^{1}CH); 162.34 (^{3}C)

EI-MS; m/z:

Calculated for [$C_7H_4N_2O$] 132.0318 found 132.0374

3.3.11 Synthesis of 1-nitro-3-nitrosobenzene

The synthesis was based on known literature protocols.[167] 3-Nitroaniline (2.5 g, 18.1 mmol) was dissolved in DCM (50 ml). To this solution Oxone® (22.25 g, 36.4 mmol) dissolved in water (200 ml) was added. The solution was stirred under nitrogen at room temperature until TLC monitoring indicated complete consumption of the starting material (2 h). After separation of the layers, the aqueous layer was extracted with DCM twice. The combined organic layers were washed with 1N HCl, sat. sodium bicarbonate solution, water, brine and the two phases were separated using a hydrophobic filter. Removal of the solvent in vacuo yielded 2.70 g (17.7 mmol, 98 %) of the desired product as a yellowish solid.

Characterization:

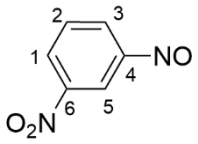

^{1}H-NMR (700 MHz, $CDCl_3$-d_1):

δ (ppm) = 7.89 (t; $^3J_{HH}$ = 7.9 Hz; 1H; ^{2}CH); 8.32 – 8.36 (m; 1H; ^{3}CH); 8.57 – 8.62 (m; 2H; $^{1+5}$CH)

^{13}C-NMR (125 MHz, $CDCl_3$-d_1):

δ (ppm) = 114.73 (^{5}CH); 126.69 (^{3}CH); 128.91 (^{1}CH); 131.03 (^{2}CH); 149.29 (^{6}C); 163.49 (^{4}C)

EI-MS; m/z:

Calculated for [$C_6H_4N_2O_3$] 152.0222 found 152.0374

3.3.12 Synthesis of methyl 3-nitrosobenzoate

The synthesis was based on known literature protocols.[167] Methyl 3-aminobenzoate (2.0 g, 13.2 mmol) was dissolved in DCM (40 ml). To this solution Oxone® (16.2 g, 26.5 mmol) dissolved in water (160 ml) was added. The solution was stirred under nitrogen at room temperature until TLC monitoring indicated complete consumption of the starting material (3 h). After separation of the layers, the aqueous layer was extracted with DCM twice. The combined organic layers were washed with 1N HCl, sat. sodium bicarbonate solution, water, brine and the two phases were separated using a hydrophobic filter. Removal of the solvent in vacuo yielded 2.20 g (13.2 mmol, quant.) of the crude product as an amber solid.

Characterization:

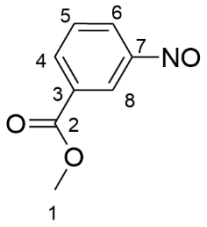

^{1}H-NMR (700 MHz, $CDCl_3$-d_1):

δ (ppm) = 3.99 (s; 3H; $^{1}CH_3$); 7.70 (t; $^{3}J_{HH}$ = 7.7 Hz; 1H; ^{5}CH); 7.99 – 8.01 (m; 1H; ^{6}CH); 8.37 – 8.40 (m; 1H; ^{4}CH); 8.60 (s; 1H; ^{8}CH)

^{13}C-NMR (125 MHz, $CDCl_3$-d_1):

δ (ppm) = 52.70 ($^{1}CH_3$); 122.49 (^{8}CH); 123.77 (^{6}CH); 129.54 (^{5}CH); 131.77 (^{3}C); 135.72 (^{4}C); 164.83 (^{7}C); 165.74 (^{2}C)

EI-MS; m/z:

Calculated for [$C_8H_7NO_3$] 165.0426 found 165.0283

3.3.13 Synthesis of 3-nitrosobenzonitrile

The synthesis was based on known literature protocols.[167] 3-Aminobenzonitrile (2.5 g, 21.15 mmol) was dissolved in DCM (250 ml). To this solution Oxone® (26.0 g, 42.3 mmol) dissolved in water (500 ml) was added. The solution was stirred under nitrogen at room temperature until TLC monitoring indicated complete consumption of the starting material (3 h). After separation of the layers, the aqueous layer was extracted with DCM twice. The combined organic layers were washed with 1N HCl, sat. sodium bicarbonate solution, water, brine and the two phases were separated using a hydrophobic filter. Removal of the solvent in vacuo yielded 2.74 g (20.7 mmol, 96 %) of the crude product as an amber solid with a purity of ≥ 90% as determined by ^{1}H-NMR spectroscopy. Column chromatography on silica gel (pentane : ethyl acetate 100 : 1) resulted in partial decomposition. R_f = 0.77 (DCM).

Characterization:

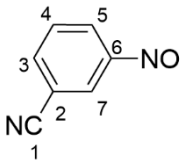

^{1}H-NMR (700 MHz, $CDCl_3$-d_1):

δ (ppm) = 7.81 (t; $^{3}J_{HH}$ = 7.8 Hz; 1H; ^{4}CH); 7.98 (d; $^{3}J_{HH}$ = 7.7 Hz; 1H; ^{3}CH); 8.12 (d; $^{3}J_{HH}$ = 8.1 Hz; 1H; ^{5}CH); 8.17 (s; 1H; ^{7}CH)

^{13}C-NMR (125 MHz, $CDCl_3$-d_1):

δ (ppm) = 114.43 (^{2}CH); 117.55 (^{1}C); 124.58 (^{5}CH); 124.77 (^{7}CH); 131.07 (^{4}C); 138.16 (^{3}C); 163.28 (^{6}C)

EI-MS; m/z:

Calculated for [$C_7H_4N_2O$] 132.0318 found 132.0274

3.3.14 Synthesis of 1-chloro-4-nitrosobenzene

The synthesis was based on known literature protocols.[167] 4-chloroaniline (2.5 g, 19.60 mmol) was dissolved in DCM (45 ml). To this solution Oxone® (23.4 g, 38.3 mmol) dissolved in water (200 ml) was added. The solution was stirred under nitrogen at room temperature until TLC monitoring indicated complete consumption of the starting material (4 h). After separation of the layers, the aqueous layer was extracted with DCM twice. The combined organic layers were washed with 1N HCl, sat. sodium bicarbonate solution, water, brine and the two phases were separated using a hydrophobic filter. Removal of the solvent in vacuo yielded 2.66 g (18.8 mmol, 96 %) of the desired product as a yellowish solid.

Characterization:

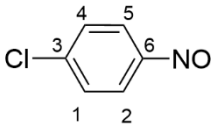

^{1}H-NMR (700 MHz, $CDCl_3$):

δ (ppm) = 7.59 (d; $^{3}J_{HH}$ = 8.8 Hz; 2H; $^{1+4}$CH); 8.85 (d; $^{3}J_{HH}$ = 8.5 Hz; 2H; $^{2+5}$CH)

^{13}C-NMR (125 MHz, $CDCl_3$-d_1):

δ (ppm) = 122.20 ($^{2/5}$CH); 129.71 ($^{1/4}$CH); 142.52 (^{3}C); 163.76 (^{6}C)

EI-MS; m/z:

Calculated for [C_6H_4ClNO] 140.9981 found 140.9965

3.3.15 Synthesis of 1-bromo-4-nitrosobenzene

The synthesis was based on known literature protocols.[167] 4-Bromoaniline (2.5 g, 14.90 mmol) was dissolved in DCM (45 ml). To this solution Oxone® (17.9 g, 29.8 mmol) dissolved in water (180 ml) was added. The solution was stirred under nitrogen at room temperature until TLC monitoring indicated complete consumption of the starting material (4 h). After separation of the layers, the aqueous layer was extracted with DCM twice. The combined organic layers were washed with 1N HCl, sat. sodium bicarbonate solution, water, brine and the two phases were separated using a hydrophobic filter. Removal of the solvent in vacuo yielded 2.68 g (14.5 mmol, 97 %) of the desired product as a light green to almost colorless solid.

Characterization:

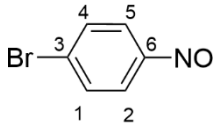

^{1}H-NMR (700 MHz, $CDCl_3$-d_1):

δ (ppm) = 7.88 (d; $^{3}J_{HH}$ = 7.9 Hz; 2H; $^{2+5}$CH); 8.99 (d; $^{3}J_{HH}$ = 8.6 Hz; 2H; $^{1+4}$CH)

^{13}C-NMR (125 MHz, $CDCl_3$-d_1):

δ (ppm) = 122.36 ($^{2/5}$CH); 131.65 (^{3}C); 133.01 ($^{1/4}$CH); 164.16 (^{6}C)

EI-MS; m/z:

Calculated for [C_6H_4BrNO] 184.9476 found 184.9405

3.3.16 Synthesis of methyl 4-nitrosobenzoate

The synthesis was based on known literature protocols.[167] Methyl 4-aminobenzoate (5.0 g, 33.1 mmol) was dissolved in DCM (100 ml). To this solution Oxone® (40.7 g, 66.2 mmol) dissolved in water (400 ml) was added. The solution was stirred under nitrogen at room temperature until TLC monitoring indicated complete consumption of the starting material (40 min). After separation of the layers, the aqueous layer was extracted with DCM twice. The combined organic layers were washed with 1N HCl, sat. sodium bicarbonate solution, water, brine and the two phases were separated using a hydrophobic filter. Removal of the solvent in vacuo yielded the crude product. The crude solid residue was recrystallized from DCM to yield 4.91 g (29.9 mmol, 90 %) of the desired product as a yellowish solid.

Characterization:

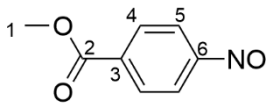

^{1}H-NMR (700 MHz, $CDCl_3$-d_1):

δ (ppm) = 3.97 (s; 3H; $^{1}CH_3$); 7.92 (d; $^{3}J_{HH}$ = 8.4 Hz; 2H; ^{5}CH); 8.29 (d; $^{3}J_{HH}$ = 7.2 Hz; 2H; ^{4}CH)

^{13}C-NMR (125 MHz, $CDCl_3$-d_1):

δ (ppm) = 53.14 ($^{1}CH_3$); 120.76 (^{5}CH); 131.43 (^{4}CH); 135.57 (^{3}C); 164.76 (^{6}C); 166.11 (^{2}C)

EI-MS; m/z:

Calculated for [$C_8H_7NO_3$] 165.0426 found 164.9018

3.3.17 Synthesis of 3-bromo-1-nitrosobenzene

The synthesis was based on known literature protocols.[167] 3-Bromoaniline (2.5 g, 14.90 mmol) was dissolved in DCM (45 ml). To this solution Oxone® (17.9 g, 29.8 mmol) dissolved in water (180 ml) was added. The solution was stirred under nitrogen at room temperature until TLC monitoring indicated complete consumption of the starting material (3.5 h). After separation of the layers, the aqueous layer was extracted with DCM twice. The combined organic layers were washed with 1N HCl, sat. sodium bicarbonate solution, water, brine and the two phases were separated using a hydrophobic filter. Removal of the solvent in vacuo yielded 2.62 g (14.1 mmol, 95 %) of the desired product as greenish solid.

Characterization:

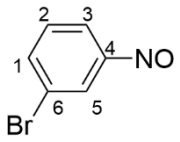

^{1}H-NMR (700 MHz, $CDCl_3$-d_1):

δ (ppm) = 7.55 (t; $^{3}J_{HH}$ = 7.8 Hz; 1H; ^{2}CH); 7.74 (s; 1H; ^{5}CH); 7.81 (d; $^{3}J_{HH}$ = 7.9 Hz; 1H; ^{1}CH); 8.09 (d; $^{3}J_{HH}$ = 7.7 Hz; 1H; ^{3}CH)

^{13}C-NMR (125 MHz, $CDCl_3$-d_1):

δ (ppm) = 121.77 (^{5}CH); 122.12 (^{3}CH); 124.01 (^{6}C); 131.22 (^{2}C); 138.04 (^{1}C); 165.21 (^{4}C)

EI-MS; m/z:

Calculated for [C_6H_4BrNO] 184.9476 found 184.9425

3.3.18 Synthesis of 2-nitrosobenzonitrile

The synthesis was based on known literature protocols.[167] 2-Aminobenzonitrile (2.5 g, 21.15 mmol) was dissolved in DCM (125 ml). To this solution Oxone® (26 g, 42.3 mmol) dissolved in water (200 ml) was added. The solution was stirred under nitrogen at room temperature until TLC monitoring indicated complete consumption of the starting material (3 h). After separation of the layers, the aqueous layer was extracted with DCM twice. The combined organic layers were washed with 1N HCl, sat. sodium bicarbonate solution, water, brine and the two phases were separated using a hydrophobic filter. Removal of the solvent in vacuo yielded 2.67 g (20.2 mmol, 95 %) of the crude product as an brownish solid with a purity of ≥ 90% as determined by ^{1}H-NMR spectroscopy. Column chromatography on silica gel (pentane : ethyl acetate 100 : 1) resulted in partial decomposition.

Characterization:

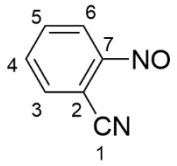

^{1}H-NMR (700 MHz, $CDCl_3$-d_1):

δ (ppm) = 6.99 (d; $^{3}J_{HH}$ = 8.1 Hz; 1H; ^{3}CH); 7.76 (t; $^{3}J_{HH}$ = 7.6 Hz; 1H; ^{5}CH); 7.85 (t; $^{3}J_{HH}$ = 7.6 Hz; 1H; ^{4}CH); 8.06 (d; $^{3}J_{HH}$ = 7.4 Hz; 1H; ^{6}CH)

^{13}C-NMR (125 MHz, $CDCl_3$-d_1):

δ (ppm) = 112.34 (^{6}CH); 114.17 (^{2}C); 116.76 (^{1}C); 133.63 (^{5}CH); 134.61 (^{3}CH); 135.53 (^{4}CH); 161.95 (^{7}C)

EI-MS; m/z:

Calculated for [$C_7H_4N_2O$] 132.0318 found 132.0294

3.3.19 Synthesis of 2-bromo-1-nitrosobenzene

The synthesis was based on known literature protocols.[167] 2-Bromoaniline (2.5 g, 14.90 mmol) was dissolved in DCM (45 ml). To this solution Oxone® (17.9 g, 29.8 mmol) dissolved in water (180 ml) was added. The solution was stirred under nitrogen at room temperature until TLC monitoring indicated complete consumption of the starting material (3.5 h). After separation of the layers, the aqueous layer was extracted with DCM twice. The combined organic layers were washed with 1N HCl, sat. sodium bicarbonate solution, water, brine and the two phases were separated using a hydrophobic filter. Removal of the solvent in vacuo yielded 2.75 g (14.8 mmol, 99 %) of the crude product as a greenish to grey solid.

Characterization:

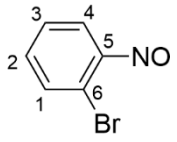

^{1}H-NMR (700 MHz, $CDCl_3$-d_1):

δ (ppm) = 6.21 (d; $^{3}J_{HH}$ = 8.1 Hz; 1H; ^{4}CH); 7.28 (t; $^{3}J_{HH}$ = 7.6 Hz; 1H; ^{3}CH); 7.53 (t; $^{3}J_{HH}$ = 7.6 Hz; 1H; ^{2}CH); 7.99 (d; $^{3}J_{HH}$ = 7.9 Hz; 1H; ^{1}CH)

^{13}C-NMR (125 MHz, $CDCl_3$-d_1):

δ (ppm) = 109.18 (^{4}CH); 127.52 (^{3}C); 133.42 (^{6}C); 135.41 (^{1}CH); 136.85 (^{2}CH); 161.38 (^{5}C)

EI-MS; m/z:

Calculated for [C_6H_4BrNO] 184.9476 found 184.9409

3.3.20 Synthesis of 1-ethyl-4-nitrosobenzene

The synthesis was based on known literature protocols.[167] 4-Ethylaniline (2.42 g, 19.99 mmol) was dissolved in DCM (65 ml). To this solution Oxone® (25 g, 40.9 mmol) dissolved in water (250 ml) was added. The solution was stirred under nitrogen at room temperature until TLC monitoring indicated complete consumption of the starting material (12 h). After separation of the layers, the aqueous layer was extracted with DCM twice. The combined organic layers were washed with 1N HCl, sat. sodium bicarbonate solution, water, brine and the two phases were separated using a hydrophobic filter. After removal of the solvent the residue was distilled at ambient temperature in vacuo ($p = 7 \cdot 10^{-3}$ mbar) to give 1.06 g (7.84 mmol, 40 %) of the product as a green liquid.

Characterization:

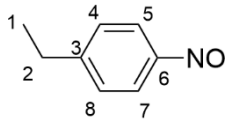

^{1}H-NMR (700 MHz, $CDCl_3$-d_1):

δ (ppm) = 1.29 (t; $^3J_{HH}$ = 7.6 Hz; 3H; $^1CH_3$); 2.73 (q; $^3J_{HH}$ = 7.9 Hz; 2H; $^2CH_2$); 7.40 (d; $^3J_{HH}$ = 8.4 Hz; 2H; $^{4+8}$CH); 7.82 (d; $^3J_{HH}$ = 7.9 Hz; 2H; $^{5+7}$CH)

^{13}C-NMR (125 MHz, $CDCl_3$-d_1):

δ (ppm) = 15.05 ($^1CH_3$); 29.36 ($^2CH_2$); 121.55 ($^{5/7}$CH); 128.74 ($^{4/8}$CH); 153.38 (^{3}C); 165.86 (^{6}C)

EI-MS; m/z:

Calculated for [C_8H_9NO] 135.0684 found 135.0716

3.4 Setup of the Continuous Microfluidic Reactor

In the following, all necessary steps are described in order to set up a microfluidic system. This is based on the technical developments of the "Leibniz Institute for Polymer Research Dresden" (IPF). The reactor is a PTFE layer milled with the desired shape. The processed reactor shape on the forming layer is shown in Figure 25.

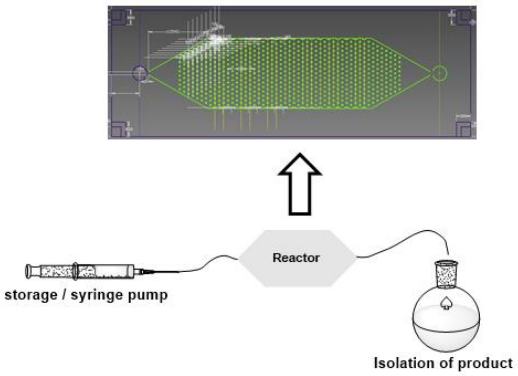

Figure 25: Schematic representation of the reactor setup (bottom). Enlargement of the reactor chamber and the dimensions produced (top).

The polymers attached to glass substrates were covered with the respective mold and clamped in an aluminum holder (Figure 26). The reactor can be connected to capillary tubing using the aluminum holder. Starting from a "Legato 200" type syringe pump obtained from "KD-Scientific", two separately available reactant solutions can be conveyed and initially brought together in a T-junction. In the present work, only one syringe with the desired educt solution was used. The mixture was introduced into the reactor via capillary tubes and detected at its outlet with the aid of NMR as a discontinuous analysis method.

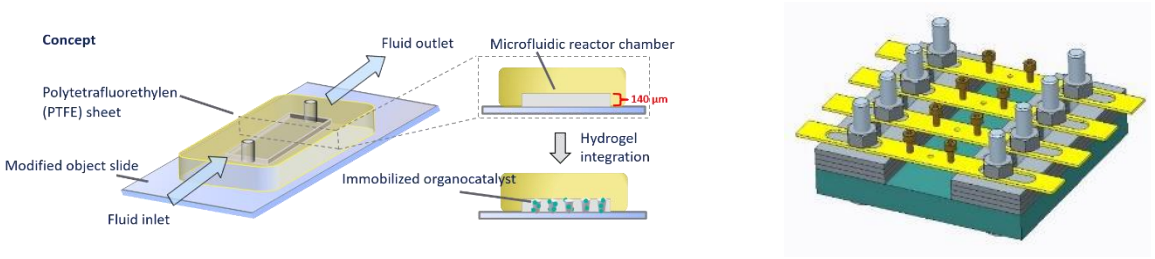

Figure 26: Schematic illustration of the various components of the microfluidic system.

To determine the residence time of the reactants in the system, the volumes of the installed components are decisive. The volumes are listed below in Table 5. With the help of the volume of the built-in components, a dwell time of 42 min can be calculated for an applied flow of $2\ \frac{\mu l}{min}$, from the fluid inlet to the detection (fluid outlet). The volume of the reactor chamber results from its base area and the height produced (140 µm).

Table 5: Specifications for calculating the volumes of the components installed in the reactor to determine the residence time.

Component	Longitude [mm]	iD [mm]	Volume [µl]
Connection between syringe and reactor inlet	300	0.25	14.7
Reactor chamber	Height = 140 µm		100
Connection between reactor outlet and detection/work up	175	0.25	8.6

3.5 Surface Modification

The gels were bound to glass object slides (7.6 cm x 2.6 cm). The microscope slides were washed with *iso*-propanol under supersonic treatment at 70 °C for 10 min. Afterwards, also under supersonic treatment at 70 °C, the microscopy slides were cleaned using water followed by ethanol. As a final cleaning and activation step the object slides were treated with a solution of 100 ml deionized water, 20 ml ammonia solution (25 %) and 20 ml H_2O_2 (35 %) at 70 °C for 10 min in an supersonic bath. After drying in nitrogen flow, these substrates were modified by gas deposition. 20 of the dried slides were placed in a desiccator with 300 µl of 3-(trichlorosilyl)-propylmethacrylate (3TCSPMA) at a pressure of 50 mbar for at least 2 h. The desiccator was ventilated with argon for removal and subsequent storage.

3.6 Contact Angle Measurement

To track the surface modification of the object slides, contact angle measurements of unmodified slides (top row) and modified slides (bottom row) were performed with water and diiodomethane (Figure 27).

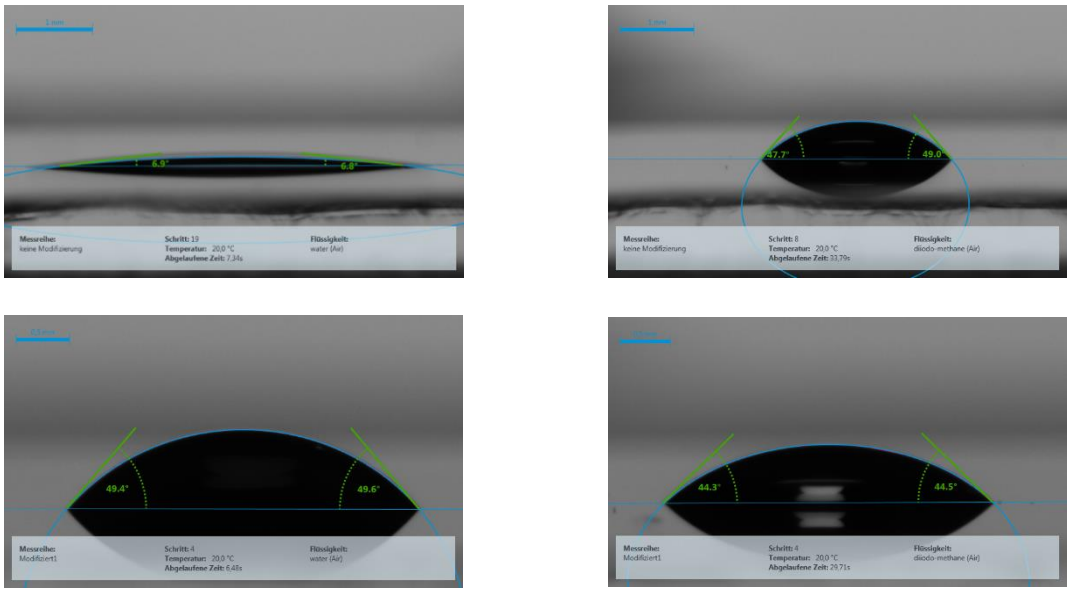

Figure 27: Surface modification of the slides, contact angle measurements of unmodified slides (top row) and modified slides (bottom row).

3.7 Photopolymerization

The photopolymerization was carried out via an "Omnicure® S1500" UV-Lamp combined with an UV-Filter (320 – 480 nm) from "Lumen Dynamics". UV irradiation for photopolymerization was performed with an intensity of 428 mW (intensity = 20 %) at the end of the lighting cable, with 8 cm distance of light source to substrate. 15 mmol of monomers were mixed in the desired ratios and were dissolved in 1.7 ml deionized water in case of catalyst structure A (cf. 3.3.3) or ethanol for catalyst structure B (cf. 3.3.8) with an initiator concentration of 26.25 $\frac{mg}{ml}$. 800 µl of the resulting monomer solution were transferred into a mold, made from dark grey polyoxymethylene to minimize scattered radiation. The incubation chamber gasket was covered by a modified microscopy slide and the photopolymerization mask (diamond shaped position of 662 dots) on the back side (Figure 28). This stack was half covered with an opaque cover and the uncovered side was centered below UV light for 12.4 s, followed by the other half. Afterwards, the incubation chamber was removed and the polymer structures were washed with water, followed by CH_2Cl_2 for 1 h. To remove the HCl-salt, washing with a mixture of methanol and triethylamine (9:1) as well as with tetrahydrofuran and triethylamine (9:1) followed by pure tetrahydrofuran and pure methanol as the last purification step was applied (1 h for each step). The substrates were dried in air and stored at room temperature till usage. The general structure of the polymer and reactor structure is shown in Figure 28 (a). A typical example of the polymer structure after workup together with the mask Figure 28 (b) used for polymerization is shown in Figure 28 (c) as well.

a)

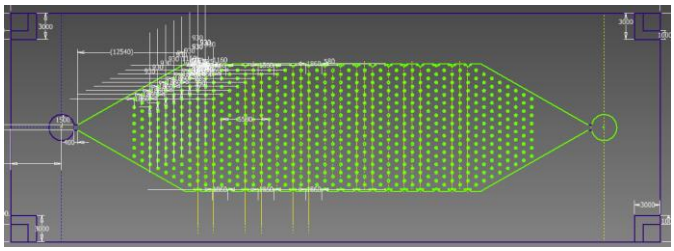

b)

c)

Figure 28: Schematic illustration of the general structure of the diamond shaped reactor with 662 polymerdots (a). Together with the mask used for polymerization (b) and a typical example of the polymer structure after workup (c).

3.8 Determination of Conversion of MFR experiments

The conversion was determined by NMR spectroscopy. NMR spectroscopy enables an offline determination of conversion and a fast screening of different reactions. For NMR spectroscopy, the outlet flow was collected into a vial with 400 µl DMSO-d_6 and was frozen immediately after the desired time of sample collection with liquid nitrogen. The sample was warmed up just before the tube was inserted into the NMR spectrometer.

3.9 Synthesis in Continuous Flow

In this chapter, all syntheses of the low molecular weight compounds as well as the characterization of the products obtained from continuous flow reactions are described.

Initially to flow reactions, the polymer dots were pre-swollen with pure solvent for at least 2 h. Therefore, the "Legato 200" syringe pump was loaded with one syringe (Braun 20 ml syringe with iD = 20.1 mm), filled up with pure solvent and the flow rate was set to 2.0 $\frac{\mu l}{min}$.

3.9.1 Synthesis of (2*S*,10*R*)-2-[hydroxy(4-nitrophenyl)methyl]cyclohexan-1-one

A solution of cyclohexanone (0.167 M) and *p*-nitrobenzaldehyde (0.033 M) in a mixture of DMSO and water (9 : 1) was injected via a "Hamilton™" 1000 Series "Gastight™" Syringe. The flow rate was adjusted to 0.5 $\frac{\mu l}{min}$, resulting in a residence time of 200 min. After 48 h of running reaction and dilution of the crude product solution using sat. NaCl-solution, the reaction mixture was extracted using EtOAc three times. After phase separation, the solvent was evaporated. Purification of the crude product via column chromatography on silica using a mixture of *n*-hexane : EtOAc (1 : 1) (R_f = 0.4) yielded 9.2 mg (0.037 mmol, 78 %) of the corresponding pure product.

Characterization:

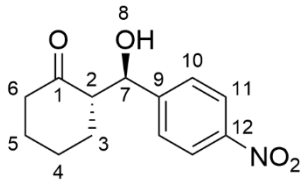

^{1}H-NMR (700 MHz, DMSO-d_6):

δ (ppm) = 1.12 – 1.24 (m; 1H; $^4CH_2$); 1.46 – 1.87 (m; 5H; $^{3\text{-}5}CH_2$); 2.22 – 2.39 (m; 2H; $^6CH_2$); 2.62 – 2.76 (m; 1H; ^2CH); 5.08 (t; $^3J_{HH}$ = 4.54 Hz, 1H; ^7CH); 5.50 (d; $^3J_{HH}$ = 4.8 Hz; 1H; ^8OH); 7.61 (d; $^3J_{HH}$ = 9.7 Hz; 2H; ^{11}CH); 8.18 (d; $^3J_{HH}$ = 8.8 Hz; 2H; ^{10}CH)

^{13}C-NMR (176 MHz, DMSO-d_6):

δ (ppm) = 23.2 ($^{4}CH_2$); 27.3 ($^{3}CH_2$); 29.5 ($^{5}CH_2$); 41.2 ($^{6}CH_2$); 57.3 (^{2}CH); 70.4 (^{7}CH); 123.0 (^{11}CH); 128.1 (^{10}CH); 146.5 (^{9}C); 151.6 (^{12}C); 210.7 (^{1}C)

Chiral HPLC: Chiralpack IA, *n*-Heptan : 2-Propanol (85 : 15), 0.8 $\frac{ml}{min}$, T = 15 °C, λ = 254 nm, t_{R1} = 26.5 min, t_{R2} = 36.1 min

ESI-MS; m/z:

Calculated for $[C_{13}H_{15}NO_4Na]^+$ 272.0899 found 272.0883

3.9.2 Synthesis of (*2S,10R*)-2-[hydroxy(3-nitrophenyl)methyl]cyclohexan-1-one

A solution of cyclohexanone (0.167 M) and 3-nitrobenzaldehyde (0.033 M) in a mixture of DMSO and water (9 : 1) was injected via a "Hamilton™" 1000 Series "Gastight™" Syringe. The flow rate was adjusted to 0.5 $\frac{\mu l}{min}$, resulting in a residence time of 200 min. After 48 h of running reaction and dilution of the crude product solution using sat. NaCl-solution, the reaction mixture was extracted using EtOAc three times. After phase separation, the solvent was evaporated. Purification of the crude product via column chromatography on silica using a mixture of *n*-hexane : EtOAc (1 : 1) (R_f = 0.44) yielded 11 mg (0.044 mmol, 93 %) of the corresponding pure product.

Characterization:

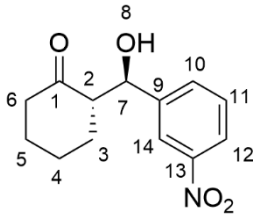

^{1}H-NMR (700 MHz, $CDCl_3$-d_1):

δ (ppm) = 1.33 – 1.45 (m; 1H; $^{3}CH_2$); 1.51 – 1.62 (m; 3H; $^{3\text{-}5}CH_2$); 1.79 – 1.86 (m; 1H; $^{3\text{-}5}CH_2$); 2.06 – 2.17 (m; 1H; $^{3\text{-}5}CH_2$); 2.32 – 2.42 (m; 1H; $^{6}CH_2$); 2.47 – 2.53 (m; 1H; $^{6}CH_2$); 2.59 – 2.66 (m; 1H; ^{2}CH); 3.98 – 4.25 (s; 1H; ^{8}OH); 4.89 (d; $^{3}J_{HH}$ = 8.48 Hz; 1H; ^{7}CH); 7.53 (t; $^{3}J_{HH}$ = 7.52 Hz; 1H; ^{11}CH); 7.65 – 7.69 (m; 1H; ^{10}CH); 8.15 – 8.18 (m; 1H; ^{12}CH); 8.19 – 8.23 (m; 1H; ^{14}CH)

^{13}C-NMR (176 MHz, $CDCl_3$-d_1):

δ (ppm) = 24.8 ($^{4}CH_2$); 27.8 ($^{5}CH_2$); 30.9 ($^{3}CH_2$); 42.8 ($^{6}CH_2$); 57.3 (^{2}CH); 74.2 (^{7}CH); 122.2 (^{14}CH); 123.1 (^{12}CH); 129.5 (^{11}C); 133.3 (^{10}C); 143.4 (^{9}C); 148.4 (^{13}C); 215.0 (^{1}C)

Chiral HPLC: Chiralpack IA, *n*-Heptan : 2-Propanol (95 : 5), 0.8 $\frac{ml}{min}$, T = 15 °C, λ = 254 nm, t_{R1} = 29.9 min, t_{R2} = 38.8 min

ESI-MS; m/z:

Calculated for $[C_{13}H_{15}NO_4Na]^+$ 272.0899 found 272.0893

3.9.3 Synthesis of (*2S,10R*)-2-[hydroxy(2-nitrophenyl)methyl]cyclohexan-1-one

A solution of cyclohexanone (0.167 M) and 2-nitrobenzaldehyde (0.033 M) in a mixture of DMSO and water (9 : 1) was injected via a "Hamilton™" 1000 Series "Gastight™" Syringe. The flow rate was adjusted to 0.5 $\frac{\mu l}{min}$, resulting in a residence time of 200 min. After 48 h of running reaction and dilution of the crude product solution using sat. NaCl-solution, the reaction mixture was extracted using EtOAc three times. After phase separation, the solvent was evaporated. Purification of the crude product via column chromatography on silica using a mixture of *n*-hexane : EtOAc (2 : 1) (R_f = 0.51) yielded 8.8 mg (0.035 mmol, 75 %) of the corresponding pure product.

Characterization:

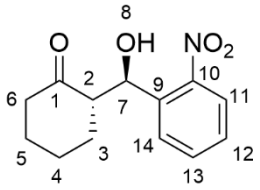

^{1}H-NMR (700 MHz, $CDCl_3$-d_1):

δ (ppm) = 1.52 – 1.90 (m; 5H; $^{3\text{-}5}CH_2$); 2.05 – 2.15 (m; 1H; $^{4+5}CH_2$); 2.29 – 2.50 (m; 2H; $^6CH_2$); 2.71 – 2.82 (m; 1H; $^2CH_2$); 3.98 – 4.42 (s; 1 H; ^8OH); 5.45 (d; $^3J_{HH}$ = 6.94 Hz; 1H; ^7CH); 7.39 – 7.45 (m; 1H; ^{12}CH); 7.60 – 7.65 (m; 1H; ^{13}CH); 7.75 – 7.79 (m; 1H; ^{14}CH); 7.82 – 7.87 (m; 1H; ^{11}CH)

^{13}C-NMR (176 MHz, $CDCl_3$-d_1):

δ (ppm) = 25.1 ($^4CH_2$); 27.9 ($^5CH_2$); 31.2 ($^3CH_2$); 42.9 ($^6CH_2$); 57.4 (^2CH); 69.9 (^7CH); 124.2 (^{11}CH); 128.5 (^{12}CH); 129.1 (^{14}C); 133.4 (^{13}C); 136.7 (^9C); 148.8 (^{10}C); 215.1 (^1C)

Chiral HPLC: Chiralpack IA, *n*-Heptan : 2-Propanol (95 : 5), 0.8 $\frac{ml}{min}$, T = 15 °C, λ = 254 nm, t_{R1} = 28.9 min, t_{R2} = 31.4 min

ESI-MS; m/z:

Calculated for $[C_{13}H_{15}NO_4Na]^+$ 272.0899 found 272.0869

3.9.4 Synthesis of (*2S,10S*)-2-[hydroxy(4-nitrophenyl)methyl]cyclopentan-1-one

A solution of cyclopentanone (0.167 M) and *p*-nitrobenzaldehyde (0.033 M) in a mixture of DMSO and water (9 : 1) was injected via a "Hamilton™" 1000 Series "Gastight™" Syringe. The flow rate was adjusted to 0.5 $\frac{\mu l}{min}$, resulting in a residence time of 200 min. After 48 h of running reaction and dilution of the crude product solution using sat. NaCl-solution, the reaction mixture was extracted using EtOAc three times. After phase separation, the solvent was evaporated. Purification of the crude product via column chromatography on silica using a mixture of *n*-hexane : EtOAc (1 : 1) (R_f = 0.45) yielded 9.3 mg (0.041 mmol, 86 %) of the corresponding pure product.

Characterization:

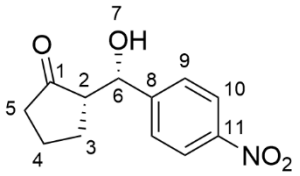

^{1}H-NMR (700 MHz, $CDCl_3$-d_1):

δ (ppm) = 1.48 – 1.64 (m; 1H; $^{3}CH_2$); 1.69 – 1.75 (m; 1H; $^{4}CH_2$); 1.90 – 2.19 (m; 3H; $^{3\text{-}5}CH_2$); 2.33 – 2.51 (m; 2H; $^{5}CH_2$, ^{2}CH); 4.73 (s; br.; 1H; ^{7}OH); 5.40 – 5.45 (m; 1H; ^{6}CH); 7.51 (d; $^{3}J_{HH}$ = 8.6 Hz; 2H; ^{9}CH); 8.21 (d; $^{3}J_{HH}$ = 8.8 Hz; 2H; ^{10}CH)

^{13}C-NMR (176 MHz, $CDCl_3$):

δ (ppm) = 20.5 ($^{4}CH_2$); 22.6 ($^{3}CH_2$); 39.1 ($^{5}CH_2$); 56.2 (^{2}CH); 70.8 (^{6}CH); 123.8 (^{10}CH); 126.5 (^{9}CH); 147.4 (^{11}C); 150.2 (^{8}C); 219.5 (^{1}C)

Chiral HPLC: Chiralpack IA, *n*-Heptan : 2-Propanol (95 : 5), 0.8 $\frac{ml}{min}$, T = 15 °C, λ = 254 nm, t_{R1} = 61.9 min, t_{R2} = 66.2 min

ESI-MS; m/z:
Calculated for $[C_{12}H_{13}NO_4Na]^+$ 258.0845 found 258.0735

3.9.5 Synthesis of (*2S,10R*)-2-[hydroxy(3-nitrophenyl)methyl]cyclopentan-1-one

A solution of cyclopentanone (0.167 M) and 3-nitrobenzaldehyde (0.033 M) in a mixture of DMSO and water (9 : 1) was injected via a "Hamilton™" 1000 Series "Gastight™" Syringe. The flow rate was adjusted to 0.5 $\frac{\mu l}{min}$, resulting in a residence time of 200 min. After 48 h of running reaction and dilution of the crude product solution using sat. NaCl-solution, the reaction mixture was extracted using EtOAc three times. After phase separation, the solvent was evaporated. Purification of the crude product via column

chromatography on silica using a mixture of *n*-hexane : EtOAc (1 : 1) (R_f = 0.49) yielded 7.0 mg (0.029 mmol, 63 %) of the corresponding pure product.

Characterization:

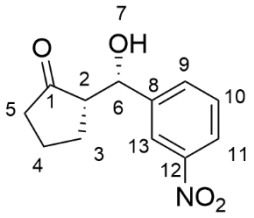

^{1}H-NMR (700 MHz, $CDCl_3$-d_1):

δ (ppm) = 1.49 – 1.60 (m; 1H; $^{3}CH_2$); 1.67 – 1.79 (m; 1 H; $^{4}CH_2$); 1.93 – 2.07 (m; 1H; $^{4}CH_2$); 2.09 – 2.43 (m; 3H; $^{3+5}CH_2$); 2.47 – 2.53 (m; 1H; ^{2}CH); 4.78 (s; br.; 1H; ^{7}OH); 5.39 – 5.45 (m; 1H; ^{6}CH); 7.49 – 7.55 (m; 1H; ^{10}CH); 7.65 – 7.72 (m; 1H; ^{9}CH); 8.02 – 8.18 (m; 1H; ^{11}CH); 8.23 (s; 1H; ^{13}CH)

^{13}C-NMR (176 MHz, $CDCl_3$):

δ (ppm) = 20.5 ($^{4}CH_2$); 22.7 ($^{3}CH_2$); 39.2 ($^{5}CH_2$); 56.3 (^{2}CH); 70.5 (^{6}CH); 120.8 (^{13}CH); 122.5 (^{11}CH); 129.6 (^{10}CH); 131.8 (^{9}CH); 145.2 (^{8}C); 148.6 (^{12}C); 219.7 (^{1}C)

Chiral HPLC: Chiralpack IA, *n*-Heptan : 2-Propanol (95 : 5), 0.5 $\frac{\text{ml}}{\text{min}}$, T = 15 °C, λ = 254 nm, t_{R1} = 42.7 min, t_{R2} = 48.8 min

ESI-MS; m/z:
Calculated for $[C_{12}H_{13}NO_4Na]^+$ 258.0845 found 258.0744

3.9.6 Synthesis of (*2S,10S*)-2-[hydroxy(2-nitrophenyl)methyl]cyclopentan-1-one

A solution of cyclopentanone (0.167 M) and 2-nitrobenzaldehyde (0.033 M) in a mixture of DMSO and water (9 : 1) was injected via a "Hamilton™" 1000 Series "Gastight™" Syringe. The flow rate was adjusted to 0.5 $\frac{\mu\text{l}}{\text{min}}$, resulting in a residence time of 200 min. After 48 h of running reaction and dilution of the crude product solution using sat. NaCl-solution, the reaction mixture was extracted using EtOAc three times. After phase separation, the solvent was evaporated. Purification of the crude product via column chromatography on silica using a mixture of *n*-hexane : EtOAc (1 : 1) (R_f = 0.58) yielded 9.2 mg (0.039 mmol, 82 %) of the corresponding pure product.

Characterization:

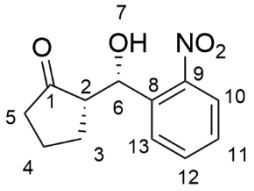

^{1}H-NMR (700 MHz, $CDCl_3$-d_1):

δ (ppm) = 1.60 – 1.82 (m; 3H; $^{3+4}CH_2$); 1.97 – 2.09 (m; 1H; $^{4}CH_2$); 2.10 – 2.47 (m; 2H; $^{3+5}CH_2$); 2.68 – 2.79 (m; 1H; ^{2}CH); 5.88 – 5.94 (m; 1H; ^{6}CH); 7.41 – 7.46 (m; 1H; ^{11}CH); 7.62 – 7.69 (m; 1H; ^{12}CH); 7.88 (m; 1H; ^{13}CH); 7.96 – 8.01 (m; 1H; ^{10}CH)

^{13}C-NMR (176 MHz, $CDCl_3$):

δ (ppm) = 20.4 ($^{4}CH_2$); 23.2 ($^{3}CH_2$); 38.8 ($^{5}CH_2$); 55.0 (^{2}CH); 66.9 (^{6}CH); 124.8 (^{10}CH); 128.3 (^{13}CH); 128.8 (^{11}CH); 133.6 (^{12}CH); 138.6 (^{8}C); 147.3 (^{9}C); 218.9 (^{1}C)

Chiral HPLC: Chiralpack IA, *n*-Heptan : 2-Propanol (95 : 5), 0.5 $\frac{ml}{min}$, T = 15 °C, λ = 254 nm, t_{R1} = 38.1 min, t_{R2} = 39.9 min

ESI-MS; m/z:
Calculated for $[C_{12}H_{13}NO_4Na]^+$ 258.0845 found 258.0738

3.9.7 Synthesis of (*4R*)-4-(4-nitroophenyl)-4-hydroxy-4-butan-2-one

A solution of acetone (0.167 M) and *p*-nitrobenzaldehyde (0.033 M) in a mixture of DMSO and water (9 : 1) was injected via a "Hamilton™" 1000 Series "Gastight™" Syringe. The flow rate was adjusted to 0.5 $\frac{\mu l}{min}$, resulting in a residence time of 200 min. After 48 h of running reaction and dilution of the crude product solution using sat. NaCl-solution, the reaction mixture was extracted using EtOAc three times. After phase separation, the solvent was evaporated. Purification of the crude product via column chromatography on silica using a mixture of *n*-hexane : EtOAc (1 : 4) (R_f = 0.68) yielded 8.1 mg (0.038 mmol, 80 %) of the corresponding pure product.

Characterization:

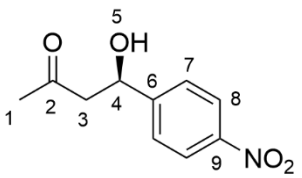

^{1}H-NMR (700 MHz, $CDCl_3$-d_1):

δ (ppm) = 2.22 (s; 3H; $^{1}CH_3$); 2.79 – 2.91 (m; 2H; $^{3}CH_2$); 3.40 – 3.52 (m; 1H; ^{5}OH); 5.23 – 5.29 (m; 1H; ^{4}CH); 7.54 (d; $^{3}J_{HH}$ = 8.5 Hz; 2H; ^{7}CH); 8.21 (d; $^{3}J_{HH}$ = 8.7 Hz; 2H; ^{8}CH)

^{13}C-NMR (176 MHz, DMSO-d_6):

δ (ppm) = 31.0 ($^{1}CH_3$); 52.9 ($^{3}CH_2$); 68.7 (^{4}CH); 123.9 (^{8}CH); 127.6 (^{7}CH); 147.1 (^{9}C); 153.8 (^{6}C); 206.9 (^{2}C)

Chiral HPLC: Chiralpack IC, *n*-Heptan : 2-Propanol (90 : 10), 0.7 $\frac{ml}{min}$, T = 15 °C, λ = 254 nm, t_{R1} = 23.9 min, t_{R2} = 25.4 min

ESI-MS; m/z:
Calculated for $[C_{10}H_{11}NO_4]^+$ 209.0688 found 209.0691

3.9.8 Synthesis of 1,2-*bis*(4-cyanophenyl)diazene oxide

A solution of 4-nitrosobenzonitrile (0.05 M) and cyclohexanone (0.025 M) in DMSO was injected via a "Hamilton™" 1000 Series "Gastight™" syringe. The flow rate was adjusted to 2.0 $\frac{\mu l}{min}$, resulting in a residence time of 50 min. After 23 h of running reaction and dilution of the crude product with sat. NH_4Cl-solution, the reaction mixture was extracted using EtOAc. After phase separation the solvent was evaporated. Purification of the crude product via column chromatography on silica using a mixture of *n*-hexane : EtOAc (8 : 1) (R_f = 0.13) yielded 15 mg (0.060 mmol, 98 %) of the corresponding pure product.

Characterization:

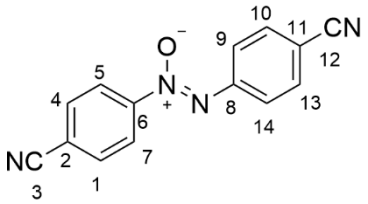

^{1}H-NMR (700 MHz, $CDCl_3$-d_1):

δ (ppm) = 7.79 (d; $^{3}J_{HH}$ = 8.5 Hz; 2H; $^{10+13}CH$); 7.87 (d; $^{3}J_{HH}$ = 8.9 Hz; 2H; ^{1+4}CH); 8.23 (d; $^{3}J_{HH}$ = 8.5 Hz; 2H; ^{9+14}CH); 8.46 (d; $^{3}J_{HH}$ = 8.5 Hz; 2H; ^{5+7}CH)

^{13}C-NMR (176 MHz, $CDCl_3$-d_1):

δ (ppm) = 113.5 (^{11}C); 116.5 (^{2}C); 117.7 (^{3}C); 118.6 (^{12}C); 123.7 ($^{5/7}CH$); 126.4 ($^{9/14}CH$); 133.2 ($^{10/13}CH$); 133.5 ($^{1/4}CH$); 146.7 (^{8}C); 150.6 (^{6}C)

LRMS (EI-TOF):
Calculated for $C_{14}H_8N_4O$ $[M]^+$ 248.0698 found 248.0425
mp = 195.7−198.1 °C

3.9.9 Synthesis of 1,2-*bis*(3-nitrophenyl)diazene oxide

A solution of 1-nitro-3-nitrosobenzene (0.05 M) and cyclohexanone (0.025 M) in DMSO was injected via a "Hamilton™" 1000 Series "Gastight™" syringe. The flow rate was adjusted to 2.0 $\frac{\mu l}{min}$, resulting in a residence time of 50 min. After 18 h of running reaction and dilution of the crude product with sat. NH_4Cl-solution, the reaction mixture was extracted using EtOAc. After phase separation the solvent was evaporated. Purification of the crude product via column chromatography on silica using a mixture of *n*-hexane : EtOAc (6 : 1) (R_f = 0.15) yielded 13 mg (0.045 mmol, 93 %) of the corresponding pure product.

Characterization:

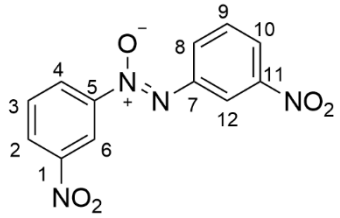

^{1}H-NMR (700 MHz, $CDCl_3$-d_1):

δ (ppm) = 7.71 (t; $^3J_{HH}$ = 8.2 Hz; 1H; ^{9}CH); 7.79 (t; $^3J_{HH}$ = 8.3 Hz; 1H; ^{3}CH); 8.31 (ddd; J_{HH} = 8.2, 2.1, 0.9 Hz; 1H; ^{8}CH); 8.49 (m; 2H; $^{2+10}$CH); 8.71 (ddd; J_{HH} = 8.2, 2.1, 0.9 Hz; 1H; ^{4}CH); 9.13 (t; $^3J_{NH}$ = 2.0 Hz; 1H; ^{12}CH); 9.22 (t; $^3J_{HH}$ = 2.0 Hz; 1H; ^{6}CH)

^{13}C-NMR (176 MHz, $CDCl_3$-d_1):

δ (ppm) = 118.1 (^{6}CH); 120.5 (^{12}CH); 124.6 (^{8}CH); 126.8 (^{2}CH); 128.0 (^{4}CH); 129.8 (^{9}CH); 130.3 (^{3}CH); 131.6 (^{10}CH); 143.9 (^{7}C); 148.4 ($^{1/11}$C); 148.5 (^{5}C)

LRMS (EI-TOF):

m/z calculated for $C_{12}H_8N_4O_5$ $[M]^+$ 288.0495 found 288.0316

mp = 145.3 − 146.4 °C

3.9.10 Synthesis of dimethyl 3,3´-diazene oxide 1,2-diyldibenzoate

A solution of 3-nitrosobenzoate (0.05 M) and cyclohexanone (0.025 M) in DMSO was injected via a "Hamilton™" 1000 Series "Gastight™" syringe. The flow rate was adjusted to 2.0 $\frac{\mu l}{min}$, resulting in a residence time of 50 min. After 17.7 h of running reaction and dilution of the crude product with sat. NH_4Cl-solution, the reaction mixture was extracted using EtOAc. After phase separation, the solvent was evaporated. Purification of the crude product via column chromatography on silica using a mixture of *n*- pentane : CH_2Cl_2 (3 : 1) (R_f = 0.46) yielded 13 mg (0.041 mmol, 86 %) of the corresponding pure product.

Characterization:

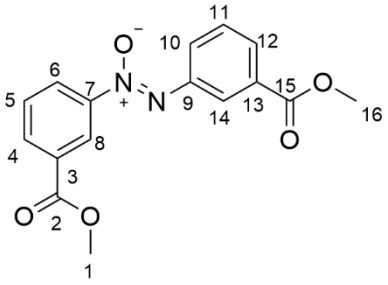

^{1}H-NMR (700 MHz, $CDCl_3$-d_1):

δ (ppm) = 3.96 (s; 3H; $^{16}CH_3$); 3.99 (s; 3H; $^{1}CH_3$); 7.58 (t; $^{3}J_{HH}$ = 8.9 Hz; 1H; ^{11}CH); 7.63 (t; $^{3}J_{HH}$ = 7.9 Hz; 1H; ^{5}CH); 8.09 (ddd; $^{3}J_{HH}$ = 7.8, 1.4, 1.4 Hz; 1H; ^{12}CH); 8.26 (ddd; $^{3}J_{HH}$ = 7.8, 1.3, 1.3 Hz; 1H; ^{4}CH); 8.43 (ddd; $^{3}J_{HH}$ = 8.1, 2.0, 1.2 Hz; 1H; ^{10}CH); 8.53 (ddd; $^{3}J_{HH}$ = 8.2, 2.3, 1.1 Hz; 1H; ^{6}CH); 8.78 (t; ^{3}JHH = 1.7 Hz; 1H; ^{14}CH); 8.97 (t; $^{3}J_{HH}$ = 1.8 Hz; 1H; ^{8}CH)

^{13}C-NMR (176 MHz, $CDCl_3$-d_1):

δ (ppm) = 52.4 ($^{16}CH_3$); 52.6 ($^{1}CH_3$); 123.6 (^{8}CH); 126.5 (^{6}CH); 127.1 (^{14}CH); 128.9 (^{11}CH); 129.1 (^{5}CH); 129.4 (^{10}CH); 130.7 (^{12}C); 130.9 (^{13}C); 131.4 (^{3}C); 132.8 (^{4}CH); 143.8 (^{9}C); 148.3 (^{7}CH); 165.7 (^{2}C); 166.5 (^{15}C)

LRMS (EI-TOF):

m/z calculated for $C_{16}H_{14}N_2O_5$ $[M]^+$ 314.0903 found 314.0493

mp = 134.2 − 136.6 °C

3.9.11 Synthesis of 1,2-*bis*(3-cyanophenyl)diazene oxide

A solution of 3-nitrosobenzonitrile (0.05 M) and cyclohexanone (0.025 M) in DMSO was injected via a "Hamilton™" 1000 Series "Gastight™" syringe. The flow rate was adjusted to 2.0 $\frac{\mu l}{min}$, resulting in a residence time of 50 min. After 21.5 h of running reaction and dilution of the crude product with sat. NH_4Cl-solution, the reaction mixture was extracted using EtOAc. After phase separation, the solvent was evaporated. Purification of the crude product via column chromatography on silica using a mixture of *n*-hexane : EtOAc (8 : 1) (R_f = 0.08) yielded 11 mg (0.044 mmol, 82 %) of the corresponding pure product.

Characterization:

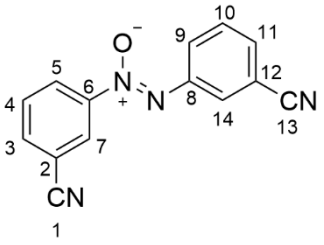

^{1}H-NMR (700 MHz, $CDCl_3$-d_1):

δ (ppm) = 7.61−7.65 (m; 1H; ^{10}CH); 7.69−7.73 (m; 2H; $^{4+11}$CH); 7.89−7.91 (dt; $^{3}J_{HH}$ = 1.5, 1.5 Hz; 1H; ^{3}CH); 8.32 (ddd; $^{3}J_{HH}$ = 8.2, 1.7, 1.3 Hz; 1H; ^{9}CH); 8.57−8.60 (m; 2H; $^{5+14}$CH); 8.65 (t; $^{3}J_{HH}$ = 1.8 Hz; 1H; ^{7}CH)

^{13}C-NMR (176 MHz, $CDCl_3$-d_1):

δ (ppm) = 113.5 (^{12}C); 113.8 (^{2}C); 117.4 (^{1}C); 118.2 (^{13}C); 126.5 (^{7}CH); 126.8 (^{5}CH); 129.1 (^{14}CH); 130.1 (^{10}CH); 130.41 (^{4}CH); 130.42 (^{9}CH); 133.4 (^{11}CH); 135.6 (^{3}CH); 143.9 (^{8}C); 148.3 (^{6}C)

LRMS (EI-TOF):

m/z calculated for $C_{14}H_8N_4O$ $[M]^+$ 248.0698 found 248.0501

mp = 133.1−134.3 °C

3.9.12 Synthesis of 1,2-*bis*(4-chlorophenyl)diazene oxide

A solution of 1-chloro-4-nitrosobenzene (0.05 M) and cyclohexanone (0.025 M) in DMSO was injected via a "Hamilton™" 1000 Series "Gastight™" syringe. The flow rate was adjusted to 2.0 $\frac{\mu l}{min}$, resulting in a residence time of 50 min. After 17 h of running reaction and dilution of the crude product with sat. NH_4Cl-solution, the reaction mixture was extracted using EtOAc. After phase separation, the solvent was evaporated. Purification of the crude product via column chromatography on silica using a mixture of *n*-hexane : EtOAc (50 : 1) (R_f = 0.25) yielded 12 mg (0.045 mmol, 66 %) of the corresponding pure product.

Characterization:

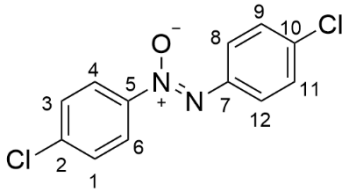

^{1}H-NMR (700 MHz, $CDCl_3$-d_1):

δ (ppm) = 7.45 (d; $^{3}J_{HH}$ = 9.0 Hz; 2H; $^{9+11}$CH); 7.49 (d; $^{3}J_{HH}$ = 9.1 Hz; 2H; $^{1+3}$CH); 8.16 (d; $^{3}J_{HH}$ = 9.0 Hz; 2H; $^{8+12}$CH); 8.25 (d; $^{3}J_{HH}$ = 9.1 Hz; 2H; $^{4+6}$CH)

^{13}C-NMR (176 MHz, $CDCl_3$-d_1):

δ (ppm) = 123.7 ($^{4/6}$CH); 127.1 ($^{8/12}$CH); 129.01 ($^{9/11}$CH); 129.08 ($^{1/3}$CH); 135.3 (^{10}C); 138.1 (^{2}C); 142.3 (^{7}C); 146.6 (^{5}C)

LRMS (EI-TOF):

m/z calculated for $C_{12}H_8Cl_2N_2O$ $[M]^+$ 266.0014 found 265.9744

mp = 152.0−154.1 °C

3.9.13 Synthesis of 1,2-*bis*(4-bromophenyl)diazene oxide

A solution of 1-bromo-4-nitrosobenzene (0.05 M) and cyclohexanone (0.025 M) in DMSO was injected via a "Hamilton™" 1000 Series "Gastight™" syringe. The flow rate was adjusted to 2.0 $\frac{\mu l}{min}$, resulting in a residence time of 50 min. After 24 h of running reaction and dilution of the crude product with sat. NH_4Cl-solution, the reaction mixture was extracted using EtOAc. After phase separation, the solvent was evaporated. Purification of the crude product via column chromatography on silica using a mixture of *n*-hexane : EtOAc (8 : 1) (R_f = 0.25) yielded 18 mg (0.05 mmol, 67 %) of the corresponding pure product.

Characterization:

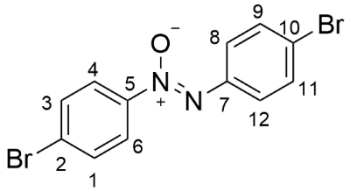

^{1}H-NMR (700 MHz, $CDCl_3$-d_1):

δ (ppm) = 7.61 (d; $^3J_{HH}$ = 8.8 Hz; 2H; $^{9+11}$CH); 7.65 (d; $^3J_{HH}$ = 8.9 Hz; 2H; $^{1+3}$CH); 8.08 (d; $^3J_{HH}$ = 8.8 Hz; 2H; $^{8+12}$CH); 8.18 (d; $^3J_{HH}$ = 8.9 Hz; 2H; $^{4+6}$CH)

^{13}C-NMR (125 MHz, $CDCl_3$-d_1):

δ (ppm) = 123.6 (^{10}C); 123.9 ($^{4/6}$CH); 126.5 (^{2}C); 127.3 ($^{8/12}$CH); 132.0 ($^{9/11}$CH); 132.1 ($^{1/3}$CH); 142.6 (^{7}C); 147.1 (^{5}C)

LRMS (EI-TOF):

m/z calculated for $C_{12}H_8Br_2N_2O$ $[M]^+$ 355.8983 found 355.8945

mp = 166.5−168.4 °C

3.9.14 Synthesis of dimethyl 4,4´-diazene oxide 1,2-diyldibenzoate

A solution of 4-nitrosobenzoate (0.05 M) and cyclohexanone (0.025 M) in DMSO was injected via a "Hamilton™" 1000 Series "Gastight™" syringe. The flow rate was adjusted to 2.0 $\frac{\mu l}{min}$, resulting in a residence time of 50 min. After 16 h of running reaction and dilution of the crude product with sat. NH_4Cl-solution, the reaction mixture was extracted using EtOAc. After phase separation, the solvent was evaporated. Purification of the crude product via column chromatography on silica using a mixture of *n*-hexane : EtOAc (3 : 1) (R_f = 0.39) yielded 9 mg (0.029 mmol, 68 %) of the corresponding pure product.

Characterization:

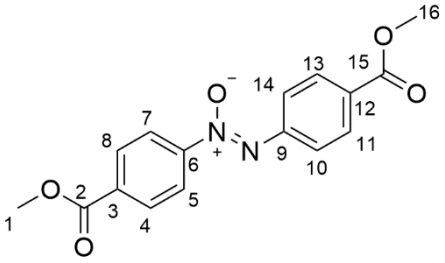

^{1}H-NMR (700 MHz, $CDCl_3$-d_1):

δ (ppm) = 3.95 (s; 3H; $^{16}CH_3$); 3.97 (s; 3H; $^{1}CH_3$); 8.15−8.22 (m; 6H; $^{4+8+10+11+13+14}CH$); 8.39 (d; $^{3}J_{HH}$ = 8.6 Hz; 2H; ^{5+7}CH)

^{13}C-NMR (176 MHz, $CDCl_3$-d_1):

δ (ppm) = 52.3 ($^{16}CH_3$); 52.6 ($^{1}CH_3$); 122.6 ($^{5/7}CH$); 125.4 ($^{10/14}CH$); 130.2 ($^{11/13}CH$); 130.4 ($^{4/8}CH$); 130.7 (^{12}C); 133.3 (^{3}C); 147.0 (^{9}C); 150.9 (^{6}C); 165.8 (^{2}C); 166.2 (^{15}C)

LRMS (EI-TOF):

m/z calculated for $C_{16}H_{14}N_2O_5$ $[M]^+$ 314.0903 found 314.0557

mp = 199.1−201.4 °C

3.9.15 Synthesis of 1,2-*bis*(3-bromophenyl)diazene oxide

A solution of 3-bromo-1-nitrosobenzene (0.05 M) and cyclohexanone (0.025 M) in DMSO was injected via a "Hamilton™" 1000 Series "Gastight™" syringe. The flow rate was adjusted to 2.0 $\frac{\mu l}{min}$, resulting in a residence time of 50 min. After 22 h of running reaction and dilution of the crude product with sat. NH_4Cl-solution, the reaction mixture was extracted using EtOAc. After phase separation, the solvent was evaporated. Purification of the crude product via column chromatography on silica using a mixture of *n*-hexane : EtOAc (7 : 1) (R_f = 0.5) yielded 15 mg (0.042 mmol, 74 %) of the corresponding pure product.

Characterization:

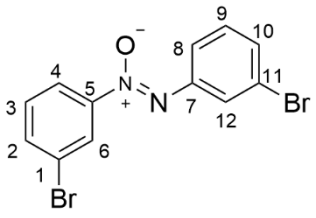

^{1}H-NMR (700 MHz, $CDCl_3$-d_1):

δ (ppm) = 7.37 (t; $^{3}J_{HH}$ = 8.1 Hz; 1H; ^{9}CH); 7.40 (t; $^{3}J_{HH}$ = 8.2 Hz; 1H; ^{3}CH); 7.53−7.56 (m; 1H; ^{10}CH); 7.69−7.73 (m; 1H; ^{2}CH); 8.04−8.07 (m; 1H; ^{8}CH); 8.23−8.26 (m; 1H; ^{4}CH); 8.41 (t; $^{3}J_{HH}$ = 1.9 Hz; 1H; ^{12}CH); 8.47 (t; $^{3}J_{HH}$ = 1.9 Hz; 1H; ^{6}CH)

^{13}C-NMR (176 MHz, $CDCl_3$-d_1):

δ (ppm) = 121.5 (^{4}CH); 122.7 (^{11}C); 122.9 (^{1}C); 124.9 (^{8}CH); 126.1 (^{6}CH); 128.7 (^{12}CH); 130.4 (^{9}CH); 130.6 (^{3}CH); 133.2 (^{10}CH); 135.3 (^{2}CH); 145.1 (^{7}C); 149.2 (^{5}C)

LRMS (EI-TOF):

m/z calculated for $C_{12}H_8Br_2N_2O$ $[M]^+$ 355.8983 found 355.8794

mp = 107.5−109.8 °C

3.9.16 Synthesis of 1,2-*bis*(2-cyanophenyl)diazene oxide

A solution of 2-nitrosobentonitrile (0.05 M) and cyclohexanone (0.025 M) in DMSO was injected via a "Hamilton™" 1000 Series "Gastight™" syringe. The flow rate was adjusted to 2.0 $\frac{\mu l}{min}$, resulting in a residence time of 50 min. After 17 h of running reaction and dilution of the crude product with sat. NH_4Cl-solution, the reaction mixture was extracted using EtOAc. After phase separation, the solvent was evaporated. Purification of the crude product via column chromatography on silica using a mixture of *n*-hexane : EtOAc (5 : 1) (R_f = 0.16) yielded 15 mg (0.047 mmol, 72 %) of the corresponding pure product.

Characterization:

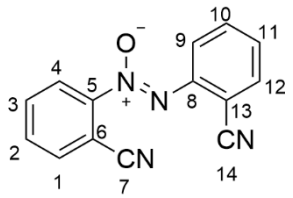

^{1}H-NMR (700 MHz, $CDCl_3$-d_1):

δ (ppm) = 7.53 (t; $^{3}J_{HH}$ = 7.6 Hz; 1H; ^{3}CH); 7.70−7.76 (m; 2H; $^{2+11}$CH); 7.77−7.85 (m; 2H; $^{1+10}$CH); 7.91 (dd; $^{3}J_{HH}$ = 7.5, 1.4 Hz; 1H; ^{12}CH); 8.47 (d; $^{3}J_{HH}$ = 8.3 Hz; 1H; ^{9}CH); 8.87 (d; $^{3}J_{HH}$ = 8.1 Hz; 1H; ^{4}CH)

^{13}C-NMR (176 MHz, $CDCl_3$-d_1):

δ (ppm) = 108.1 (^{13}C); 111.9 (^{6}C); 116.1 (^{14}C); 116.8 (^{7}C); 123.7 (^{4}CH); 125.3 (^{9}CH); 130.6 (^{3}CH); 132.5 (^{11}CH); 133.7 (^{2}CH); 133.9 (^{10}CH); 134.1 (^{1}CH); 135.6 (^{12}CH); 144.9 (^{5}C); 149.4 (^{8}C)

LRMS (EI-TOF):

m/z calculated for $C_{14}H_8N_4O$ $[M]^+$ 248.0698 found 248.0627

mp = 192.4−193.5 °C

3.9.17 Synthesis of 1,2-*bis*(2-bromophenyl)diazene oxide

A solution of 2-bromo-1-nitrosobenzene (0.05 M) and cyclohexanone (0.025 M) in DMSO was injected via a "Hamilton™" 1000 Series "Gastight™" syringe. The flow rate was adjusted to 2.0 $\frac{\mu l}{min}$, resulting in a residence time of 50 min. After 22 h of running reaction and dilution of the crude product with sat. NH_4Cl-solution, the reaction mixture was extracted using EtOAc. After phase separation, the solvent was evaporated. Purification of the crude product via column chromatography on silica using a mixture of *n*-hexane: EtOAc (5:1) (R_f = 0.16) yielded 13 mg (0.037 mmol, 61 %) of the corresponding pure product.

Characterization:

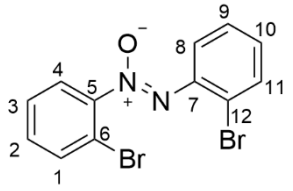

^{1}H-NMR (700 MHz, $CDCl_3$-d_1):

δ (ppm) = 7.20−7.23 (m; 1H; ^{2}CH); 7.35−7.51 (m; 3H; $^{3+9+10}$CH); 7.70−7.77 (m; 3H; $^{1+8+11}$CH); 7.97 (dd; $^{3}J_{HH}$ = 8.0, 1.5 Hz; 1H; ^{4}CH)

^{13}C-NMR (176 MHz, $CDCl_3$-d_1):

δ (ppm) = 115.2 (^{12}C); 119.5 (^{6}C); 123.6 (^{4}CH); 125.4 (^{8}CH); 127.9 (^{3}CH); 128.4 (^{9}CH); 129.9 (^{2}CH); 131.5 (^{10}CH); 133.6 (^{1}CH); 134.3 (^{11}CH); 142.4 (^{5}C); 149.2 (^{7}C)

LRMS (EI-TOF):

m/z calculated for $C_{12}H_8Br_2N_2O$ $[M]^+$ 355.8983 found 355.8829

mp = 108.2−112.5 °C

3.9.18 Synthesis of 1,2-diphenyldiazene oxide

A solution of nitrosobenzene (0.05 M) and cyclohexanone (0.025 M) in DMSO was injected via a "Hamilton™" 1000 Series "Gastight™" syringe. The flow rate was adjusted to 1.0 $\frac{\mu l}{min}$, resulting in a residence time of 100 min. After 20 h of running reaction and dilution of the crude product with sat. NH_4Cl-solution, the reaction mixture was extracted using CH_2Cl_2. After phase separation, the solvent was evaporated. Purification of the crude product via column chromatography on silica using a mixture of *n*-hexane : EtOAc (50 : 1) (R_f = 0.38) yielded 5 mg (0.025 mmol, 61 %) of the corresponding pure product.

Characterization:

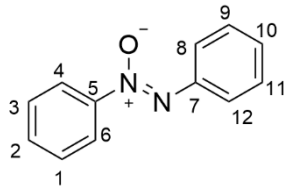

^{1}H-NMR (700 MHz, DMSO-d_6):

δ (ppm) = 7.45−7.49 (m; 1H; ^{10}CH); 7.54−7.58 (m; 2H; $^{9+11}$CH); 7.62−7.66 (m; 2H; $^{1+3}$CH); 7.72−7.80 (m; 1H; ^{2}CH); 8.06−8.09 (m; 2H; $^{8+12}$CH); 8.25−8.27 (m; 2H; $^{4+6}$CH)

^{13}C-NMR (176 MHz, $CDCl_3$-d_1):

δ (ppm) = 122.1 ($^{4/6}$CH); 125.1 ($^{8/12}$CH); 128.9 ($^{9/11}$CH); 129.3 ($^{1/3}$CH); 129.8 (^{10}CH); 132.1 (^{2}CH); 143.7 (^{7}C); 147.7 (^{5}C)

LRMS (EI-TOF):

m/z calculated for $C_{12}H_{10}N_2O$ $[M]^+$ 198.0793 found 198.0907

mp = < 35 °C

3.9.19 Synthesis of 1,2-di-*o*-tolyldiazene oxide

A solution of 2-nitrosotoluene (0.05 M) and cyclohexanone (0.025 M) in DMSO was injected via a "Hamilton™" 1000 Series "Gastight™" syringe. The flow rate was adjusted to 0.5 $\frac{\mu l}{min}$, resulting in a residence time of 200 min. After 21 h of running reaction and dilution of the crude product with sat. NH_4Cl-solution, the reaction mixture was extracted using CH_2Cl_2. After phase separation, the solvent was evaporated. Purification of the crude product via column chromatography on silica using a mixture of *n*-hexane : EtOAc (30 : 1) (R_f = 0.25) yielded 6 mg (0.027 mmol, 52 %) of the corresponding pure product.

Characterization:

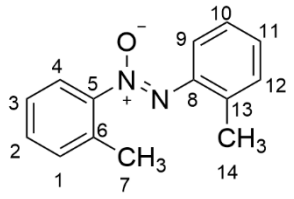

^{1}H-NMR (700 MHz, $CDCl_3$-d_1):

δ (ppm) = 2.37 (s; 3H; $^{7}CH_3$); 2.52 (s; 3H; $^{14}CH_3$); 7.23−7.36 (m; 5H; $^{1-3+11+12}$CH); 7.36−7.42 (m; 1H; ^{10}CH); 7.66−7.70 (m; 1H; ^{9}CH); 8.03 (d; $^{3}J_{HH}$ = 8.1 Hz; 1H; ^{4}CH)

^{13}C-NMR (176 MHz, $CDCl_3$-d_1):

δ (ppm) = 18.6 ($^{7}CH_3$); 18.7 ($^{14}CH_3$); 121.7 (^{4}CH); 123.8 (^{9}CH); 126.2 (^{1}CH); 126.8 (^{12}CH); 128.8 (^{2}CH); 130.2 (^{10}CH); 130.9 (^{3}CH); 131.4 (^{13}C); 131.9 (^{11}CH); 134.3 (^{6}C); 142.9 (^{5}C); 149.7 (^{8}C)

LRMS (EI-TOF):

m/z calculated for $C_{14}H_{14}N_2O$ $[M]^+$ 226.1106 found 227.1174

mp = 57.8−58.5 °C

3.9.20 Synthesis of 1,2-*bis*(4-ethylphenyl)diazene oxide

A solution of 1-ethyl-4-nitrosobenzene (0.05 M) and cyclohexanone (0.025 M) in DMSO was injected via a "Hamilton™" 1000 Series "Gastight™" syringe. The flow rate was adjusted to 0.5 $\frac{\mu l}{min}$, resulting in a residence time of 200 min. After 44 h of running reaction and dilution of the crude product with sat. NH_4Cl-solution, the reaction mixture was extracted using CH_2Cl_2. After phase separation, the solvent was evaporated. Purification of the crude product via column chromatography on silica using a mixture of *n*-hexane : EtOAc (120 : 1) (R_f = 0.16) yielded 11 mg (0.043 mmol, 73 %) of the corresponding pure product.

Characterization:

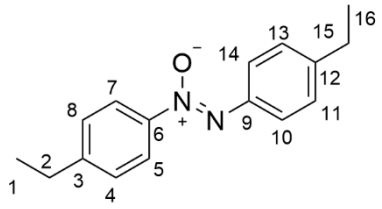

^{1}H-NMR (700 MHz, $CDCl_3$-d_1):

δ (ppm) = 1.24−1.32 (m; 6H; $^{1+16}CH_3$); 2.68−2.78 (m; 4H; $^{2+15}CH_2$); 7.29−7.35 (m; 4H; $^{4+8+11+13}CH$); 8.14 (d; $^{3}J_{HH}$ = 8.4 Hz; 2H; $^{10+14}CH$); 8.21 (d; $^{3}J_{HH}$ = 8.5 Hz; 2H; ^{5+7}CH)

^{13}C-NMR (176MHz, $CDCl_3$-d_1):

δ (ppm) = 15.5 ($^{1}CH_3$); 15.6 ($^{16}CH_3$); 28.8 ($^{2}CH_2$); 29.1 ($^{15}CH_2$); 122.4 ($^{5/7}CH$); 125.9 ($^{10/14}CH$); 128.2 ($^{4/8}CH$); 128.3 ($^{11/13}CH$); 142.2 (^{12}C); 146.4 (^{3}C); 146.6 (^{9}C); 148.3 (^{6}C)

LRMS (EI-TOF):

m/z calculated for $C_{16}H_{18}N_2O$ $[M]^+$ 254.1419 found 254.1343

4 Results and Discussion

To analyze the performance of immobilized organocatalysts in gels, various experiments and methods for characterization are necessary which are discussed in the following together with the results obtained. Some content of the following chapter has already been published.[24,25]

4.1 Assessment of the Batch Syntheses carried out

For the targeted construction of catalytically active gels and their use within the MFR, the synthesis of various low molecular weight compounds is necessary.

4.1.1 Synthesis of lithium phenyl-2,4,6-trimethylbenzoylphosphinate

The synthesis was carried out according to known protocols from literature. [161,162] In the present work the photo initiator is used to initiate the defined buildup of the polymer networks on glass surfaces by photolithography.

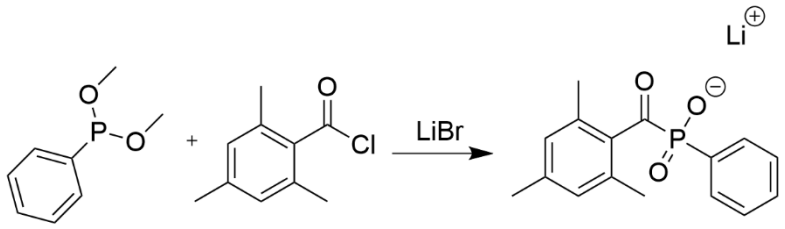

Figure 29: Synthesis of lithium phenyl-2,4,6-trimethylbenzoylphosphinate.

Overall, the desired photo initiator LAP could be synthesized successfully (Figure 29). The synthesis is based on a Michaelis-Arbuzov reaction[161] and gives an acceptable yield of 65 %. Various statements regarding the yields to be expected can be found in the literature. These range from 77 % to 100 %.[162,168] The losses in yield in the synthesis carried out are probably due to losses during precipitation and washing of the crude product. The high purity of the product obtained was successfully confirmed by various analytical methods (^{1}H, ^{13}C, ^{31}P-NMR spectroscopy and ESI-MS).

4.1.2 Synthesis of L-proline-based Catalysts

Synthesis of *o*-(2-methacryloyloxyethylsuccinoyl)-*trans*-4-hydroxy-L-proline (MAOESLP)

The synthesis of MAOESLP is a two-step synthesis which was carried out according to known protocols from literature.[163] The catalytic properties of the polymer gel are based on the immobilization of various catalysts. The basis of the catalysts used in this work is the amino acid L-proline and thus a secondary amine.

In the first reaction step, the carboxylic acid of *o*-(2-methacryloyloxyethyl) succinic acid is converted to the corresponding acid chloride using thionyl chloride. This synthesis was carried out with a conversion of 99 % and without significant impurities. Consequently, the resulting product was used immediately for the second reaction step.

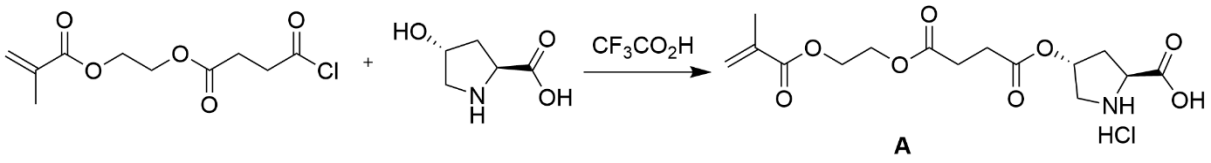

Figure 30: Synthesis of o-(2-Methacryloyloxyethylsuccinoyl)-trans-4-hydroxy-L-proline (MAOESLP).

The second synthesis step involves the formation of an ester bond through the reaction of 2-methacryloyloxyethylsuccinoylic acid chloride and *trans*-4-hydroxy-L-proline to form *o*-(2-methacryloyloxyethylsuccinoyl)-*trans*-4-hydroxy-L-proline (MAOESLP) (Figure 30). The desired product could be obtained with a yield of 72 % which is in agreement with the information in literature.[163] In this reaction step too, a product without major impurities could be obtained after the precipitation. Since the product is obtained as a hydrochloride, a longer crystallization process under cooling is necessary to obtain a solid. In this reaction, the purity of the product could again be confirmed by ^{1}H, ^{13}C-NMR spectroscopy and ESI-MS.

Synthesis of (*S*)-2-(((*R*)-1-((4-(2-(methacryloyloxy)ethoxy)-4-oxobutanoyl)oxy)-4-methylpentan-2-yl)carbamoyl)pyrrolidin-1-iumchloride

The underlying synthesis of the targeted proline amide is a four-step synthesis. The first step (Figure 31(1)) involves classic BOC protection of the secondary amine of L-prolin and was carried out in the same way as reported in previous work.[164] The literature indicates a yield of 84 % for this reaction which was exceeded with 99 % in the present case. One possible reason is the more precise adjustment of the pH value to pH 7 during the work-up. In the literature on which the procedure is based, the pH value is adjusted to 2 - 3 which could possibly have already caused another deprotection. The purity of the product could be verified without further purification using ^{1}H, ^{13}C-NMR spectroscopy.

The subsequent synthesis (2) was carried out analogously to previous work.[19,169] The amide bond formation between the carboxylic acid of the BOC-protected L-proline and the primary amine of L-leucinol was successfully carried out with a yield of 82 % and is therefore within the yield range of the literature. After successful purification by column chromatography, the purity of the product could be verified using ^{1}H, ^{13}C-NMR-spectroscopy.

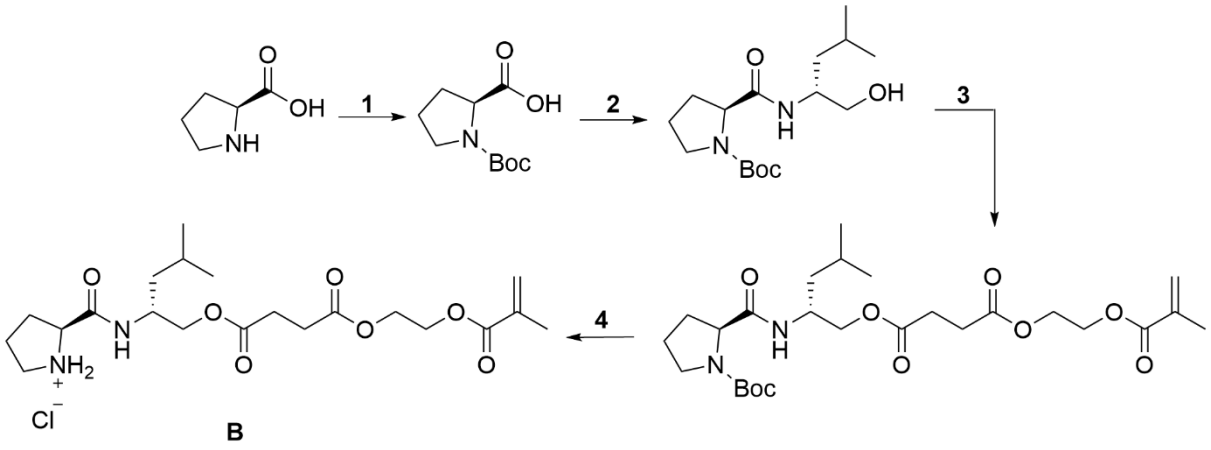

Figure 31: Synthesis of (S)-2-(((R)-1-((4-(2-(methacryloyloxy)ethoxy)-4-oxobutanoyl)oxy)-4-methylpentan-2-yl)carbamoyl)pyrrolidin-1-iumchloride.

The subsequent synthesis step (3), the formation of the ester bond between the primary alcohol of the L-leucinol residue and the carboxylic acid of 2-methacryloyloxyethylsuccinoylic acid, was carried out using the classic Steglich esterification.[165] In this reaction step, a yield of 89 % could be achieved which, however, cannot be subjected to a literature comparison due to the lack of compounds known from the literature. All impurities could be removed by means of two column chromatographic purifications and a pure product was obtained. The purity of the product could be confirmed by ^{1}H, ^{13}C-NMR-spectroscopy and ESI-MS.

The final cleavage of the BOC-protective group could also be carried out on the basis of previous work.[166] The deprotection was carried out successfully using 4N HCl in dioxane in almost quantitative yields of 97 %. The purity of the target structure could be demonstrated using ^{1}H, ^{13}C-NMR-spectroscopy and ESI-MS.

4.1.3 Synthesis of nitrosoarenes

The nitroso compounds required for the reductive dimerization of nitrosoarenes to furnish azoxyarenes could be synthesized on the basis of previous work.[167]

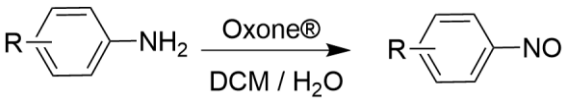

Figure 32: Oxidation of anilines to furnish nitrosoarenes.

In total, 11 differently substituted nitrosoarenes could be obtained from the corresponding anilines by oxidation (Figure 32). The synthesis in a two-phase system of DCM and water offers the advantage that the oxidizing agent Oxone®, as the potassium salt of peroxomonosulphuric acid, dissolves very well in water but is almost insoluble in DCM. As a result, the oxidation takes place primarily at the phase boundary which minimizes overoxidation to nitroaromatic compounds. Furthermore, due to the mild reaction conditions at room temperature, there are hardly any undesirable side reactions such as the formation of aryl hydroxylamines. Accordingly, the desired nitrosoarenes could be obtained in yields ranging from 90 % up to quantitative yields and lie within the range of the underlying literature.[167] The only exception is 1-ethyl-4-nitrosobenzene which was purified by distillation. The purification led to relatively high losses due to the low

liquid volume. The purity of the respective target molecules from chapter 3.3 could be verified using ^{1}H, ^{13}C-NMR-spectroscopy and ESI-MS.

4.2 Assessment of the Setup of the Microfluidic Reactor

Various work steps are necessary for the successful construction of a microfluidic reactor system, which are explained and analyzed in the following section. The gels, which contain the catalyst in immobilized form, are preserved in cylindrical shapes on glass surfaces and are therefore referred to as gel dots in the further course.

The general structure of the microfluidic reactor system is shown in Figure 25 and Figure 26. Compared to previous work[22,23], which mainly relied on PDMS, exclusively PTFE was used as the molding material. The desired reactor shape was milled into the PTFE workpiece in advance. In contrast to PDMS, PTFE has two decisive advantages: On the one hand, it is less elastic which reduces the risk of deformation and leakage when the reactor is clamped in the aluminum holder. On the other hand, it is almost completely chemically inert so that solvents such as DMSO or reactive chemicals could also be used without any significant changes to the shaping material. Nevertheless, under the given technical conditions, it was important to ensure that the screws for the connection between the glass surface and the reactor shape were adjusted evenly and not too strongly (at around 8 $\frac{cN}{m}$). Also in comparison to previous work[22,23], the threads for adjusting the flow system were milled directly into the PTFE layer. For the connection to the capillary tubes HPLC fittings were used, so that previous approaches in this area could also be further developed and problems, such as leaks, were almost eliminated. A disadvantage of using PTFE as a shaping layer is the limitation of the CNC milling machine used for production (type: WF7 CNC from "Kunzmann" milling machines). This only enables a milling width of around 100 µm. The elaboration of more filigree structures is easier with PDMS due to its fluid processing.

4.2.1 Surface Modification

Glass slides were used as the carrier material for the covalent connection of the polymer networks within the reactor chamber due to its wide range of possible uses and its chemical inertness. Commercially available glass slides (72 mm x 26 mm), onto which an adhesion promoter was applied by gas-phase diffusion, formed the basis. For this purpose, the surfaces were first cleaned with various solvents and then with an RCA 1 solution. The result of this surface protocol are free hydroxy groups on the glass surface which react with an oxophile such as functionalized chlorosilanes. In this case, 3TCSPMA was specifically used.

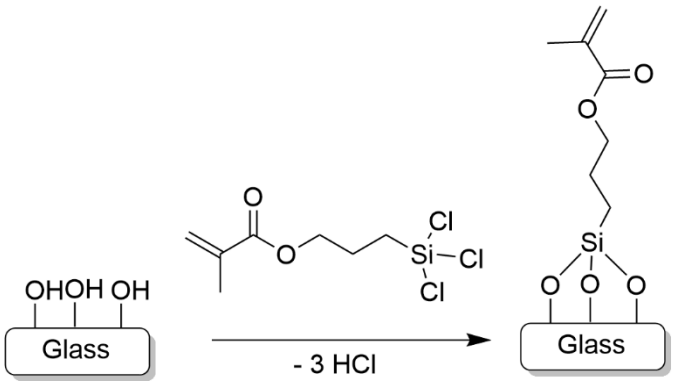

Figure 33: Reaction of 3TCSPMA with hydroxyl groups on the surface of an object slide.

The surface modification shown in Figure 33 is accompanied by a change in the surface polarity. A successful modification can thus be tracked using the contact angle measurements shown in chapter 3.6. When wetted with water, unmodified surfaces were hydrophilic with a contact angle of 6.8°. In contrast, the wetting with diiodomethane was significantly less pronounced with a contact angle of 49°. After the modification, wetting with water resulted in a contact angle of 49° and 44° with diiodomethane. In general, surface modification via gas phase diffusion has proven to be a successful and robust process. The modified slides were stable for several weeks in an argon atmosphere.

4.2.2 Photopolymerization

For the successful photopolymerization, the monomer solutions including the dissolved photoinitiator were placed in a dark gray polyoxymethylene polymerization form according to the basic principle from Figure 8. This was covered with a modified glass slide and a photo polymerization mask and irradiated accordingly. The masks used were developed and provided by the "IPF". A foil printer from "MIVA Technologies" of the type "MIVA 26100 ReSolution PHOTOPLOTTER" was used for the corresponding production. This powerful printer enables resolutions of up to 100,000 dpi. The design of the reactor chamber and the polymerization mask was continuously adapted and optimized by the "IPF" in the course of previous work.[21–23,74]

Figure 34: Picture of a single geldot (left) and the diamond-shaped arrangement of the geldots (right).

The result of this work was the diamond-shaped arrangement of the gel dots, shown in Figure 34. The gel dots obtained after the photolithography were processed in several washing steps. This work-up is essential because the structural unit of the proline is present as hydrochloride after its synthesis and polymerization

and thus hinders a subsequent catalysis. It is also important to remove excess monomer from the gel structure.

Compared to previous work[23], this work made use of methacrylate-based monomers. The obvious disadvantages of poor solubility and lower reactivity could be compensated for by the hydrochloride present and the use of water or other polar solvents such as ethanol as well as slightly longer irradiation times and higher initiator concentrations.

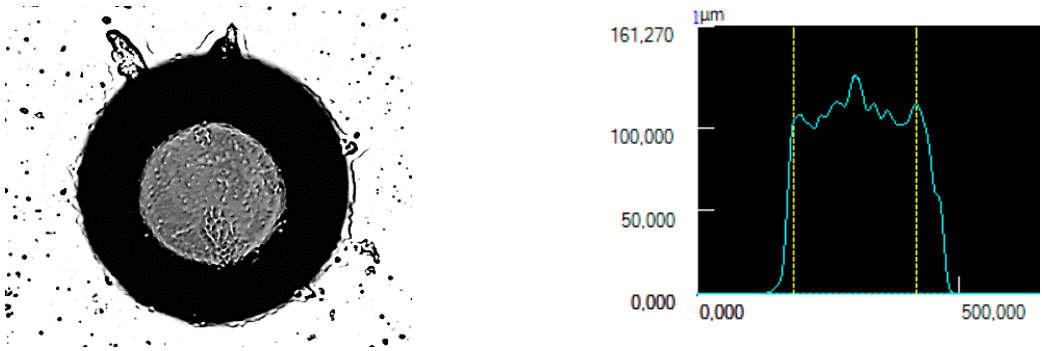

Figure 35: Exemplary representation of the data obtained by confocal microscopy with regard to the dimensions and shape of the gel dots produced. The black area (left) is caused by interference, which can be seen as a shoulder in the height profile (right).

Well-defined cylindrical gel structures should be obtained based on the conditions of the photopolymerization. Figure 35 shows the enlarged laser measurement of a single gel dot using a confocal microscope (left) and the corresponding height profile (right). An average height of 111 µm and a diameter of 236 µm were obtained for the gel structure. For the most precise evaluation possible without artifacts, the grey area within the black ring was used for the measurement. The black border and the slight shoulder formation are the result of interference from the UV laser and are caused on the edges of the dots. The resulting dimensions of the dots correspond to the dimensions of the polymerization mask.

A variation of the height of the gel structures obtained could be achieved through different irradiation times. The procedure already described was chosen again for the polymerization. The resulting gel dots were examined again using confocal microscopy. The polymerization mold was 140 µm high which also limits the maximum height of the polymer structures. In previous works, it was observed that the amount of crosslinker has a huge influence on the processes within the MFR.[23] As can be seen in following results, a relatively high crosslinker content of 5 % is necessary for sufficiently stable methacrylate-based gel structures. Gel compositions with crosslinker contents below 3 mol% did not show sufficient mechanical stability and could not be polymerized successfully. Consequently, polymers consisting of 90 mol% of catalyst B, 5 mol% methyl methacrylate (MMA) and 5 mol% ethylene glycol dimethacrylate (EGDMA) were produced. The height of the polymer dots was analyzed for different light exposure times in order to estimate an optimal use of the reactor chamber. As shown in Figure 36, the height of the hexagonally ordered gel structures increased from 23 (± 6) µm after 6 s of irradiation and 73 (± 11) µm after 9 s to 106 (± 19) µm after 12 seconds of irradiation in an almost linearly behavior. A further increase of the irradiation to 15 seconds

leaded to a height of 122 (± 12) µm and could not be increased by further extension of irradiation time. If the irradiation time is extended beyond 12 s, the spatial resolution of the photopolymerization deteriorates significantly and larger, coherent gel domains are increasingly formed. This can be continued until the individual dots have completely disbanded and the transition into a continuous layer can be observed. The other extreme is exposure times of less than 6 seconds which is not sufficient to obtain polymer structures at all. This can be explained by the gel point that must necessarily be reached within the network structure.

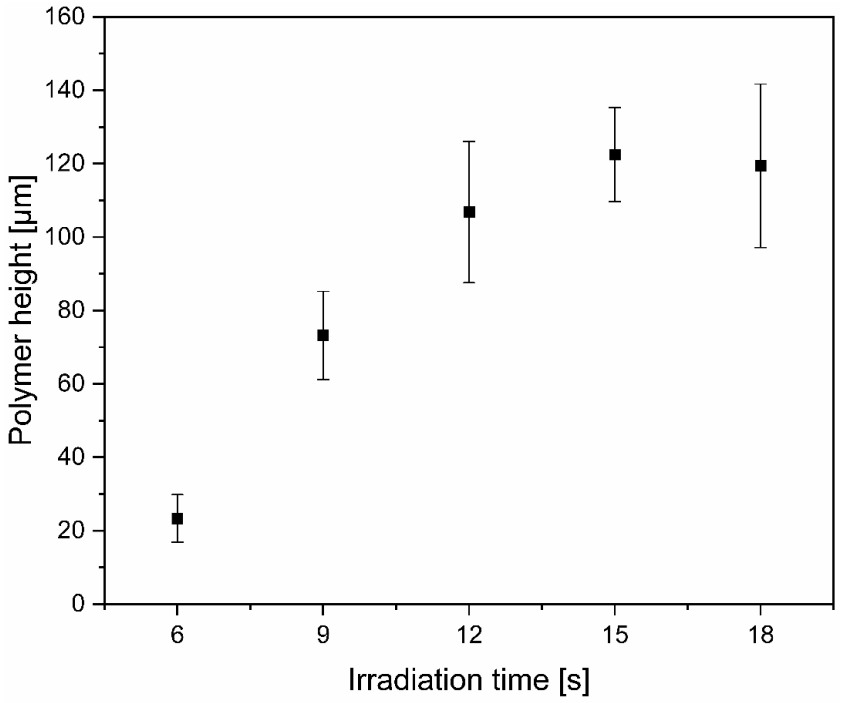

Figure 36: Plot of the average object height against the exposure time used. The error bars describe the standard deviation of the measurements. Conditions of manufacture: I = 20 %, c = 3.34 M, h = 8 cm.

On the basis of previous work[23] and the results of the analysis of methacrylate-based polymer gels, the optimal conditions for the polymerization could be derived. These are summarized below in Table 6.

Table 6: Optimized conditions of the photopolymerization for the synthesis of the gel dots by photolithography.

Intensity	Distance to the light source	Irradiation time	Monomer amount[a]	Crosslinker content
20 %	8 cm	12 s	15 mmol	5 mol%

[a] Solution in 1.7 ml of distilled water/ethanol

Using the conditions shown in Table 6 and using the methacrylate-based catalyst structure B, object heights of 106 µm result. Accordingly, the object heights obtained by photopolymerization can be adjusted in a targeted manner. Nevertheless, moderate deviations from the targeted object heights are obtained, especially for shorter irradiation times.

4.2.3 Analysis of the Degree of Swelling of the Gel Structures

Based on previous work, a further analysis of the swelling of the gel structures was made.[23] In addition to reliable and reproducible photopolymerization with high spatial resolution, the efficient use of the given dimensions of the microfluidic reactor depends on the behavior of the gels. Within the reactor, the gels are subject to a swelling process. As a result, a change in volume occurs. Unhindered swelling changes the height as well as the width of the gel in equal measure, so that the degree of volume swelling is characteristic of both the solvent and the gel composition.

Completely swollen gels are in a state of equilibrium. To achieve this, without the swelling processes taking place influencing the reactions within the MFR, the gel structures were pre-swollen with pure solvent in advance of each reaction. There are three possible states for the swollen structures inside the reactor chamber, of which only one is particularly promising. In the completely swollen state, the gel structures can on the one hand hypothetically exceed the maximum height of the reactor chamber and are therefore actually compressed by it. On the other hand, even when swollen, they can be too small for the given reactor geometry which leads to inaccessible volumes in the reactor chamber. The third and most promising option is swelling right up to the top of the reactor chamber but with little or no compression. This does not result in any inaccessible volume but also not in a deformation of the gel structure. A swelling of the gels, that is as well adapted as possible to the reactor geometry, is essential for efficient catalysis within the gel due to the desired diffusion of reactants into the gel structure - and adducts out of it. Too high or too low a degree of swelling would inhibit diffusion and efficient catalysis. The degree of swelling and the diffusion process can be influenced and controlled by the degree of crosslinking of the gels. This assumes that diffusion processes in polymer gels with a higher proportion of crosslinking require more time than in less crosslinked gel structures. A calculation of the degree of swelling of the isotropic swelling is possible as a ratio of the parameters H2 and H1, illustrated in Figure 37.

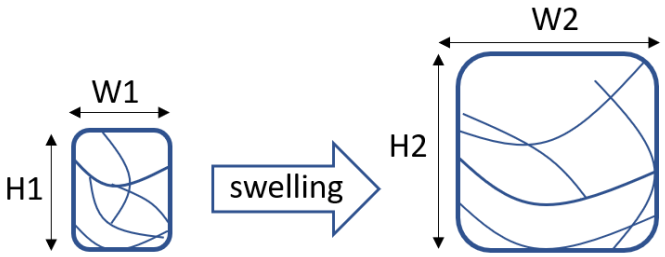

Figure 37: Schematic illustration of the change in the dimensions of a gel from the dry (left) to the swollen state (right).

In accordance with this relationship of isotropic swelling, there is also a geometric correlation for bound polymers and consequently a relationship between the degree of swelling and the layer thickness can be established as follows:

$$\left(\frac{H_2}{H_1}\right)_{SA} = \sqrt[3]{Q_{Iso.}} \qquad (18)$$

$Q_{Iso.}$ = Degree of swelling of isotropically swollen gels $[/]$

H_1 = Height in the dried state $[cm]$

H_2 = Height in the swollen state $[cm]$

The relationship described in Equation 18 has already been examined in previous studies.[46] This work is based on the swelling behavior of thin layers (≥ 100 nm) which, due to the surface connection, cannot swell freely along the x- and y-axes. As a result, there is increased swelling along the z-axis and Equation 18 is no longer valid. Instead, an empirical connection was sought for the swelling along the z-axis. The corresponding results are as follows:

$$Q_{SA} = Q_{Iso.}^{\frac{5}{9}} \qquad (19)$$

Q_{SA} = Degree of swelling of surface attached gels $[/]$

The corresponding degree of swelling results from the measured layer thickness. The following can also be formulated accordingly:

$$\left(\frac{H_2}{H_1}\right)_{SA} = Q_{Iso.}^{\frac{5}{9}}$$

The validity of the corresponding results has so far been imitated to thin layers. In further work, however, it was successfully shown that the corresponding relationship is also valid for greater layer thicknesses.[170] Nevertheless, it is also known that a surface connection limits the swelling of gels in the z-direction.[171] In order to adapt the swelling of the gels to the reactor geometry as best as possible, various measurements based on the isotropic degree of swelling were carried out.

4.2.4 Analysis of the Isotropic Degree of Swelling

To determine the isotropic degree of swelling, macroscopic gel workpieces in a cylindrical shape and in the desired composition were produced. For this purpose, about 0.6 ml of the monomer solution were drawn into a 1 ml Pasteur pipette and irradiated for 12 s (I = 40 %, d = 8 cm). The pipettes were then cut open and the workpieces obtained were divided up for multiple determinations. Prior to the analysis of the degree of swelling, the samples were worked up as described in 3.7. Afterwards, the degree of swelling was determined using the volume as well as the mass of the samples.

Table 7: Compilation of the determined degrees of volume swelling for isotropically swelling gel workpieces of different composition in DMSO.

Amount of crosslinker [mol%]	Amount of catalyst[a] [mol%]	Degree of volume swelling [-]
3	90	2.43 (±0.14)
5	50	1.28 (±0.04)
5	90	2.28 (±0.12)

[a] Using catalyst structure B.

The degrees of swelling summarized in Table 7 show a clear relationship to both the crosslinker content and the catalyst content. The degree of swelling is greatest when, as has happened using 3 mol%, the lowest proportion of crosslinking agent has been polymerized into the network structure. A lower proportion of crosslinking agents enables the gel structure to absorb more solvent which leads to more pronounced swelling. Gel compositions with crosslinker contents below 3 mol% did not show sufficient mechanical stability and could not be polymerized successfully. Furthermore, the degree of swelling when using 90 mol% catalyst was 2.28 and was thus significantly higher compared to 1.28, when using 50 mol% catalyst. If the amount of catalyst is reduced, this proportion of the gel is balanced out by adding MMA. The increased MMA content leads to an increasingly non-polar character which reduces swelling due to polar solvents such as DMSO. The degree of swelling of the corresponding gel composition with catalyst structure A was determined to be 1.8 (± 0.03) and is thus in the range of the previous results. The lower swelling compared to catalyst structure B is due to the structural differences between the catalysts. Catalyst A has a carboxylic acid functionality which reduces swelling in DMSO due to its hydrophilicity.

Since the asymmetric aldol reaction should be carried out in mixtures of DMSO and water, the degree of swelling was also investigated for the solvent water. Again, a gel composition of 90 mol% catalyst, 5 mol% MMA and 5 mol% EGDMA was used. For this gel composition, a degree of swelling of 1.38 (± 0.18) was found. Compared to the degree of swelling in pure DMSO, this is much less pronounced in water. The reason for this behavior is the more polar character of water as solvent compared to DMSO and therefore less pronounced swelling of methacrylate-based gels is to be expected.

Table 8: Weight degree of swelling of gel samples containing 90 mol% catalyst, 5 mol% MMA and 5 mol% EGDMA.

	Gel containing catalyst structure A	Gel containing catalyst structure B
Weight degree of swelling [-]	1.90 (± 0.03)	2.38 (±0. 48)

A comparison of the degree of volume swelling and the weight degree of swelling (Table 8) shows that overall comparable results were obtained, but that the degree of mass swelling is slightly higher independently of the catalyst structure used. This deviation is given intrinsically by the correlation of the density with the degree of volume and weight swelling. The density of DMSO is given as 1.1 $\frac{g}{ml}$, accordingly the degree of mass swelling is necessarily greater than the degree of volume swelling.

4.2.5 Influence of Different Irradiation Times on the MFR

The asymmetric aldol reaction is carried out within the MFR in pure DMSO or a solvent mixture of DMSO and water. Previous work formed the basis for estimating the object heights in the swollen state which is the reason for using an exposure time of 12 seconds and an object height in the dry state of 106 µm for further analysis based on Table 6.[46] Using the appropriate approximation and catalyst structure B, an expansion by a factor of 1.19 to 1.58 is to be expected for 90 mol% catalyst loading and 5 mol% crosslinker content. When using pure DMSO, this would correspond to a filling of the reactor chamber of slightly more than 100 % which is, however, reduced by adding water and the associated lower degree of swelling and thus results in an almost optimal filling of the reactor chamber. Using the expansion factor of 1.58, the following polymer heights, shown in Figure 38, result for the various exposure times between 6 and 18 seconds in the dried and in the swollen state.

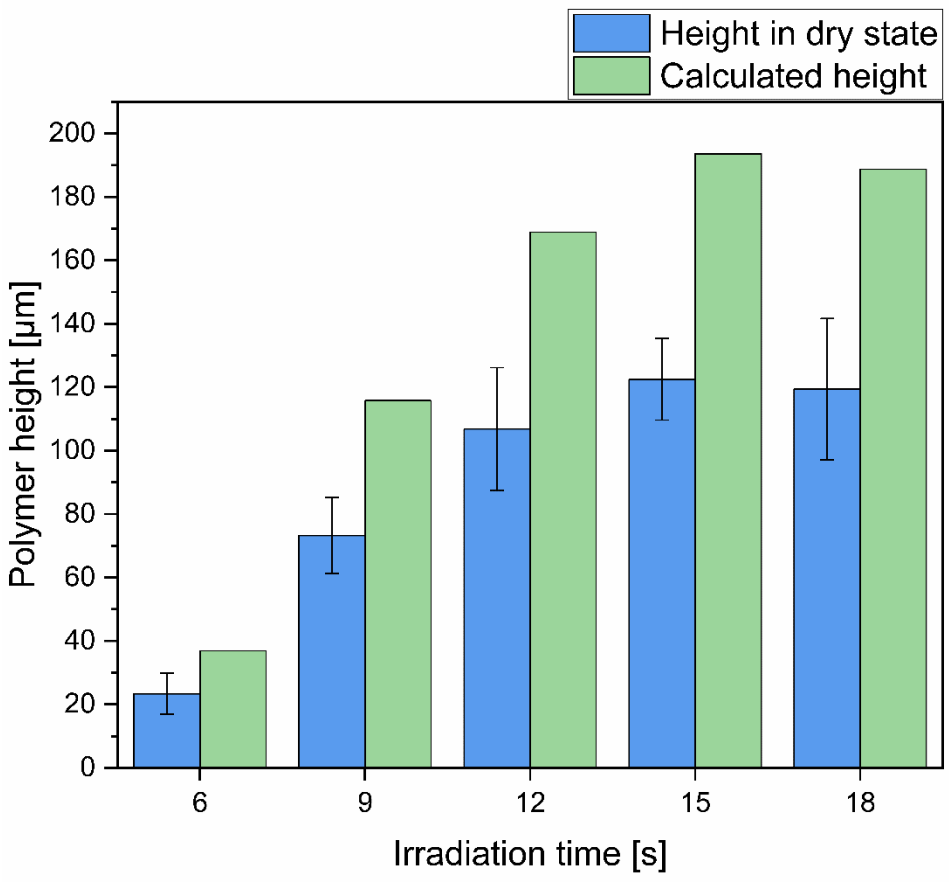

Figure 38: Average polymer height for different light exposure times in dry state determined by confocal microscopy (blue bars). Calculated polymer height in swollen state (green bars). Polymer composition: 90% catalyst B, 5% crosslinker, 5% methyl methacrylate.

For a more in-depth analysis of the relationship between conversion behavior and polymer structure height, reactor surfaces with attached gel structures of different heights were prepared and used to determine the conversion of the asymmetric aldol reaction of the model system 4-nitrobenzaldehyde and cyclohexanone. The corresponding results are summarized in Figure 39. The surfaces with polymer structures prepared with 6 and 9 seconds of UV-light irradiation and heights of 23 (± 6) µm and 73 (± 11) µm, respectively, provide a similar conversion of 54 % and 56 % after a reaction time of 6 hours. After reaction times of 12 and 18 hours, both polymer structures showed an almost constant conversion behavior with a conversion of around 30 % and 45 % respectively. After 24 hours the conversion dropped significantly in both cases. After a polymerization time of 12 seconds and a polymer height of 106 (± 19) µm, the polymer structures deliver an almost constant conversion of 97 % after 6 hours and 92 % after 24 hours of reaction time. In contrast to this, no further increase in conversion can be achieved by additional extension of the polymerization time. A further increase in irradiation time leads to an increasingly unselective polymerization and thus to the formation of larger polymer domains without a fine structure. Consequently, efficient diffusion of the reactants into the gel is made more difficult by the smaller surface area. However, applying 15 seconds of irradiation, leading to polymer structures of 122 (± 12) µm, the reactor delivers 87 % conversion after 6 hours and 82 % after 24 hours. The importance of diffusion into the gel becomes clear when gels with a higher crosslinker content are produced. A doubling of the crosslinker content led on the one hand to more difficult diffusion processes of the educts into the gel structure and on the other hand to a more difficult release of the product formed from the gel. As a result of these effects, after 12 seconds of light exposure, significantly lower conversions of slightly above 70 % can be observed.

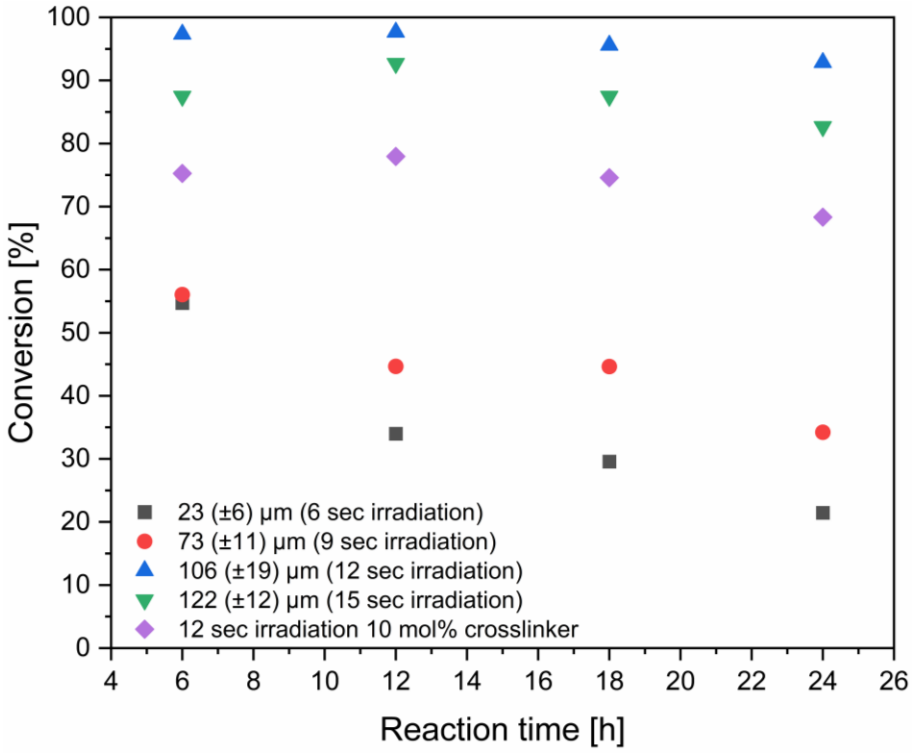

Figure 39: Relationship between the height of the polymer structures and the conversion behavior of the asymmetric aldol reaction of 4-nitrobenzaldehyde and cyclohexanone, analyzed by ^{1}H-NMR over a total reaction time of 24 hours with a residence time of 3.34 hours. Using 0.034 M of aldehyde respective 0.167 M of ketone in a 9:1 DMSO : water mixture.

4.2.6 Summary of the Optimized Preparation Process

The parameters discussed in the previous chapters 4.2.4 and 4.2.5 and the corresponding results are the basis for the optimal conditions for the reactions within the MFR. First, the photopolymerization and the resulting influences on the catalyst-bearing gel elements within the MFR were examined. In particular, the crosslinker content and the catalyst content were varied and analyzed. Then, the isotropic swelling behavior of the gels in DMSO and water was also examined. Unless otherwise explicitly stated, the following conditions and combinations have been used for polymer preparation.

Table 9: Summary of the optimized conditions for the photopolymerization and composition of the gel.

Photopolymerization	
Intensity [%]	20
Distance to light source [cm]	8
Irradiation time [s]	12
Amount of monomer used [mmol][a]	15

[a] dissolved in 1.7 ml of destilled water.

Polymer composition	
Calatyst [mol%]	90
MMA [mol%]	5
EGDMA [mol%]	5

4.3 Asymmetric Aldol Reaction inside the MFR

With the optimized conditions of the photopolymerization and the knowledge of the swelling behavior of the polymer gels, a detailed analysis of the asymmetric aldol reaction within the MFR is carried out. In addition to optimizing the solvent mixture and the temperature of the reaction, the product spectrum is examined in order to finally examine the reusability and long-term stability of the system, also in terms of selectivity.

4.3.1 Optimization of Solvent Composition and Temperature

The organocatalyzed asymmetric aldol reaction was analyzed regarding different parameters such as solvent composition and temperature. As an initial investigation, different solvent compositions of DMSO and water were screened regarding conversion and selectivity. As illustrated in the summarized results in Table 10, neither pure DMSO nor larger proportions of water yield good conversions and selectivity at room temperature (~ 23 °C)

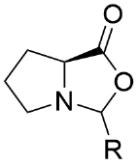

Figure 40: Structure of the L-proline-oxazolidine derivative.

(Table 10, entries 1 and 4). This is due to the gel's swelling properties examined in 4.2.4. Larger proportions of water lead to a significantly reduced degree of swelling which inhibits efficient catalysis within the gel. It is also known that small amounts of water show a positive influence on the conversion and the selectivity of the asymmetric aldol reaction[172] so that the lower conversion and the lower selectivity for pure DMSO are understandable.[173] The addition of water does not increase the activity of the catalyst but rather reduces the deactivation of proline due to the formation of an oxazolidine derivative (Figure 40). The water hydrolyzes the oxazolidine structure formed between the educts and the catalyst and thus reduces the increasing deactivation of the catalyst over time.[173] While all of the reaction conditions analyzed led to sufficient conversions with moderate selectivity, the solvent composition DMSO : water (9 : 1) with 95 % conversion and an anti-selectivity of 67 : 33 gave the best results at room temperature (Table 10, entry 2). At a reaction temperature of 40 °C, all solvent compositions show weaker results for conversion or selectivity than their counterparts at room temperature.

Table 10: Optimization of reaction conditions for the asymmetric aldol reaction of p-nitrobenzaldehyde and cyclohexanone.

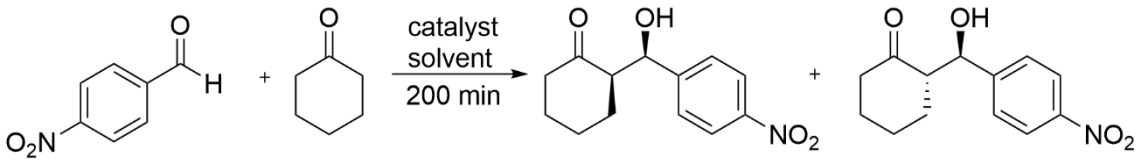

Entry	DMSO-water ratio (v : v)	Temperature [°C]	Conversion [%][a]	Diastereomeric ratio syn/anti [%][a]
1	10 : 0	rt	26	36/64
2	9 : 1	rt	95	33/67
3	8 : 2	rt	58	35/65
4	7 : 3	rt	80	41/59
5	9 : 1	40 °C	78	41/59
6	8 : 2	40 °C	73	43/57
7	7 : 3	40 °C	82	41/59

[a] Determined by ^{1}H-NMR after 24 h of sample collection. Using 0.034 M of aldehyde respective 0.167 M of ketone.

Based on the results obtained, all the following results were carried out in a 9 : 1 DMSO : water mixture at room temperature.

4.3.2 Product Scope of the direct Asymmetric Aldol Reaction inside the MFR

For the evaluation of the substrate generality of this organocatalyzed asymmetric aldol reaction inside the MFR, the reaction of various aromatic aldehydes with different ketones was investigated, applying the optimized conditions. As can be seen in Table 11, different aromatic aldehydes and ketones can effectively be transformed to the corresponding aldol products inside the MFR.

Table 11: Substrate scope of the direct asymmetric aldol reaction inside the MFR[a]

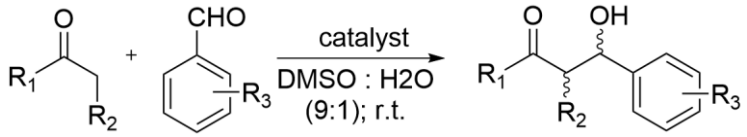

Entry	Product	Yield [%]	dr[a] [anti : syn]	ee[b] [%]
1	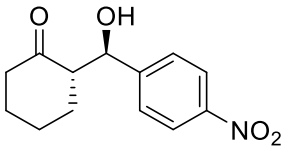	78	67 : 33	87
2	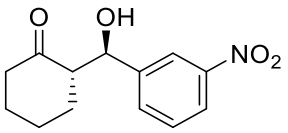	93	68 : 32	57
3	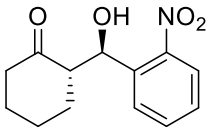	75	71 : 29	72
4	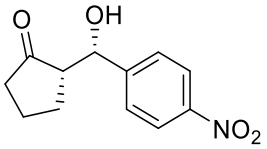	86	26 : 74	18
5	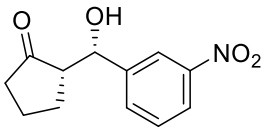	63	25 : 75	67
6	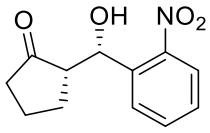	82	21:79	76

7	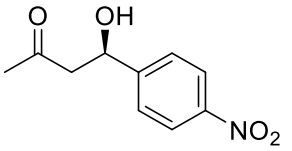	80	-	19

[a] Determined by ^{1}H-NMR after 48 h of sample collection. Using 0.034 M of aldehyde respective 0.167 M of ketone at dwell times of 3.34 h. [b] determined by chiral HPLC analysis (IA, IC columns).

Using a mixture of DMSO : water (9 : 1 v : v) as solvent, the feasibility of different cyclic and acyclic ketones as donors for the asymmetric aldol reaction was examined. As shown in Table 11 when cyclohexanone serves as donor part of the aldol reaction, good yields ranging from 75 - 93 % with moderate to good ee values (57 - 87 %) for the anti-isomer were received. In contrast, however, the diastereomeric ratios obtained were only 67 : 33, 68 : 32 and 56 : 44, respectively, for the three different aldehydes investigated. With the use of cyclopentanone, moderate to good yields of 63 - 86 %, but attenuated enantioselectivities with 18 - 76 % ee, could be obtained in this case for the syn product, which is in line with previous findings.[174] When using cyclopentanone, the diastereomeric ratio was between 21 : 79 and 26 : 74. Furthermore, acetone, a non-cyclic ketone, was also investigated as a donor in the aldol reaction within the MFR. The reaction of acetone with 4-nitrobenzaldehyde also provides a good yield of 80 % but again attenuated ee selectivity of only 19 %. TANG et al.[175] also investigated the basic structure of proline amide B without immobilization for the asymmetric aldol reaction of acetone with various aldehydes. The comparison between the immobilized catalyst and this low molecular weight catalyst shows a comparable yield which suggests that the catalyst is equally active, even in immobilized form. However, a difference can be seen when comparing the ee values. In the case of the free catalyst, these are slightly higher at 33 % than in the case of the immobilized catalyst. A possible explanation could be seen in the mechanism of the proline-catalyzed aldol reaction and the conformations that are necessary for a high selectivity. The immobilization could inhibit the formation of only one conformation and thus reduce the selectivity. Oppositely the reaction time is dramatically decreased. The reaction of the free catalyst takes place within 12 hours, whereas the residence time within the MFR is only 3.34 hours and consequently significantly shorter reaction times are needed in case of the MFR concept. An in-depth comparison and discussion of the amount of catalyst needed is given in 4.3.5.

4.3.3 Reusability of Catalyst System

In order to serve as an efficient catalyst system in a continuous process, a catalyst system must be robust, versatile and deliver high conversions and good selectivity over a long period of time. Using a 9 : 1 mixture of DMSO and water as a solvent, the reusability and robustness of the MFR system were analyzed in a recycling study. To investigate the corresponding behavior of the polymer gel produced, different ketones were alternately reacted with 4-nitrobenzaldehyde. After a reaction time of 24 hours in each case, the reactor system was flushed with pure DMSO for 24 hours and then the contrary ketone was injected. The corresponding conversions and diastereoselectivities were analyzed using ^{1}H-NMR and are shown in Figure 41. After performing the first reaction with cyclohexanone and 4-nitrobenzaldehyde (mixture A) a conversion of 93 % with an anti-selectivity of 66 % was achieved. After rinsing with pure DMSO, the second educt

solution of cyclopentanone and 4-nitrobenzaldehyde (mixture B) was injected which could be converted to the desired product in 94 % with a syn-selectivity of 74 %. The second reaction run with A delivered a conversion of 64 % and an anti-selectivity of 74 % over further 24 hours of reaction time. After rinsing again for 24 hours with pure DMSO, conversions of 85 % and syn-selectivities of 72 % could still be obtained in a second reaction with B. Even after a total reaction time of 168 h, the presented reactor system still delivers good conversions with acceptable selectivities and can thus serve as a solid foundation for further investigations.

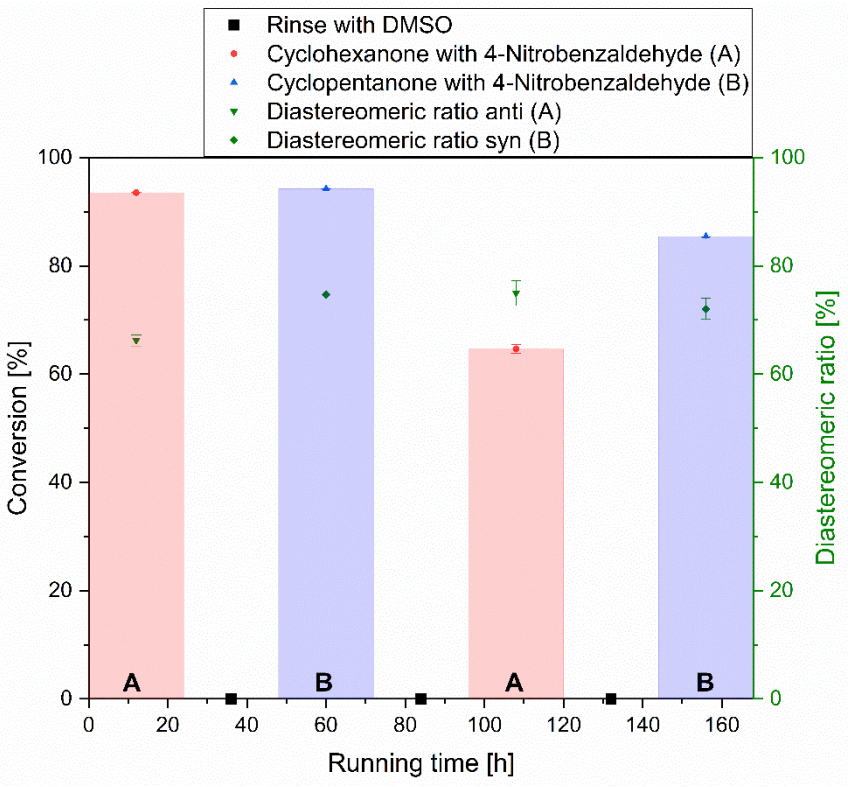

Figure 41: Reusability of MFR with different ketones at dwell times of 3.34 h in DMSO/ water (9:1 v : v). Reaction of 0.167 M of the ketone and 0.033 M of 4-nitrobenzaldehyde.

4.3.4 Catalytic Long-Term Behavior of MFR System

For a satisfactory, long-term, continuous process, it is necessary to achieve consistently high conversions over long periods of time with good selectivities at the same time. As shown in Figure 42 and Figure 43, the behavior of the reactor was analyzed over a period of 144 hours (6 days).

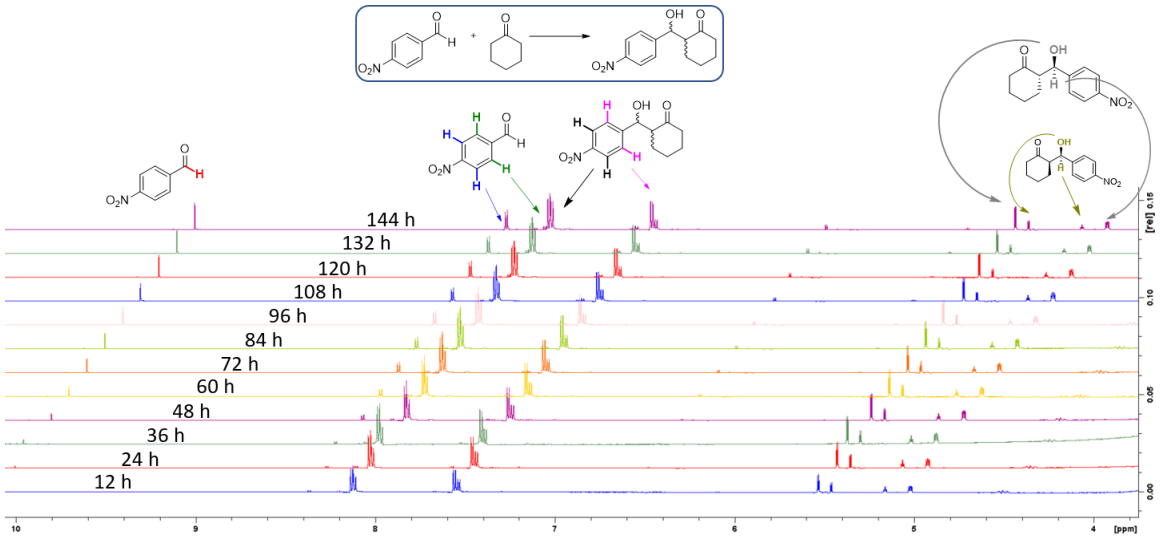

Figure 42: Example of the time depending NMR spectra for the aldol reaction of 4-nitrobenzaldehyde and cyclohexanone for the determination of the conversion and diastereomeric ratio via NMR.

Even after 144 hours of continuous operation, a conversion of 75 (± 5) % can still be achieved with an anti-selectivity of 71 (± 4) %. The maximum conversion could be reached after an operating time of 24 hours with 94 (± 5) %. Subsequently, the conversion decreases slightly, whereby the decrease seems to gradually slow down with increasing reaction time as indicated by the third order polynomial fit. After about 140 hours, an almost constant conversion level can be assumed. In contrast, the anti-selectivity increases slightly with increasing reaction time. After 24 hours, an anti-selectivity of 65 (± 3) % was obtained, whereas it slightly increased to 71 (± 4) % after 144 hours.

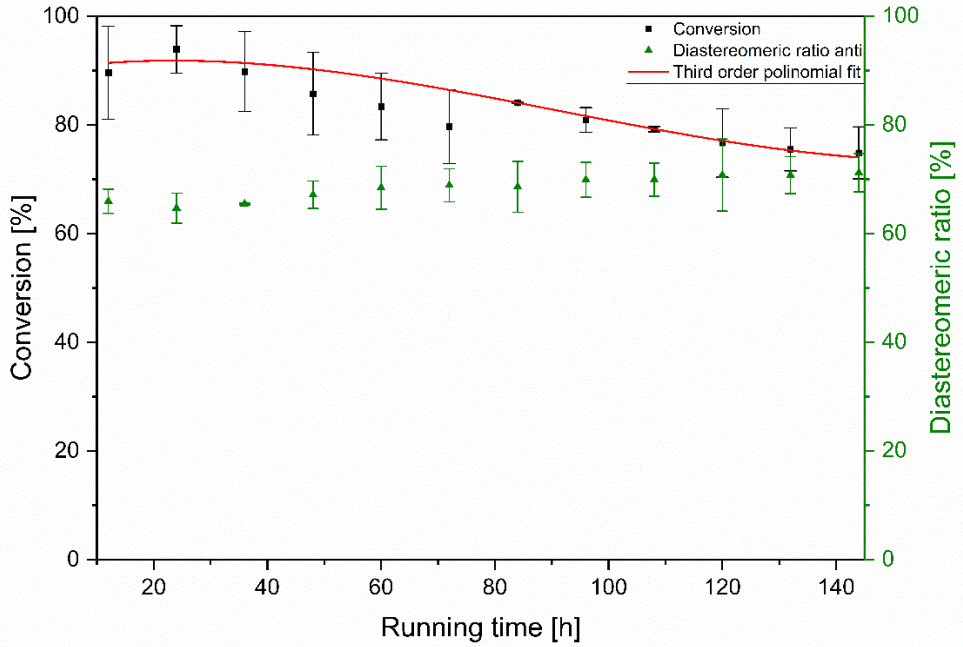

Figure 43: Long-term conversion and diastereomeric ratio of the aldol reaction of 4-nitrobenzaldehyde and cyclohexanone at dwell times of 3.34 h in DMSO/water (9 : 1 v : v). Reaction of 0.167 M of the ketone and 0.033 M of aldehyde.

4.3.5 Comparison of the MFR Approach and a Batch Reaction

Based on previous work, a further comparison was made between a reaction in the MFR and a classic batch reaction using the model reaction of cyclohexanone and 4-nitrobenzaldehyde.[23] The first step is to calculate the appropriate amount of catalyst for the batch reaction. A density of 0.28 (± 0.1) $\frac{g}{ml}$ was determined for the gels based on catalyst structure B. On the basis of this, the mass of the gels immobilized on the surface can be calculated using the following Equation 20.

$$m = N \cdot \rho \cdot V = N \cdot \rho \cdot \pi \cdot r^2 \cdot H \qquad (20)$$

m = Mass $[mg]$

N = Number of gel dots $[/]$

H = Height $[cm]$

r = Radius $[cm]$

Since the substance concentration of the monomers used is known during the polymerization, an amount of substance within the irradiated volume can be calculated:

$$n = N \cdot c \cdot V = N \cdot c \cdot \pi \cdot r^2 \cdot H \qquad (21)$$

n = Amount of substance $[mmol]$

c = Substance concentration $\left[\frac{mmol}{ml}\right]$

As a result, the amounts of substance of the immobilized gel constituents are obtained and can be converted into masses using the molar mass. An amount of 8.68 µmol results for the catalyst structure synthesized in chapter 3.3.6. Since the corresponding flow experiments were analyzed over 48 hours and operated at a flow rate of 0.5 $\frac{\mu l}{min}$, the result is a volume of 1.44 ml for the educt solution. A catalyst concentration of 6.02 $\frac{\mu mol}{ml}$ was used based on the volume of educt conveyed. In order to achieve a comparable catalyst concentration, around 0.6 mol% of catalyst, based on the educt, must be used in a batch reactor with an educt concentration of $3.4 \cdot 10^{-2}$ $\frac{mmol}{ml}$.

After a reaction time of 200 minutes, which corresponds to the residence time in the reactor, no conversion was detected for the batch experiment. These findings appear reasonable as the lower turnover efficiency of organocatalysts typically makes larger amounts necessary. In the case of the prolinamide already mentioned in chapter 4.3.2, 20 mol% are used, for example.[175] Opposingly, the lower turnover efficiency is compensated by the high local catalyst concentration inside the reactor chamber. While in case of the batch

reaction the catalyst concentration is 6.02 $\frac{\mu mol}{ml}$, the low volume of the reactor chamber of 100 µl corresponds with a catalyst concentration of $8.6 \cdot 10^{-2} \frac{mmol}{ml}$ in the case of the MFR concept. This provides an approximately 15-fold higher catalyst concentration within the microfluidic reactor chamber compared to the corresponding batch experiment.

This result shows that the MFR also provides higher efficiency for more complex organocatalyzed reactions such as the asymmetric aldol reaction, compared to classic batch reactions.

4.3.6 Evaluation of TOF and TON

The TOF and TON were calculated to enable a comparison of the MFR approach with other systems. The results are summarized in Table 12. In case of the MFR approach, TON between 5.08 and 3.43 and TOF values ranging from 1.52 h^{-1} to 1.03 h^{-1} were obtained. In contrast, typical proline-based catalyst systems without immobilization deliver TON in the range of 8 to 50 in batch reactors.[176] Fewer comparative data are available for immobilized proline systems. Proline, which has been grafted onto silica supports, is reported to deliver TOF between 0.4 and 3.6 h^{-1}.[177] Additionally, proline as a catalyst for the asymmetric aldol reaction immobilized in polymers delivers a TOF of 0.33 h^{-1} and a TON of 9.[178] As a result, the efficiency of the MFR approach lies below typical systems in batches without immobilization but is shown to be equivalent or even superior when comparing different immobilized catalyst systems. In spite of this, in comparison to the presented MFR approach, significantly longer reaction times, typically around or above 24 hours, are required for the direct asymmetric aldol reaction using proline as a catalyst in one form or another in all of the cases mentioned.

Table 12: Calculated TON and TOF for different reactions. $8.68 \cdot 10^{-3}$ mmol of catalyst B (immobilized on surface).[a]

Aldol-product [-]	TON [-]	TOF [h^{-1}]
1	4.25	1.28
2	5.08	1.52
3	4.06	1.22
4	4.55	1.37
5	3.43	1.03
6	4.51	1.35
7	4.43	1.33

[a] An educt solution of 0.167 M of the ketone and 0.033 M of aldehyde were used. The yields and reaction dwell times (200 min) were used for TOF calculations.

4.4 Synthesis of Azoxybenzenes by Reductive Dimerization of Nitrosobenzenes within the MFR

In addition to the asymmetric aldol reaction within the MFR, a detailed analysis of the reductive dimerization of nitrosobenzenes to yield azoxybenzenes was carried out as well. In addition to optimizing the solvent mixture of the reaction, the product spectrum is examined in order to finally survey the reusability and long-term stability of the system, also in terms of selectivity. The trans-selectivity of the products was therefore analyzed using single crystal X-ray diffraction spectroscopy. Finally, the TOF as well as the TON were analyzed.

4.4.1 Optimization of Reaction Conditions

The reductive dimerization of the unsubstituted nitrosobenzene was evaluated as model reaction. Following key issues, summarized in Table 13, could be validated: Since the solvent is responsible for both the solubility of the educts and products as well as for the swelling of the polymer gel, DMF and DMSO were chosen for further analysis. In DMF and DMSO (entries 1 and 2), no conversion was detected without the additive being present. With 1 eq of cyclohexanone as additive in DMF, 58 % conversion was obtained (entry 3). A conversion of 72 % after a residence time of 100 min was detected using 1 eq of cyclohexanone in DMSO (entry 4). Under the same reaction conditions using a gel without catalyst, no conversion was detected (entry 5). Halving the residence time to 50 min (entry 6) or performing reactions at higher concentrations of nitrosobenzene at 0.4 M and the additive at 0.2 M, led to a decreased conversion (entry 8), possibly because of the generally low turnover number for organocatalysts.[20] Using other ketones such as acetone (entry 7) as an additive, only traces of the desired product were obtained. This finding can possibly be attributed to a faster condensation kinetic and the ability of cyclohexanone to act as an excellent donor compared with acetone.[102]

Table 13: Optimization of reaction conditions for the reductive dimerization of nitrosobenzene to form azoxybenzene.

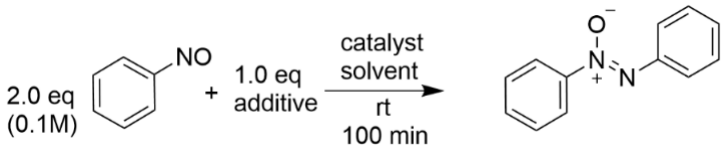

Entry	Solvent	Additive	Conversion [%][a]
1	DMF	-	-
2	DMSO	-	-
3	DMF	Cyclohexanone	58
4	DMSO	Cyclohexanone	72
5[b]	DMSO	Cyclohexanone	-
6[c]	DMSO	Cyclohexanone	56
7	DMSO	Acetone	traces
8[d]	DMSO	Cyclohexanone	43

[a] Determined by ^{1}H-NMR. [b] Conversion of reference sample under the same reaction conditions using a gel without catalyst. Determined from ^{1}H-NMR of crude product. [c] Dwell time of 50 min. [d] Reaction of 0.4 M of starting material respective 0.2 M additive.

4.4.2 Product Scope of the Reductive Dimerization inside the MFR

A wide variety of differently substituted nitrosobenzenes was subjected to the reaction conditions, the results are shown in Table 14. The reductive dimerization of nitrosoarenes yielding azoxybenzenes could be applied to a wide scope of differently substituted nitrosobenzenes.

Table 14: Substrate scope of the reductive dimerization inside the MFR.[a]

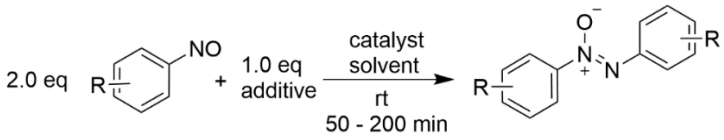

Entry	Product	Yield [%]	Conversion [%]	Dwell time [min]
1	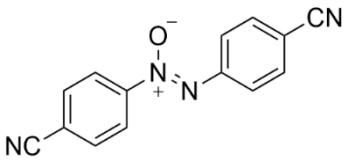	98	99	50
2	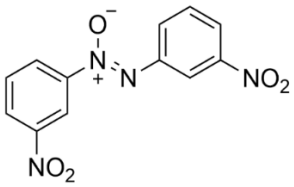	93	98	50
3	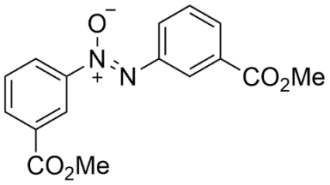	86	98	50
4	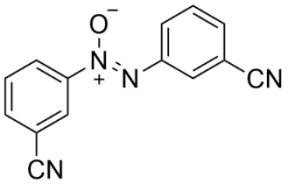	82	99	50
5	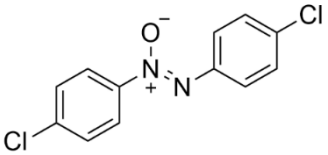	66	98	50
6	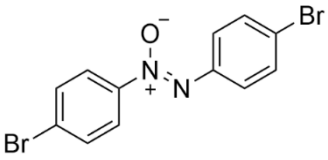	67	98	50

7	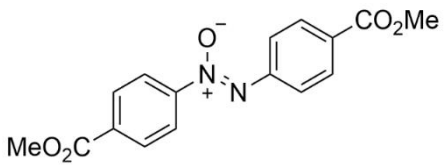	68	93	50
8	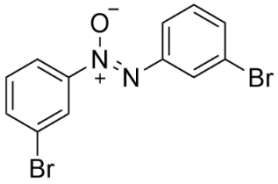	74	93	50
9	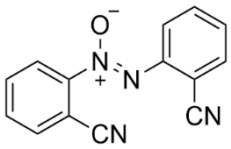	72	95	50
10	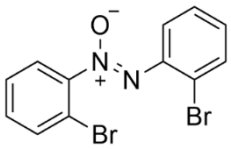	61	84	50
11	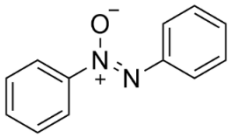	61	72	100
12	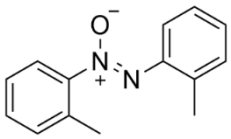	52	58	200
13	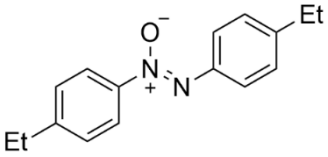	73	91	200
14	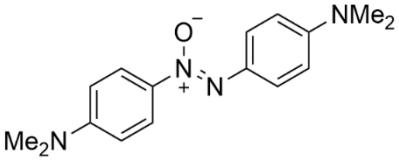	0	0	200

[a] Determined by ^{1}H-NMR of crude product. Using 0.05 M of nitrosoarene respective 0.025 M of cyclohexanone.

The reactions were studied with two equivalents of nitrosobenzene and one equivalent of cyclohexanone as additive. Regardless of the nature and position of the substituents at the ring, the conversions and yields being good to excellent, ranging from 58 % to 99 % and 52 % to 99 %, respectively. It was observed that, in cases of electron-donating substituents such as alkyl groups, the reaction times to reach high conversions were longer compared to electron withdrawing ones such as halides, esters and cyanides. Nitrosobenzenes with electron-withdrawing groups such as cyano (entries 1 and 9), nitro (entry 2), and ester (entries 3 and 7) at different positions were converted to the corresponding products in 93 - 99 %, respective 68 - 98 % isolated yields. Reactions of halogene-substituted nitrosobenzenes (entries 5, 6, 8 and 10) led to conversions of 84 - 98 % and isolated yields of 66 - 74 %. Furthermore, reactions of unsubstituted nitrosobenzene (entry 11) and reactions with electron-donating groups of alkyls at different positions (entries 12 and 13) were found to give lower conversions and required a longer reaction time with conversions from 58 % to 91 % and isolated yields ranging from 52 % to 73 %. A possible origin of the observed differences between conversion and yield could be enrichment processes of different degrees, in particular of the dipolar product molecules into the gel matrix. In case of the *p*-dimethylamino group (entry 14), only starting material was recovered. This is attributable to the electron abundance of the benzene moiety due to the particularly pronounced plus-I effect of the *p*-dimethylamino substituent and the resulting low formation of the dimer structure.[179,180] An evaluation of the reactions mentioned above indicates that both substituents in *ortho* position and electron-donating substituents inhibit the conversion of the nitroso compounds into the corresponding azoxy compounds which is in agreement with results reported in literature.[121]

4.4.3 Crystal Structures

The purity of the products obtained in chapter 4.4.2 allows the growth of suitable single crystals for X-ray diffraction spectroscopy by solvent evaporation or gas phase diffusion of isopropanol into a solution of the respective compound in chloroform. Suitable crystals could be obtained repeatedly within a few days. At the macroscopic level, the shape and color of the resulting crystals varied as shown in Figure 44.

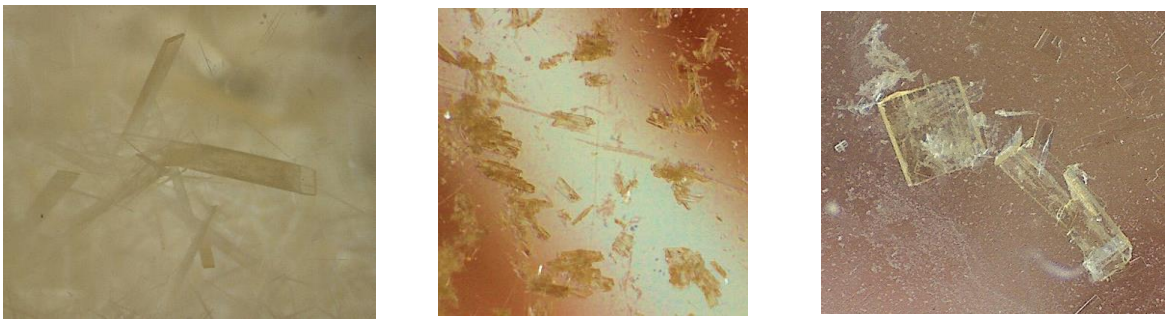

Figure 44: Crystal pictures of 1,2-Bis(4-chlorophenyl)diazene oxide (left), 1,2-Bis(4-bromophenyl)diazene oxide (middle), Dimethyl 3,3´-Diazene Oxide 1,2-Diyldibenzoate (right).

Dimethyl 3,3´-diazene oxide 1,2-diyldibenzoate (right) and 1,2-bis(4-bromophenyl)diazene oxide (middle) both tend to form plate shaped crystals. In contradistinction to 1,2-bis(4-bromophenyl)diazene oxide, 1,2-bis(4-chlorophenyl)diazene oxide (left) builds up rectangular shaped plates. Corresponding single crystals could be obtained for the products 1,2-bis(4-chlorophenyl)diazene oxide, 1,2-bis(4-bromophenyl)diazene

oxide and 3,3´-diazene oxide 1,2-diyldibenzoate. While the bromo derivative crystalized monoclinic in the $P2_1/c$ space group, the 1,2-bis(4-chlorophenyl)diazene oxide crystalized triclinic in the P-1 space group. In the examples examined, all molecules show the characteristic planar C_2N_2O core. In Table 15 and Table 16, the bond lengths together with a selection of the respective binding angles of the analyzed crystal structures are summarized.

Table 15: Bond lengths and angles of 1,2-bis(4-chlorophenyl)diazene oxide.

Bond lengths					
Bond	**Length [Å]**	**Average [Å]**	**Bond**	**Length [Å]**	**Average [Å]**
Cl(11)-C(4) Cl(12)-C(4)	1.7440(14) 1.786(4)	1.765(20)	Cl(21)-C(10) Cl(22)-C(10)	1.7382(17) 1.785(5)	1.761(85)
N(1)-C(1)	1.4213(14)		N(2)-C(7)	1.4521(14)	
O(12)-N(1)	1.433(4)		O(11)-N(2)	1.2980(14)	
N(1)-N(2)	1.2749(14)				
Angle [°]					
N(2)-N(1)-C(1)	119.30(9)				
N(2)-N(1)-O(12)	128.3(2)				
C(1)-N(1)-O(12)	109.1(2)				
N(1)-N(2)-O(11)	127.62(10)				
N(1)-N(2)-C(7)	116.80(9)				
O(11)-N(2)-C(7)	115.33(10)				

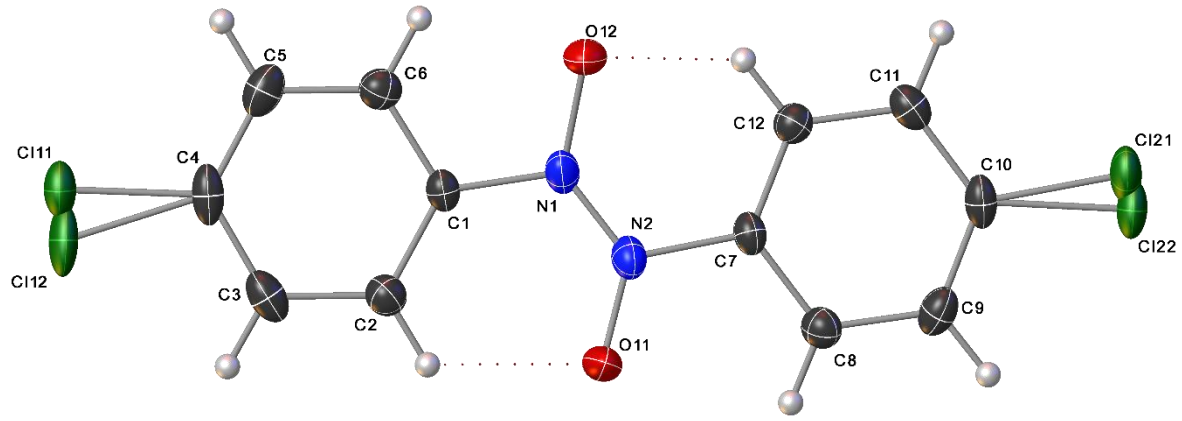

Figure 45: ORTEP diagram of 1,2-bis(4-chloroophenyl)diazene oxide. Representation as an ellipsoid with a 50 % probability of presence.

Detailed analyses of the crystals showed comparable, albeit slightly different, bond lengths and angles. These differences result from the electronic influences of the substituents on the aromatic rings. While in the case of unsubstituted azoxybenzene the N-N and N-O bond lengths are almost identical at 1.23 Å, the picture is different for the chlorine and bromine derivatives.[181] For both derivatives, the N-O bond is significantly longer than the N-N bond. While there are basically *cis* and *trans* isomers of azoxybenzenes, from the bond angles obtained it becomes clear that the formation of the thermodynamically more stable trans isomer is preferred when using the MFR concept for the reductive dimerization of nitrosoarenes to form azoxyarenes.

Table 16: Bond lengths and angles of 1,2-bis(4-bromophenyl)diazene oxide.

Bond	**Length [Å]**
Br(1)-C(1)	1.894(3)
O(1)-N(1)	1.342(6)
N(1)-C(4)	1.440(4)
N(1)-N(1)	1.267(5)

	Angle [°]
N(1)-N(1)-C(4)	117.3(4)
N(1)-N(1)-O(1)	129.6(4)
O(1)-N(1)-C(4)	112.9(3)

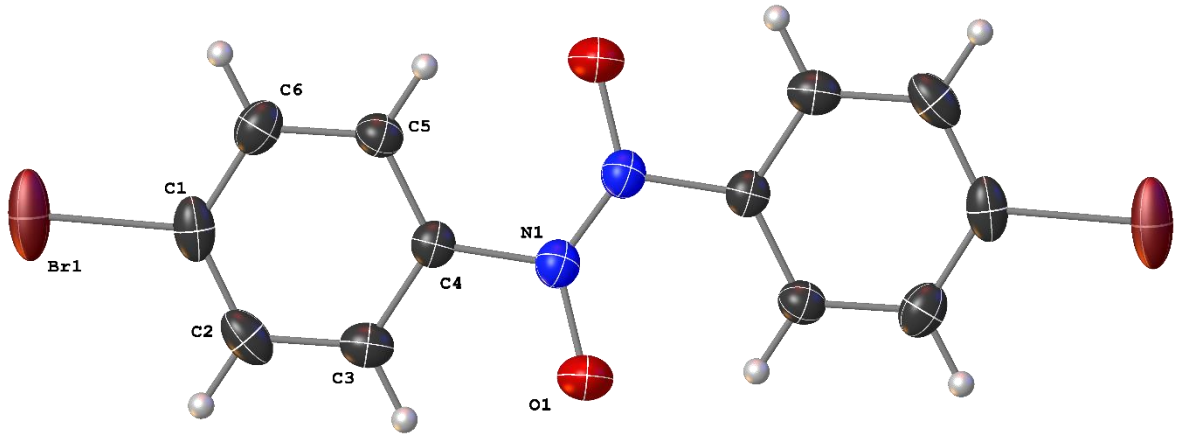

Figure 46: ORTEP diagram of 1,2-bis(4-bromophenyl)diazene oxide. Representation as an ellipsoid with a 50 % probability of presence.

In Figure 45 to Figure 47 the ORTEP diagrams of 1,2-Bis(4-chloroophenyl)diazene oxide and 1,2-Bis(4-bromophenyl)diazene oxide as well as 3,3´-diazene oxide 1,2-diyldibenzoate are shown as examples for the obtained crystal structures. In all cases, the compounds obtained are characterized by an inversion center in the middle of the N-N double bond. Furthermore, the positions of the oxygen atoms are half occupied due to the statistical distribution of the oxygen atoms bound to the nitrogen atoms. The oscillations of the substituents on the benzene rings, which also occur within the crystal lattice, lead to a blurring and less precise resolution of the position of the substituents within the ORTEP diagram. In extreme cases such as the chlorine derivative, this leads to allegedly four instead of two chlorine substituents being dissolved. In less pronounced examples, such as the bromine derivative, only pronounced blurring results in the distribution of the electron density (cf. Figure 46). As stated above, the high oscillation of the bromine atoms is visible due to the distorted ellipsoid. In Figure 47 the high impact of oscillation is especially visible within the aromatic ring.

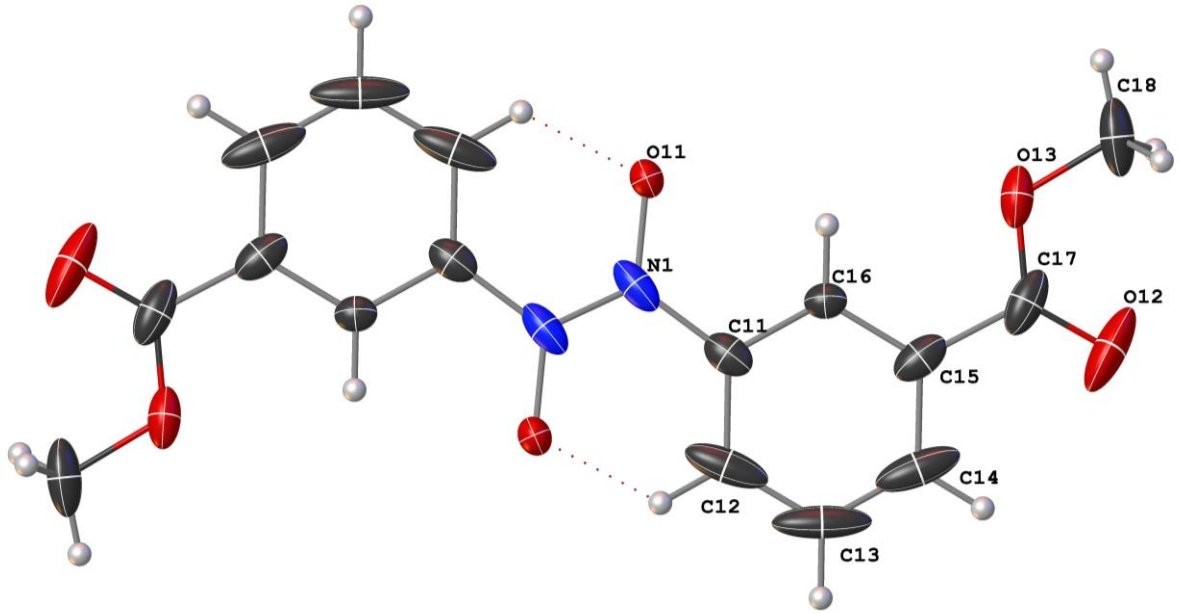

Figure 47: ORTEP diagram of 3,3´-diazene oxide 1,2-diyldibenzoate. Representation as an ellipsoid with a 50 % probability of presence.

By refining the results accordingly, ORTEP diagrams are provided for the respective structures, as shown in Figure 48.

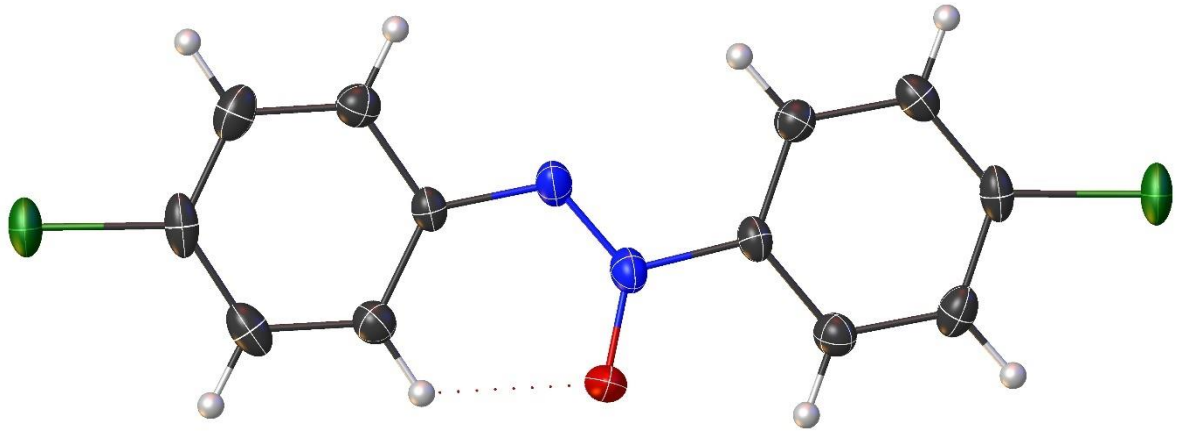

Figure 48: ORTEP diagram of 1,2-bis(4-chloroophenyl)diazene oxide. Representation as an ellipsoid with a 50 % probability of presence.

4.4.4 Catalytic Long-Term Behavior of the MFR system

To produce larger quantities of product, a gel-bound organocatalyst is required to have an outstanding stability and reusability.

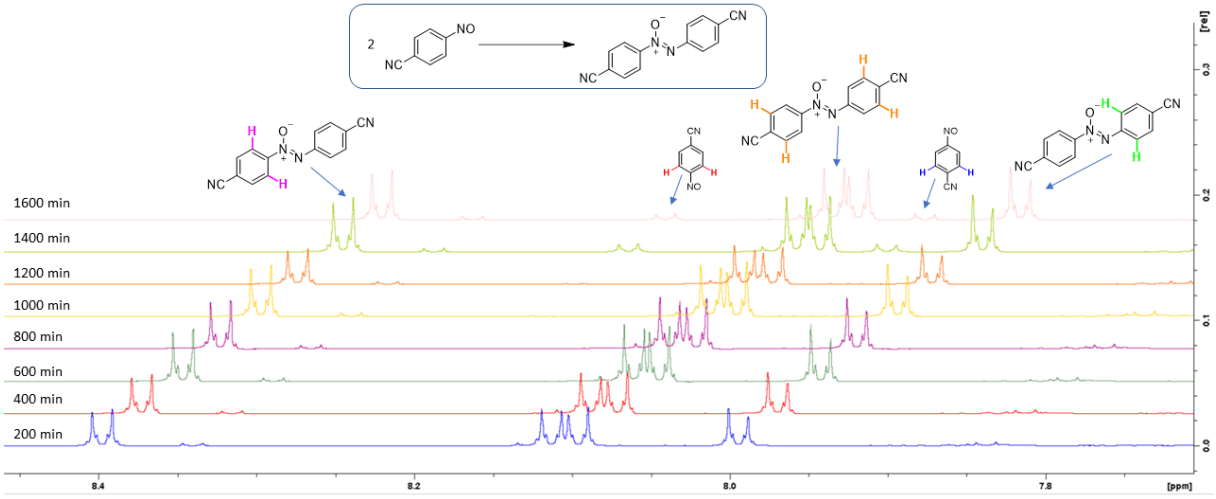

Figure 49: Example of the time depending NMR spectra for the reductive dimerization of 4-nitrosobenzonitrile to 1,2-bis(4-cyanophenyl)diazene oxide for the determination of the conversion via NMR.

As shown in Figure 49 and Figure 50, the conversion of 4-nitrosobenzonitrile only slightly decreases with longer reaction time. Specifically, after almost 24 h of reaction time, 91 (± 11) % conversion can be retained when the flow rate is kept at 1.0 $\frac{\mu l}{min}$.

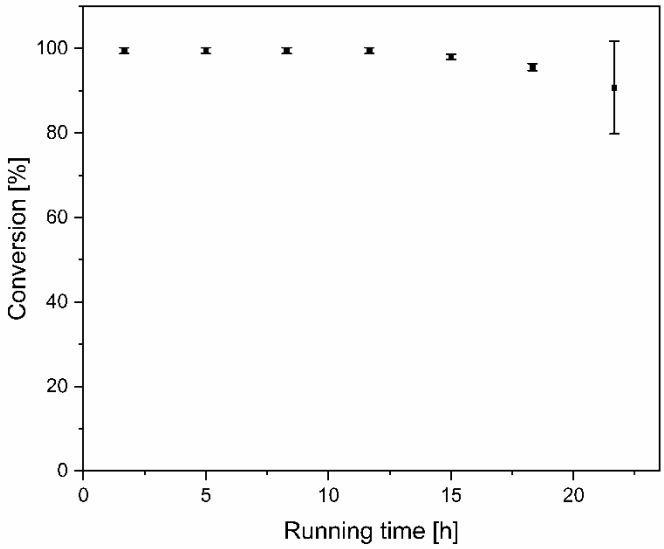

Figure 50: Long-term conversion behavior of the MFR measured by NMR when 4-nitrosobenzonitrile is injected at 1.0 $\frac{\mu l}{min}$ the reaction time is 100 min.

The running time was further extended to five days, applying a flow rate of 2.0 $\frac{\mu l}{min}$ (cf. Figure 51). Even after five days a conversion of still 67 (± 9) % was observed.

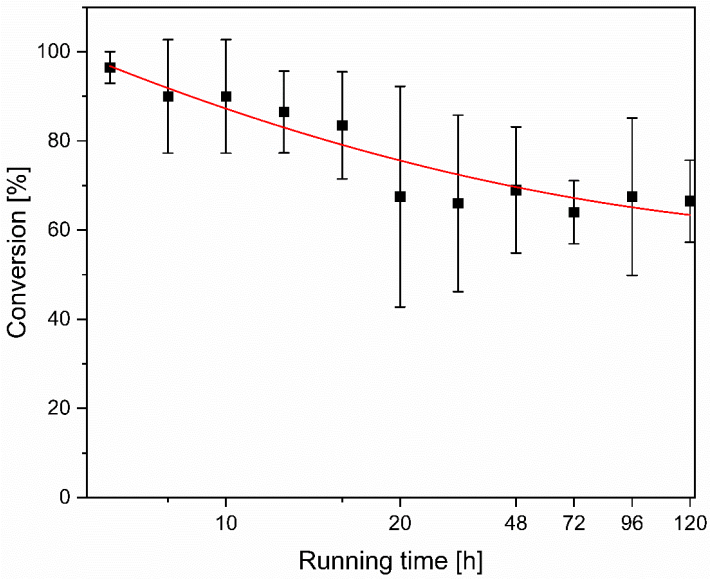

Figure 51: Long-term conversion of the reductive dimerization of 4-nitrosobenzonitrile at dwell times of 100 min in DMSO.

The decrease in conversion of 4-nitrosobenzonitrile can be explained by two different factors. The first factor is the inactivation of the catalyst due to repeated uses over time. The second factor is a possible enrichment of reactant as well as of azoxybenzene-molecules inside the gel dots due to undesired non-covalent interactions. This hypothesis would correspond to the observable color change of the gel dots shown in Figure 52 as an example which was also observed in previous works.[22,23] Figure 52 shows the gradual color change of the gel dots from the reactor inlet to the reactor outlet. The intensity of the coloring of the polymer dots decreased along the direction of flow of the reactant solution within the MFR. This could indicate a progressive accumulation of product within the gel dots. For the synthesis of 1,2-bis(4-cyanophenyl)diazene oxide from 4-nitrosobenzonitrile with cyclohexanone as an additive, the educt solution has a light green color, whereas a sample of the product solution collected over 24 h has an intense yellowish color (Figure 52).

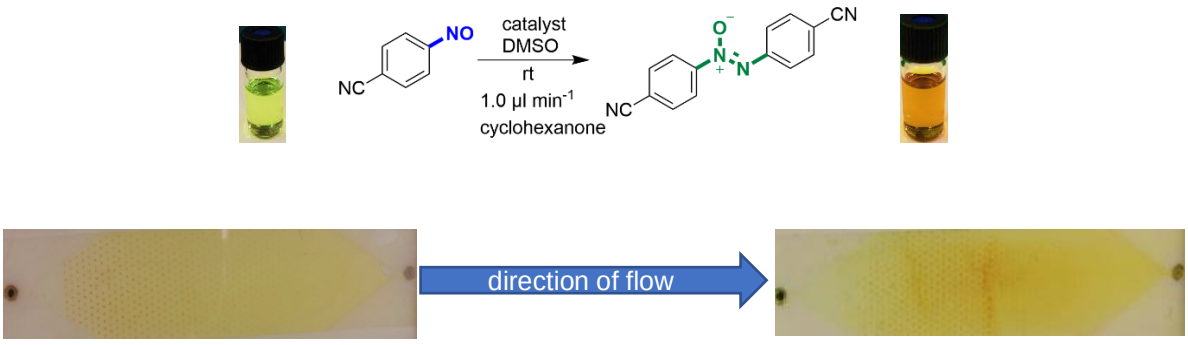

Figure 52: Color change of the MFR from light yellow after 1 h on the left to intense yellow after 24 h on the right, when 4-nitrosobenzonitrile is injected at 1.0 $\frac{\mu l}{min}$. Educt solution on the left, typical product solution on the right.

4.4.5 Attempt to Synthesize Asymmetric Azoxy Aromatics within the MFR

In addition to the production of "symmetrical" azoxycompounds, the examination of the MFR-concept for the synthesis of "asymmetric" adducts was also of interest (Figure 53). In principle, the mixing of two differently substituted nitrosobenzenes should result in four different azoxy compounds after the reaction. After a reaction of methyl 3-nitrosobenzoate with 1-bromo-4-nitrosobenzene and 1-nitro-3-nitrosobenzene with methyl 4-nitrosobenzoate, almost exclusively symmetrical adducts of both nitroso compounds were detected in the reaction mixture. Compounds 1 and 2 (Figure 53) were detected in traces in the reaction mixture only. This is in line with the results of CHUANG[121], where symmetrical azoxybenzenes were also obtained as the dominant product species. In the case of the MFR concept, this tendency seems to be reinforced, possibly by the different concentration of reactants and the low reaction temperature which does not lead to the formation of mixed dimers.

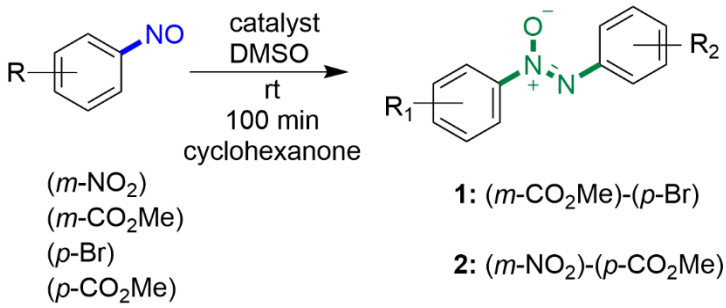

Figure 53: Overview reaction for the synthesis of asymmetric adducts. In both reactions, small amounts of starting materials were recovered.

4.4.6 Mechanistic Studies of the Reductive Dimerization of Nitrosoarenes

The improved reactivity of electron-poor nitroso compounds and the identification of hydroxycyclohexanone in the reaction solution indicate a possible reaction mechanism. As can be seen in Figure 55, the characteristic ^{1}H-NMR-signals as described previously[182] as well as a detailed analysis of the coupling of the hydroxy group and the proton in alpha position to the carbonyl function in hydroxycyclohexanone via 1D selective gradient COSY spectra are shown in Figure A1 to Figure A4. Nitrosobenzenes are well known to form dimers in a reversible equilibrium.[179] Nitrosobenzenes carrying electron-withdrawing substituents tend to favor the formation of dimers.[179] A key to a possible mechanism is the presence of the dimer structures as shown in Figure 54. In the MFR, a relatively high concentration of nitrosobenzenes were used[180,182,183] favoring dimer formation in conjunction with longer periods of rest in the syringe within the syringe pump. Further, no or only very little α-aminoxylated cyclohexanone[183] and no formation of asymmetric azoxybenzenes was detected.

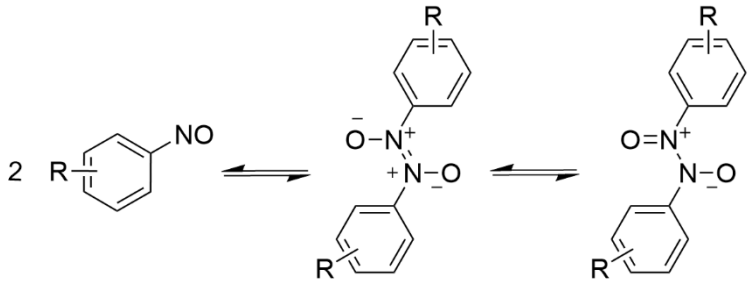

Figure 54: Equilibrium between monomer and dimer structures of nitrosobenzenes.

As shown in Figure 55, a possible mechanism for the formation of azoxybenzenes from nitrosobenzenes is proposed. The mechanism can be seen as a supplement to the work of BARBAS and colleagues who were able to produce α-hydroxy-ketones using L-proline, cyclic ketones and nitrosobenzene.[182] First, the secondary amine and the keto-species condense under formation of an iminium ion A. This is followed by a nucleophilic attack of the condensation product to the oxygen attached to a cationic nitrogen of the dimer B which forms intermediate C. Besides this, nucleophilic addition of the condensation product to excess nitrosobenzene may also take place, furnishing the α-aminoxy ketone.[182] Addition to excess nitrosoarene again leads to intermediate C.[118] However, as stated above, this seems not to be favorable. Tautomerization and hydrolysis of C leads to the formation of the *trans*-azoxyarene 1 and hydroxycyclohexanone D. Spectroscopic analyzes, which, however, also indicate that further reaction paths being taken, support the formation of α-hydroxycyclohexanone. In this context in particular, the poorer results for acetone appear to be reasonable.[102]

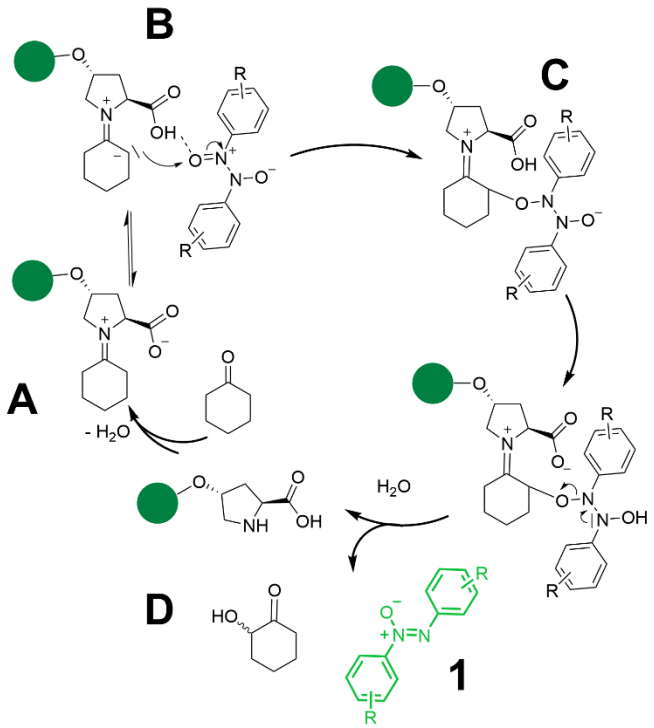

Figure 55: Proposed mechanism for the reductive dimerization of nitrosoarenes forming azoxyarenes using an immobilized proline catalyst.

4.4.7 Evaluation of the Turnover Frequency and Turnover Number

The TOF and TON were calculated to enable a comparison of our synthetic approach with other systems. The results are summarized in Table 17. In case of the MFR approach, TON between 3.34 and 1.27 and TOF values ranging from 3.02 h^{-1} to 0.31 h^{-1} were obtained. In contrast to that, mainly metal-based catalysts were described for the synthesis of azoxyarenes under batch conditions with TON between 8 and 32 and TOF between 0.5 h^{-1} and 2 h^{-1}.[184] Although a comparison of different TON and TOF is hardly possible due to the many influencing parameters, the results obtained for the MFR system are within the range of systems described in literature.[184] Nevertheless, higher TON and TOF values for the synthesis of azoxyarenes from different starting materials can be achieved using metal catalysts under batch conditions.[185] In spite of this, in comparison to the presented MFR approach, higher temperatures or significantly longer reaction times in combination with other harsh additives, such as H_2O_2 are required for the synthesis of azoxy compounds in all of the cases mentioned.

Table 17: Calculated TON and TOF for different reactions. $2.41 \cdot 10^{-2}$ mmol of catalyst A (immobilized on surface).[a]

Product [-]	Reaction running time [h]	TON [-]	Dwell time [min]	TOF [h^{-1}]
1	23	2.53	50	3.02
2	18	1.97	50	2.25
3	17.7	1.92	50	2.07
4	21.5	2.22	50	2.21
5	17	1.82	50	2.25
6	24	2.02	50	2.52
7	16	1.64	50	1.43
8	22	2.23	50	2.10
9	17	3.34	50	3.02
10	22	2.02	50	0.91
11	20	1.49	100	0.31
12	21	1.27	200	0.33
13	44	2.49	200	0.54

[a] A 0.05 M reactant solution was used. The conversions and reaction running times were used for TON calculations, isolated yields and dwell times of the MFR were used for TOF calculations.

5 Conclusion

The aim of the present work was to determine the potentials and possibilities, but also possible challenges, of using gels as carriers for organocatalysts in various reactions. Starting of the establishment of reliable and efficient synthesis routes for the desired organocatalyst structures which also run safely and selectively on the required scale. This could be achieved for both proline-based catalyst structures. The next task was to build up the appropriate methacrylate-based gels in a targeted manner and also to polymerize those with high spatial resolution. Furthermore, the reactor design had to be made more robust and the susceptibility to errors reduced in order to increase reproducibility at the same time. A further adaptation of the reactor design was made with a view to longer residence times and usage for more complex reactions. As a result of these modifications, it was possible to obtain a functional and efficient microfluidic reactor structure.

Using confocal laser microscopy, it was possible to determine the heights and to confirm the high spatial resolution of the polymer structures obtained. Based on these results, the polymer composition and synthesis were adapted to the reactor chamber in order to ensure the most efficient use of the MFR. Various parameters, such as irradiation time and crosslinker content, were varied and the influences examined in detail. As a result, the height of the network structures obtained could already be specifically adapted to the conditions and requirements within the MFR during the synthesis. The systems adjusted in this way were then built into the MFR and examined by performing various organocatalyzed reactions.

On the one hand, a classic organocatalyzed reaction within the MFR was investigated with the asymmetric aldol reaction. For this purpose, a catalyst structure based on a proline-amide was established. The corresponding in-depth analysis shows the general and extensive applicability of the MFR concept with immobilized L-proline based organocatalyst for carrying out the asymmetric aldol reaction with various substrates. In addition to determining the optimal reaction conditions, in particular targeted temperature control and solvent composition, other influencing factors were varied and examined in detail. Particularly, a direct relation between the height of the gel matrix and the conversion behavior of the MFR could be verified. Furthermore, with cyclohexanone and cyclopentanone as well as acetone, various ketones could be successfully converted as donors in the aldol reaction with different substituted aldehydes in relatively short reaction times. The yields and selectivities obtained are satisfactory to good. Based on this, the reusability of the reactor over several cycles with different ketones could also be demonstrated. Thus, investigations over 144 hours were carried out which showed the good long-term stability using the model substrates cyclohexanone and 4-nitrobenzaldehyde. Due to the longer operating times, the MFR is more efficient than comparable batch systems. This consideration was examined in the following based on a comparison of the MFR concept with a corresponding batch reaction. The analysis of the comparator system and the MFR revealed that the conversion achieved by both approaches differs dramatically. This advantage of the MFR concept could be due to the significantly higher local catalyst concentration within the reactor chamber of the MFR. In the case of the MFR, this is around 15 times higher than in a comparable batch system. A further comparison with catalyst systems for the asymmetric aldol reaction known from literature was carried out by comparing

TON and TOF. Here, too, it was shown that the MFR concept is inferior when compared to free catalysts in classic batch reactions but equivalent or even superior compared to other approaches to immobilize proline-based catalysts.

On the other hand, the application of the MFR concept for the synthesis of rather unusual organic compounds, the azoxy aromatic compounds, was applied and analyzed. In this case, too, a proline-based catalyst formed the foundation of the gel. And also in this study, the properties of a proline carrying polymer network were successfully adjusted in order to develop a versatile synthesis approach for the production of azoxybenzenes from nitrosobenzenes. Gel-bound proline served as a catalyst and cyclohexanone as an additive for this reductive dimerization. The properties of the methacrylate-based gel were adjusted in such a way that they enabled sufficient swelling but at the same time could withstand the mechanical stresses of continuous operation. With the optimized parameters in hand, the MFR was successfully used for the synthesis of a wide range of differently substituted azoxybenzenes. The different tendencies of nitroso compounds to form dimer structures and their influence on reaction time, conversion and yield agreed with previous findings. Apart from that, the established MFR also presents a good long-term activity for the continuous production of azoxybenzenes over 24 hours and 120 hours, respectively. Furthermore, it could also be shown in this reaction that the performance of the catalyst system, determined by TON and TOF, especially in view of the short reaction times and the mild conditions, can compete with established systems. In the case of reductive dimerization, an ongoing reaction with associated more diverse processes and a possible enrichment of educts and products within the gel dots could already be visually followed on the intensive color gradient during the reaction.

Some of the products obtained could also be analyzed in more detail based on corresponding single crystals. These investigations using single crystal X-ray diffractometry enabled further insights into the *trans*-selectivity of the reductive dimerization within the MFR.

A high long-term activity of the catalyst system could be determined for both of the observed reactions which, after an initial decline in conversion, changes into an increasingly constant conversion behavior. As a result, a high long-term activity could be determined based on the data obtained.

6 Outlook

Based on previous work, the focus of the present work was on expanding the application possibilities of the MFR concept to other, occasionally more sophisticated reactions. This was successfully demonstrated by means of two different reactions. Nevertheless, there is also great potential for future work. For example, the selectivity of the asymmetric aldol reaction could be increased by using other catalysts. With *(S)-N-((1S, 2S)*-2-hydroxy-1,2-diphenylethyl)pyrrolidine-2-carboxamide (Figure 56), a proline-based catalyst could also be immobilized via the primary alcohol function which might deliver higher selectivities and yields due to the higher steric demand of the phenyl substituents.[175] The analysis of whether the good yields and selectivities from batch operation can also be transferred to continuous operation of an MFR would be particularly interesting.

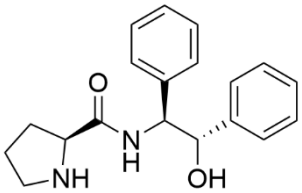

Figure 56: (S) -N - ((1S, 2S) -2-hydroxy-1,2-diphenylethyl) pyrrolidine-2-carboxamide.

Furthermore, by immobilizing other catalysts such as various diaryl-proline-ethers, other more complex reactions, including domino reactions, could be made accessible. A domino Michael aldol reaction of 1,2-diketones with various aldehydes offers enantioselective access to chiral cycloheptanones, tetrahydrochromenones and polyfunctionalized bicyclo [3.2.1] octanes. As shown in Figure 57, using cinnamaldehyde, dicyclo [3.2.1] octane-6-carbaldehyde was obtained in batch operation as a single diasteromer with the creation of four sterogenic centers.[186]

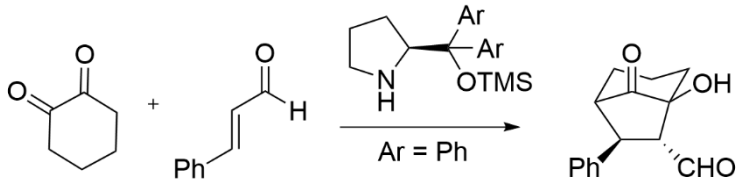

Figure 57: Example for the domino Michael aldol reaction of 1,2-cyclohexanedione with cinnamaldehyde.

Additionally, a further adaptation of the reactor design appears to be useful, especially for domino reactions. Multi-chamber systems could be used and established in order to catalyze the various stages of such a reaction selectively in individual reactor chambers.[74]

Moreover, on the basis of previous work, the Knoevenagel reaction could be investigated using more active, possibly secondary amines.[22]

Another aspect of particular interest would be an in-depth analysis of the various processes that take place within the polymer gels. So far, changes in the color of the gels over the operating time have only been determined on a purely visual basis and it is assumed that these may result from undesired enrichment

processes of the educts and products inside the gels. This could be analyzed more precisely by varying the crosslinker content and the size of the crosslinker used. So far, only low-molecular crosslinkers have been used to build up the gels, but the immobilization of macromolecular crosslinkers would also be of interest with regard to mesh size and enrichment processes. Specifically, poly(ethylene glycol)dimethacrylate (Figure 58) of varying molecular weights could be used.

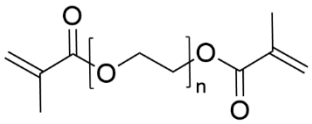

Figure 58: Structure of poly(ethylene glycol)dimethacrylate.

On the basis of this, the diffusion of various analytes into the gel structure could be followed through more in-depth analyzes such as Coherent Antistokes Raman Scattering (CARS).

7 List of Abbreviations

abs.	absolute
ATRP	Atom Transfer Radical Polymerization
aq	aqueous solution
BA	benzaldehyde
BOC	di-*tert*-butyl dicarbonate
br.	broad
BR	batch reactors
c	substance concentration
CARS	Coherent Antistokes Raman Scattering
$CDCl_3$	deuterated chloroform
cf.	confer
CH	cyclohexanone
CSTR	Continuous Stirred Tank Reactor
D	dispersion coefficient
Đ	dispersity
d	distance to light source
d (in context of NMR)	doublet
DCC	Dicyclohexylcarbodiimide
DCM	methylene chloride
DIPEA	*N*,*N*-Diisopropylethylamine
DHAP	dihydroxyacetone phosphate
D_2O	deuterated water
DMAP	4-(Dimethylamino)pyridine
DMF	*N*,*N*-Dimethylformamide

DMSO	dimethylsulfoxide
DMSO-d_6	deuterated DMSO
EDC-HCl	*N*-(3-Dimethylaminopropyl)-*N*'-ethylcarbodiimidehydrochloride
ee	enantiomeric excess
EGDMA	ethylene glycol dimethacrylate
EI-MS	Electron Impact Ionization Mass Spectrometry
ESI-MS	Electrospray Ionization Mass Spectrometry
EWG	electron withdrawing group
eq	equivalents
FR	flow reactors
GAP	glyceraldehyde-3-phosphate
h	hour
H	height
High Performance Liquid Chromatography	HPLC
HOBt	1-hydroxybenzotriazole hydrate
I	intensity
iD	inside diameter
*i*Prop	*iso*-propanol
IPF	Leibniz Institute for Polymer Research Dresden
LAP	lithium phenyl-2,4,6-trimethylbenzoylphosphinate
LCST	lower critical solution temperature
Lit.	literature
m (in context of NMR)	multiplet
MP	melting point
MFR	microfluidic reactor

MAOESLP	O-(2-methacryloyloxyethylsuccinoyl)-*trans*-4-hydroxy-L-prolin
MMA	methyl methacrylate
m/z	mass-charge-ratio
NIPAAm	*N*-isopropylacrylamide
NMR	Nuclear Magnetic Resonance
p.a.	pro analysis
PDMS	polydimethylsiloxane
PFR	Plug Flow Reactor
Pt (in context of NMR)	pseudo triplet
ppm	parts per million
PTFE	polytetrafluoroethylene
PVD	physical vapor deposition
Quant.	quantitative
Q_m	degree of mass swelling
QTOF	Quadrupole-Time-of-Flight
Q_v	degree of volume swelling
Re	Reynolds number
r.I.	relative intensity
S	styrene
s (in context of NMR)	singlet
sat.	saturated
sBR	semi-batch reactor
SPR	surface plasmon resonance spectroscopy
t	time
t (in context of NMR)	triplet
3TCSPMA	3-(trichlorosilyl)propyl methacrylate

TEA	triethylamine
THF	tetrahydrofuran
TOF	turnover frequency
TON	turnover number
UV/Vis	ultraviolet/visible
vs	versus
β	mass concentration
η	refractive index
ϱ	density
τ	dwell time

8 Conference Contributions and Publications

Table 18: List of poster presentations

Place	Meeting	Date
Halle (Saale)	Physical-Organic Chemistry at its Best: The Art of Chemical Problem Solving	09/2018
Dresden	Active Polymeric Materials and Microsystems	09/2019

Table 19: List of Publications

1.	C. J. Schmiegel, P. Berg, F. Obst, R. Schoch, D. Appelhans, D. Kuckling, „Continuous flow synthesis of azoxybenzenes by reductive dimerization of nitrosobenzenes with gel-bound catalysts", Eur. J. Org. Chem.. https://doi.org/10.1002/ejoc.202100006
2.	C. J. Schmiegel, R. Baier, D. Kuckling, „Direct asymmetric aldol reaction in continuous flow using gel-bound organocatalysts", Eur. J. Org. Chem.. https://doi.org/10.1002/ejoc.202100268

9 Publication Permission

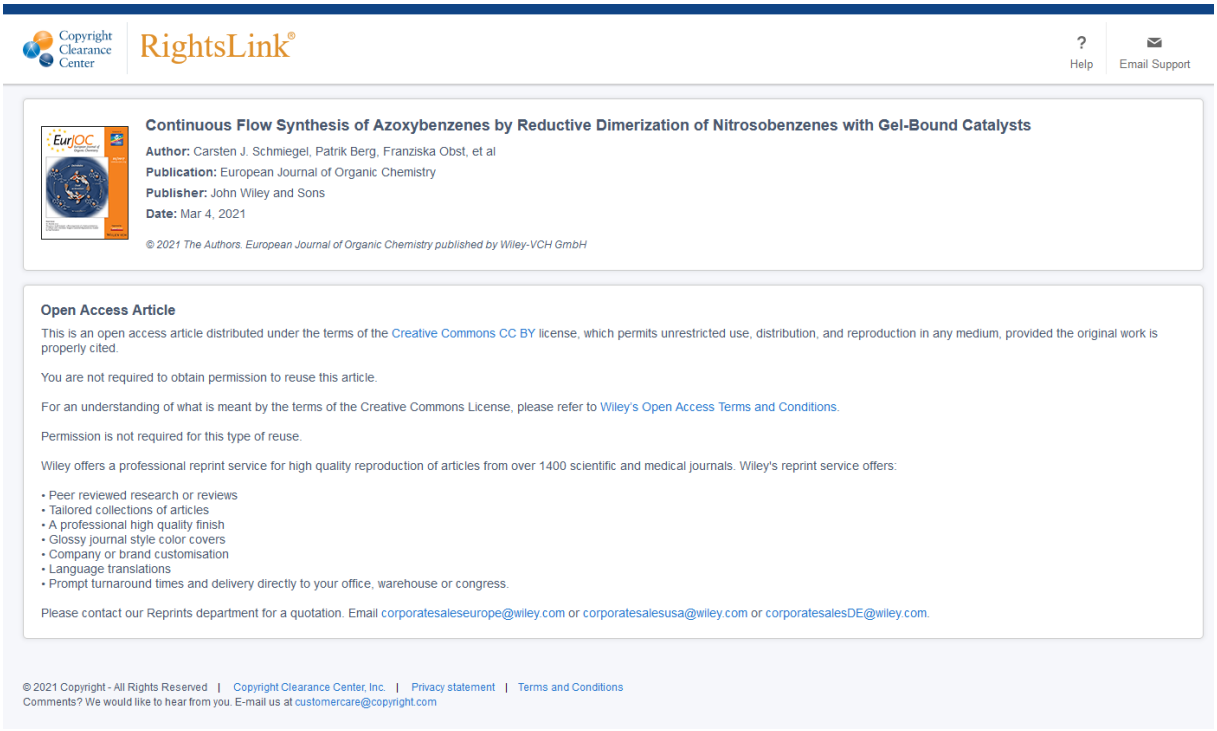

Copyright Clearance Center RightsLink® Help Email Support

Continuous Flow Synthesis of Azoxybenzenes by Reductive Dimerization of Nitrosobenzenes with Gel-Bound Catalysts

Author: Carsten J. Schmiegel, Patrik Berg, Franziska Obst, et al
Publication: European Journal of Organic Chemistry
Publisher: John Wiley and Sons
Date: Mar 4, 2021

© 2021 The Authors. European Journal of Organic Chemistry published by Wiley-VCH GmbH

Open Access Article

This is an open access article distributed under the terms of the Creative Commons CC BY license, which permits unrestricted use, distribution, and reproduction in any medium, provided the original work is properly cited.

You are not required to obtain permission to reuse this article.

For an understanding of what is meant by the terms of the Creative Commons License, please refer to Wiley's Open Access Terms and Conditions.

Permission is not required for this type of reuse.

Wiley offers a professional reprint service for high quality reproduction of articles from over 1400 scientific and medical journals. Wiley's reprint service offers:

- Peer reviewed research or reviews
- Tailored collections of articles
- A professional high quality finish
- Glossy journal style color covers
- Company or brand customisation
- Language translations
- Prompt turnaround times and delivery directly to your office, warehouse or congress.

Please contact our Reprints department for a quotation. Email corporatesaleseurope@wiley.com or corporatesalesusa@wiley.com or corporatesalesDE@wiley.com.

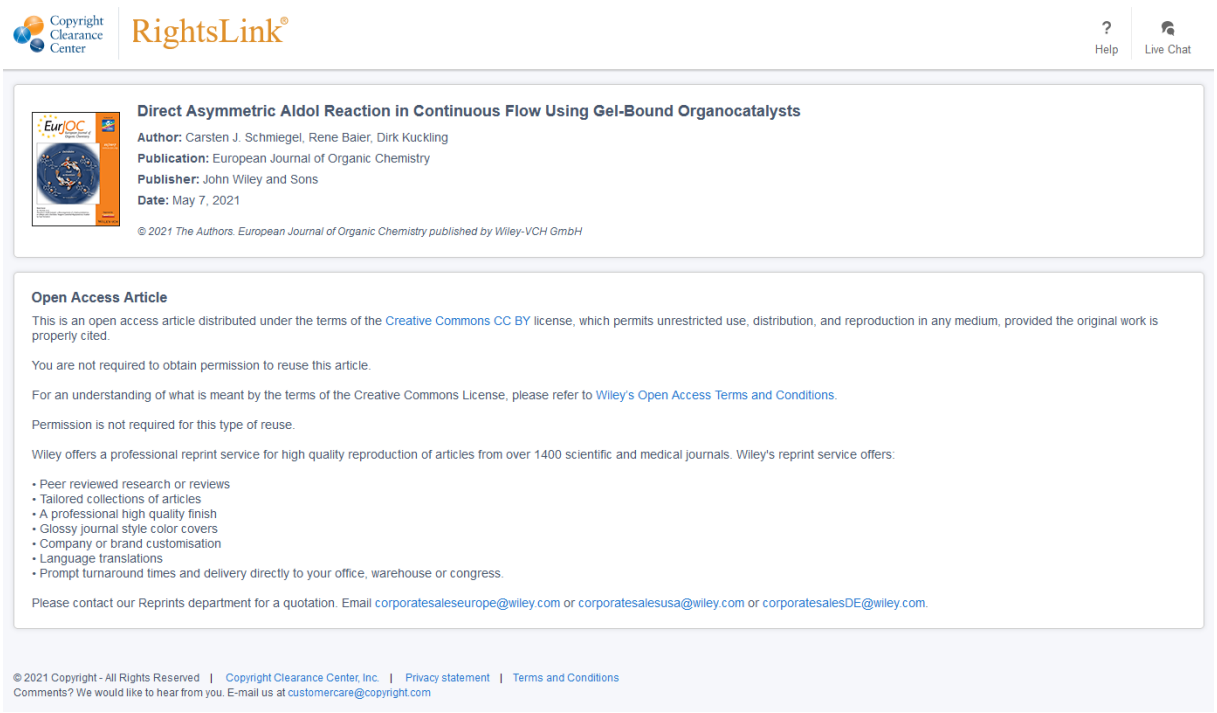

Copyright Clearance Center RightsLink® Help Live Chat

Direct Asymmetric Aldol Reaction in Continuous Flow Using Gel-Bound Organocatalysts

Author: Carsten J. Schmiegel, Rene Baier, Dirk Kuckling
Publication: European Journal of Organic Chemistry
Publisher: John Wiley and Sons
Date: May 7, 2021

© 2021 The Authors. European Journal of Organic Chemistry published by Wiley-VCH GmbH

Open Access Article

This is an open access article distributed under the terms of the Creative Commons CC BY license, which permits unrestricted use, distribution, and reproduction in any medium, provided the original work is properly cited.

You are not required to obtain permission to reuse this article.

For an understanding of what is meant by the terms of the Creative Commons License, please refer to Wiley's Open Access Terms and Conditions.

Permission is not required for this type of reuse.

Wiley offers a professional reprint service for high quality reproduction of articles from over 1400 scientific and medical journals. Wiley's reprint service offers:

- Peer reviewed research or reviews
- Tailored collections of articles
- A professional high quality finish
- Glossy journal style color covers
- Company or brand customisation
- Language translations
- Prompt turnaround times and delivery directly to your office, warehouse or congress.

Please contact our Reprints department for a quotation. Email corporatesaleseurope@wiley.com or corporatesalesusa@wiley.com or corporatesalesDE@wiley.com.

10 List of Figures

11 List of Tables

12 Formula Directory

$$d = \frac{V_{swollen}}{V_{dry}} \quad (1)$$

d = Degree of volume swelling [-]

$V_{swollen}$ = Volume of swollen gel [mm³]

V_{dry} = Volume of dry gel [mm³]

$$d_w = \frac{m_{swollen}}{m_{dry}} \quad (2)$$

d_w = Degree of weight swelling [-]

$m_{swollen}$ = Mass of swollen gel [g]

m_{dry} = Mass of dry gel [g]

$$TON = \frac{n_{Product}}{n_{Catalyst}} \quad (3)$$

TON = Turnover Number [-]

$n_{Product}$ = Amount of product $\left[\frac{mol}{l}\right]$

$n_{Catalyst}$ = Amount of catalyst $\left[\frac{mol}{l}\right]$

$$TOF = \frac{n_{Product}}{n_{Catalyst} \cdot t} \quad (4)$$

TOF = Turnover Frequency $\left[\frac{1}{h}\right]$

t = Time $[h]$

$$a = \frac{U}{m} \tag{5}$$

a = Enzyme activity $\left[\frac{\mu mol}{s \cdot mg}\right]$

U = Conversion rate of the enzyme for a substrate $\left[\frac{\mu mol}{s}\right]$

m = Amount of enzyme $[mg]$

$$v = k \cdot [A]^n \cdot [B]^m \tag{6}$$

v = Reaction rate $\left[\frac{mol}{l \cdot s}\right]$

k = reaction rate constant $\left[\left(\frac{1}{mol}\right)^{n+m-1} \cdot \frac{1}{s}\right]$

$[A]$ = Concentration reactant A $\left[\frac{mol}{l}\right]$

$[B]$ = Concentration reactant B $\left[\frac{mol}{l}\right]$

n, m = stoichiometric factors

$$v = -\frac{d[A]}{dt} = k \cdot [A]^n \cdot [B]^m \tag{7}$$

t = Time $[s]$

$$-\frac{d[A]}{dt} = k \cdot [A]^2 \tag{8}$$

$$[A]_t = \frac{[A]_0}{1 + k \cdot t \cdot [A]_0} \tag{9}$$

$[A]_0$ = Concentration reactant A at time t = 0 $\left[\frac{mol}{l}\right]$

$[A]_t$ = Concentration reactant A at time t $\left[\frac{mol}{l}\right]$

$$q_{ac} = q_r + q_{ex} + q_{fd} + q_s + q_{loss} \quad (10)$$

q_{ac} = Total thermal energy $[J]$

q_r = Thermal energy of the reaction $[J]$

q_{ex} = Thermal energy through exchange with heating or cooling element $[J]$

q_{fd} = Thermal energy of reactant solution $[J]$

q_s = Thermal energy generated by stirring $[J]$

q_{loss} = Thermal energy loss through exchange with environment $[J]$

$$-\frac{d[A]_t}{dt} = \frac{\dot{V}[A]_t}{V_0 + \dot{V}\,t} + k\,[A]_t^2 + k[A]_t\left(\frac{\dot{V}[B]_F\,t - [A]_0\,V_0}{V_0 + \dot{V}\,t}\right) \quad (11)$$

$$\frac{d[B]_t}{dt} = \frac{\dot{V}([B]_F - [B]_t)}{V_0 + \dot{V}\,t} - k[A]_t^2 + k[B]_t\left(\frac{\dot{V}[B]_F\,t - [A]_0\,V_0}{V_0 + \dot{V}\,t}\right) \quad (12)$$

$\dot{V}$ = Speed of influx $\left[\frac{m}{s}\right]$

$[B]_F$ = Concentration of reactant B in volume flow $\left[\frac{mol}{l}\right]$

V_0 = Volume of the submitted reactant solution A $[l]$

$$\tau = \frac{V_{Reactor}}{\dot{V}} \quad (13)$$

$\dot{V}$ = Volume influx $\left[\frac{l}{s}\right]$

$V_{Reactor}$ = Reactor volume $[l]$

τ = Residence time $[s]$

$$\dot{V} = \frac{V}{t} \tag{14}$$

V = Volume conveyed $[l]$

$$RD = \frac{D}{F \cdot L} \tag{15}$$

RD = Reaction dispersion number $[/]$

D = Dispersion coefficient $\left[\frac{1}{s}\right]$

F = Flow rate $\left[\frac{m}{s}\right]$

L = Length of the reactor $[m]$

$$F = \frac{\dot{V}}{A} \tag{16}$$

A = Cross sectional area $[m^2]$

$$Re = \frac{\rho \cdot F \cdot d}{\eta} \tag{17}$$

Re = Reynolds number $[/]$

ρ = Density of solvent $\left[\frac{kg}{l}\right]$

η = Viscosity $\left[\frac{kg}{m \cdot s}\right]$

d = Reactor diameter $[m]$

$$\left(\frac{H_2}{H_1}\right)_{SA} = \sqrt[3]{Q_{Iso.}} \tag{18}$$

$Q_{Iso.}$ = Degree of swelling of isotropically swollen gels $[/]$

H_1 = Height in the dried state $[cm]$

H_2 = Height in the swollen state $[cm]$

$$Q_{SA} = Q_{Iso.}^{\frac{5}{9}} \tag{19}$$

Q_{SA} = Degree of swelling of surface attached gels $[/]$

$$m = N \cdot \rho \cdot V = N \cdot \rho \cdot \pi \cdot r^2 \cdot H \tag{20}$$

m = Mass $[mg]$

N = Number of gel dots $[/]$

H = Height $[cm]$

r = Radius $[cm]$

$$n = N \cdot c \cdot V = N \cdot c \cdot \pi \cdot r^2 \cdot H \tag{21}$$

n = Amount of substance $[mmol]$

c = substance concentration $\left[\frac{mmol}{ml}\right]$

13 References

[1] a) J. H. Clark, *Green Chem.* **1999**, *1*, 1; b) P. T. Anastas, J. C. Warner, *Green chemistry. Theory and practice*, Oxford University Press, Oxford, **2000**.

[2] M. O'Brien, I. R. Baxendale, S. V. Ley, *Org. Lett.* **2010**, *12*, 1596.

[3] C. B. McPake, C. B. Murray, G. Sandford, *Tetrahedron Lett.* **2009**, *50*, 1674.

[4] a) F. Hammes, T. Broger, H.-U. Weilenmann, M. Vital, J. Helbing, U. Bosshart, P. Huber, R. P. Odermatt, B. Sonnleitner, *Cytometry. Part A.* **2012**, *81*, 508; b) D. Parida, C. A. Serra, F. Bally, D. K. Garg, Y. Hoarau, *Green Processing and Synthesis* **2012**, *1*.

[5] R. W. Coughlin, M. Aizawa, B. F. Alexander, M. Charles, *Biotechnol. Bioeng.* **1975**, *17*, 515.

[6] D. Steinborn, *Grundlagen der metallorganischen Komplexkatalyse*, Teubner, Wiesbaden, **2007**.

[7] J. M. Berg, J. L. Tymoczko, L. Stryer, *Biochemie*, Spektrum Akad. Verl., Heidelberg, **2003**.

[8] D. W. C. MacMillan, *Nature* **2008**, *455*, 304.

[9] B. List, R. A. Lerner, C. F. Barbas, *J. Am. Chem. Soc.* **2000**, *122*, 2395.

[10] S. G. Nelson, *Tetrahedron: Asymmetry* **1998**, *9*, 357.

[11] H.-D. Jakubke, H. Jeschkeit, *Aminosäuren, Peptide, Proteine*, Verl. Chemie, Weinheim, **1982**.

[12] a) C. Y. Lai, N. Nakai, D. Chang, *Science (New York, N.Y.)* **1974**, *183*, 1204; b) J. J. Marsh, H. G. Lebherz, *Trends Biochem. Sci.* **1992**, *17*, 110.

[13] J.-W. Lee, T. Mayer-Gall, K. Opwis, C. E. Song, J. S. Gutmann, B. List, *Science (New York, N.Y.)* **2013**, *341*, 1225.

[14] S. Itsuno, M. M. Hassan, *RSC Adv* **2014**, *4*, 52023.

[15] M. Gruttadauria, F. Giacalone, R. Noto, *Chem. Soc. rev.* **2008**, *37*, 1666.

[16] M. Benaglia, G. Celentano, F. Cozzi, *Adv. Synth. Catal.* **2001**, *343*, 171.

[17] M. Benaglia, M. Cinquini, F. Cozzi, A. Puglisi, G. Celentano, *Adv. Synth. Catal.* **2002**, *344*, 533.

[18] E. Huerta, P. J. M. Stals, E. W. Meijer, A. R. A. Palmans, *Angew. Chem.* **2013**, *125*, 2978.

[19] X. Yu, A. Herberg, D. Kuckling, *Eur. Polym. J.* **2019**, *120*, 109207.

[20] H. A. Zayas, A. Lu, D. Valade, F. Amir, Z. Jia, R. K. O'Reilly, M. J. Monteiro, *ACS Macro Lett.* **2013**, *2*, 327.

[21] D. Simon, F. Obst, S. Haefner, T. Heroldt, M. Peiter, F. Simon, A. Richter, B. Voit, D. Appelhans, *React. Chem. Eng.* **2019**, *4*, 67.

[22] P. Berg, F. Obst, D. Simon, A. Richter, D. Appelhans, D. Kuckling, *Eur. J. Org. Chem.* **2020**.

[23] P. Berg, UB-PAD - Paderborn University Library, **2020**.

[24] C. J. Schmiegel, P. Berg, F. Obst, R. Schoch, D. Appelhans, D. Kuckling, *Eur. J. Org. Chem.* **2021**, *2021*, 1628.

[25] C. J. Schmiegel, R. Baier, D. Kuckling, *Eur. J. Org. Chem.* **2021**, *2021*, 2578.

[26] J. e. a. Nič, *IUPAC Compendium of Chemical Terminology*, **2019**.

[27] M. Rubinstein, R. H. Colby, *Polymer physics*, Oxford University Press, Oxford, **2008**.

[28] J. Li, C. Ji, X. Yu, M. Yin, D. Kuckling, *Macromol. Rapid Commun.* **2019**, *40*, e1900189.

[29] Z. Gong, G. Zhang, X. Zeng, J. Li, G. Li, W. Huang, R. Sun, C. Wong, *ACS Appl. Mater. interfaces* **2016**, *8*, 24030.

[30] X. Li, Q. Yang, Y. Zhao, S. Long, J. Zheng, *Soft matter* **2017**, *13*, 911.

[31] H. J. Naghash, O. Okay, H. Yildirim, *J. Appl. Polym. Sci.* **1995**, *56*, 477.

[32] M. Tomida, M. Yabe, Y. Arakawa, M. Kunioka, *Polymer* **1997**, *38*, 2791.

[33] S. Buathong, F. Peruch, F. Isel, P. J. Lutz, *Des. Monomers Polym.* **2004**, *7*, 583.

[34] C. Decker, C. Bianchi, *Polym. Int.* **2003**, *52*, 722.

[35] P. Kovacic, R. W. Hein, *J. Am. Chem. Soc.* **1959**, *81*, 1187.

[36] Ji Li, *UB-Pad - Paderborn University Libary*, **2018**.

[37] A. Keller, *Faraday Disc.* **1995**, *101*, 1.

[38] L. Z. Rogovina, V. G. Vasil'ev, E. E. Braudo, *Polym. Sci. Ser. C* **2008**, *50*, 85.

[39] P. J. Flory, *Faraday Discuss. Chem. Soc.* **1974**, *57*, 7.

[40] M. Heskins, J. E. Guillet, *J. Macromol. Sci. Pure Appl. Chem.* **1968**, *2*, 1441.

[41] S. Sun, J. Hu, H. Tang, P. Wu, *J. Phys. Chem. B* **2010**, *114*, 9761.

[42] J. P. Cohen Addad, *Physical properties of polymeric gels*, J. Wiley, Chichester, New York, **1996**.

[43] M. L. Wolfrom, R. Montgomery, J. V. Karabinos, P. Rathgeb, *J. Am. Chem. Soc.* **1950**, *72*, 5796.

[44] S. J. Craythorne, C. L. Pollock, A. J. Blake, M. Nieuwenhuyzen, A. C. Marr, P. C. Marr, *New J. Chem.* **2009**, *33*, 479.

[45] B. H. Cipriano, S. J. Banik, R. Sharma, D. Rumore, W. Hwang, R. M. Briber, S. R. Raghavan, *Macromolecules* **2014**, *47*, 4445.

[46] R. Toomey, D. Freidank, J. Rühe, *Macromolecules* **2004**, *37*, 882.

[47] J. W. Gunn, S. D. Turner, B. K. Mann, *J. Biomed. Mater. Res. A* **2005**, *72*, 91.

[48] T. Çaykara, E. Turan, *Colloid Polym. Sci.* **2006**, *284*, 1038.

[49] a) K. Haraguchi, T. Takehisa, *Adv. Mater.* **2002**, *14*, 1120; b) K. Haraguchi, H.-J. Li, *Macromolecules* **2006**, *39*, 1898.

[50] A. Srivastava, E. Jain, A. Kumar, *Mater. Sci. Eng. A* **2007**, *464*, 93.

[51] a) S. Zheng, T. Wang, D. Liu, X. Liu, C. Wang, Z. Tong, *Polymer* **2013**, *54*, 1846; b) B. Strachota, M. Šlouf, J. Hodan, L. Matějka, *Colloid Polym. Sci.* **2018**, *296*, 753.

[52] D. Ceylan, M. M. Ozmen, O. Okay, *J. Appl. Polym. Sci.* **2006**, *99*, 319.

[53] K. Y. Lee, J. A. Rowley, P. Eiselt, E. M. Moy, K. H. Bouhadir, D. J. Mooney, *Macromolecules* **2000**, *33*, 4291.

[54] a) I. Anac, A. Aulasevich, M. J. N. Junk, P. Jakubowicz, R. F. Roskamp, B. Menges, U. Jonas, W. Knoll, *Macromol. Chem. Phys.* **2010**, *211*, 1018; b) B. W. Garner, T. Cai, S. Ghosh, Z. Hu, A. Neogi, *Appl. Phys. Express* **2009**, *2*, 57001.

[55] A. Röseler, *Infrared Physics* **1981**, *21*, 349.

[56] L. Y. Tyng, M. R. Ramli, M. B. H. Othman, R. Ramli, Z. A. M. Ishak, Z. Ahmad, *Polym. Int.* **2013**, *62*, 382.

[57] W. T. Truong, Y. Su, J. T. Meijer, P. Thordarson, F. Braet, *Chem. Asian J.* **2011**, *6*, 30.

[58] a) T. A. Burdon, D. C. Miller, P. E. Oyer, R. S. Mitchell, E. B. Stinson, V. A. Starnes, N. E. Shumway, *J. Thorac. Cardiovasc. Surg.* **1992**, *103*, 238; b) W. K. Wan, G. Campbell, Z. F. Zhang, A. J. Hui, D. R. Boughner, *J. Biomed. Mater. Res.* **2002**, *63*, 854.

[59] O. WICHTERLE, D. LÍM, *Nature* **1960**, *185*, 117.

[60] N. A. Peppas, *Curr. Opin. Colloid Interface Sci.* **1997**, *2*, 531.

[61] G. Yang, H. Han, C. Du, Z. Luo, Y. Wang, *Polymer* **2010**, *51*, 6193.

[62] A. Dehennis, M. A. Mortellaro, S. Ioacara, *J. Diabetes Sci. Technol.* **2015**, *9*, 951.

[63] H. L. Fisher, *Ind. Eng. Chem.* **1939**, *31*, 1381.

[64] D. Díaz Díaz, D. Kühbeck, R. J. Koopmans, *Chem. Soc. rev.* **2011**, *40*, 427.

[65] a) T. Kureha, Y. Nagase, D. Suzuki, *ACS omega* **2018**, *3*, 6158; b) K. S. Sivudu, N. M. Reddy, M. N. Prasad, K. M. Raju, Y. M. Mohan, J. S. Yadav, G. Sabitha, D. Shailaja, *J. Mol. Catal. A- Chem.* **2008**, *295*, 10.

[66] A. Pimpin, W. Srituravanich, *EJ* **2012**, *16*, 37.

[67] A. Revzin, R. J. Russell, V. K. Yadavalli, W. G. Koh, C. Deister, D. D. Hile, M. B. Mellott, M. V. Pishko, *Langmuir* **2001**, *17*, 5440.

[68] O. Prucker, M. Schimmel, G. Tovar, W. Knoll, J. Rühe, *Adv. Mater.* **1998**, *10*, 1073.

[69] J. T. Fourkas, *J. Phys. Chem. Lett.* **2010**, *1*, 1221.

[70] S. Guillon, R. Lemaire, A. V. Linares, K. Haupt, C. Ayela, *Lab on a chip* **2009**, *9*, 2987.

[71] M. Kuwahara, T. Nakano, J. Tominaga, M. B. Lee, N. Atoda, *Jpn. J. Appl. Phys.* **1999**, *38*, L1079-L1081.

[72] a) A. V. Linares, A. Falcimaigne-Cordin, L. A. Gheber, K. Haupt, *Small (Weinheim an der Bergstrasse, Germany)* **2011**, *7*, 2318; b) M. F. Montague, C. J. Hawker, *Chem. Mater.* **2007**, *19*, 526.

[73] J.-F. Chang, M. C. Gwinner, M. Caironi, T. Sakanoue, H. Sirringhaus, *Adv. Funct. Mater.* **2010**, *20*, 2825.

[74] F. Obst, D. Simon, P. J. Mehner, J. W. Neubauer, A. Beck, O. Stroyuk, A. Richter, B. Voit, D. Appelhans, *React. Chem. Eng.* **2019**, *4*, 2141.

[75] J. Clayden, N. Greeves, S. G. Warren, *Organische Chemie*, Springer Spektrum, Berlin, Heidelberg, **2013**.

[76] P. W. Atkins, J. de Paula, *Physikalische Chemie*, Wiley-VCH, Weinheim, **2010**.

[77] a) S. W. Ragsdale, *Chem. Rev.* **2006**, *106*, 3317; b) R. H. Crabtree, *Chem. Rev.* **2012**, *112*, 1536.

[78] J. A. Ewen, R. L. Jones, A. Razavi, J. D. Ferrara, *J. Am. Chem. Soc.* **1988**, *110*, 6255.

[79] C. Kaes, A. Katz, M. W. Hosseini, *Chem. Rev.* **2000**, *100*, 3553.

[80] a) K. Hou, H. T. Poh, W. Y. Fan, *Chem. Commun.* **2014**, *50*, 6630; b) M. L. Helm, M. P. Stewart, R. M. Bullock, M. R. DuBois, D. L. DuBois, *Science (New York, N.Y.)* **2011**, *333*, 863.

[81] a) K. Ziegler, E. Holzkamp, H. Breil, H. Martin, *Angew. Chem.* **1955**, *67*, 541; b) G. Natta, *Angew. Chem.* **1964**, *76*, 553.

[82] J. A. Keith, R. J. Nielsen, J. Oxgaard, W. A. Goddard, *J. Am. Chem. Soc.* **2007**, *129*, 12342.

[83] G. J. Sunley, D. J. Watson, *Catal.* **2000**, *58*, 293.

[84] W. J. Choi, *Appl. Microbiol. Biotechnol.* **2009**, *84*, 239.

[85] F. Horn, *Biochemie des Menschen*, Thieme, Stuttgart, New York, **2021**.

[86] T. Ke, A. M. Klibanov, *Biotechnol. Bioeng.* **1998**, *57*, 746.

[87] a) L. Ceci, J. Lozano, *Food Chem.* **1998**, *61*, 237; b) E. Lee, Y. Oh, Y. K. Choi, M.-J. Kim, *ACS Catal.* **2014**, *4*, 3590; c) C. Madden, M. D. Vaughn, I. Díez-Pérez, K. A. Brown, P. W. King, D. Gust, A. L. Moore, T. A. Moore, *J. Am. Chem. Soc.* **2012**, *134*, 1577.

[88] K. A. Ahrendt, C. J. Borths, D. W. C. MacMillan, *J. Am. Chem. Soc.* **2000**, *122*, 4243.

[89] W. S. Jen, J. J. M. Wiener, D. W. C. MacMillan, *J. Am. Chem. Soc.* **2000**, *122*, 9874.

[90] N. A. Paras, D. W. MacMillan, *J. Am. Chem. Soc.* **2001**, *123*, 4370.

[91] M. P. Brochu, S. P. Brown, D. W. C. MacMillan, *J. Am. Chem. Soc.* **2004**, *126*, 4108.

[92] T. D. Beeson, D. W. C. MacMillan, *J. Am. Chem. Soc.* **2005**, *127*, 8826.

[93] M. T. Hechavarria Fonseca, B. List, *Angew. Chem.* **2004**, *116*, 4048.

[94] a) B. R. Buckley, *Annu. Rep. Prog. Chem., Sect. B: Org. Chem.* **2009**, *105*, 113; b) J. G. Hernández, E. Juaristi, *Chem. Commun.* **2012**, *48*, 5396.

[95] a) J. L. Methot, W. R. Roush, *Adv. Synth. Catal.* **2004**, *346*, 1035; b) T. Werner, *Adv. Synth. Catal.* **2009**, *351*, 1469.

[96] D. Enders, O. Niemeier, A. Henseler, *Chem. Rev.* **2007**, *107*, 5606.

[97] B. List, *Asymmetric Organocatalysis*, Springer Berlin Heidelberg, Berlin, Heidelberg, **2009**.

[98] J. Wang, P. Li, P. Y. Choy, A. S. C. Chan, F. Y. Kwong, *ChemCatChem* **2012**, *4*, 917.

[99] K. Schulz, L. Ratjen, J. Martens, *Tetrahedron* **2011**, *67*, 546.

[100] V. Maya, M. Raj, V. K. Singh, *Org. Lett.* **2007**, *9*, 2593.

[101] L. Kürti, B. Czako, *Strategic applications of named reactions in organic synthesis. Background and detailed mechanisms*, Elsevier Academic, Burlington, MA, **2005**.

[102] A. Córdova, W. Zou, P. Dziedzic, I. Ibrahem, E. Reyes, Y. Xu, *Chemistry (Weinheim an der Bergstrasse, Germany)* **2006**, *12*, 5383.

[103] L.-W. Xu, J. Luo, Y. Lu, *Chem. Commun.* **2009**, 1807.

[104] a) X. Yu, W. Wang, *Org. Biomol. Chem.* **2008**, *6*, 2037; b) A. J. A. Cobb, D. M. Shaw, D. A. Longbottom, J. B. Gold, S. V. Ley, *Org. Biomol. Chem.* **2005**, *3*, 84.

[105] X. Chen, J. Wang, Y. Zhu, D. Shang, B. Gao, X. Liu, X. Feng, Z. Su, C. Hu, *Chemistry (Weinheim an der Bergstrasse, Germany)* **2008**, *14*, 10896.

[106] J. Seayad, B. List, *Org. Biomol. Chem.* **2005**, *3*, 719.

[107] M. Ahmed, A. G. Barrett, D. Braddock, S. M. Cramp, P. A. Procopiou, *Tetrahedron Lett.* **1999**, *40*, 8657.

[108] N. T. Phan, D. H. Brown, P. Styring, *Tetrahedron Lett.* **2004**, *45*, 7915.

[109] M. Gruttadauria, F. Giacalone, A. Mossuto Marculescu, P. Lo Meo, S. Riela, R. Noto, *Eur. J. Org. Chem.* **2007**, *2007*, 4611.

[110] S. Bahmanyar, K. N. Houk, *J. Am. Chem. Soc.* **2001**, *123*, 12911.

[111] S. Mukherjee, J. W. Yang, S. Hoffmann, B. List, *Chem. Rev.* **2007**, *107*, 5471.

[112] B. List, L. Hoang, H. J. Martin, *Proceedings of the National Academy of Sciences of the United States of America* **2004**, *101*, 5839.

[113] a) D. Campbell, *Dyes Pigm.* **1995**, *29*, 77; b) S. Patai (Ed.) *The chemistry of functional groups. Supplement F*, John Wiley & Sons, Chichester, **1982**; c) B. M. Trost, I. Fleming (Eds.) *Comprehensive organic synthesis. Selectivity, strategy & efficiency in modern organic chemistry*, Pergamon Press, Oxford, **1991**; d) T. Ikeda, O. Tsutsumi, *Science (New York, N.Y.)* **1995**, *268*, 1873.

[114] a) S. B. Waghmode, S. M. Sabne, S. Sivasanker, *Green Chem.* **2001**, *3*, 285; b) A. B. E. Vix, P. Müller-Buschbaum, W. Stocker, M. Stamm, J. P. Rabe, *Langmuir* **2000**, *16*, 10456; c) A. Rezaeifard, M. Jafarpour, M. A. Naseri, R. Shariati, *Dyes Pigm.* **2008**, *76*, 840.

[115] a) H. Kagechika, T. Himi, K. Namikawa, E. Kawachi, Y. Hashimoto, K. Shudo, *J. Med. Chem.* **1989**, *32*, 1098; b) H. Takahashi, T. Ishioka, Y. Koiso, M. Sodeoka, Y. Hashimoto, *Biol. Pharm. Bull.* **2000**, *23*, 1387.

[116] a) L. Hou, X. Chen, S. Li, S. Cai, Y. Zhao, M. Sun, X.-J. Yang, *Org. Biomol. Chem.* **2015**, *13*, 4160; b) H. Li, P. Li, Q. Zhao, L. Wang, *Chem. Commun.* **2013**, *49*, 9170; c) H. Li, X. Xie, L. Wang, *Chem. Commun.* **2014**, *50*, 4218; d) D. Zhang, X. Cui, F. Yang, Q. Zhang, Y. Zhu, Y. Wu, *Org. Chem. Front.* **2015**, *2*, 951.

[117] L. Ke, G. Zhu, H. Qian, G. Xiang, Q. Chen, Z. Chen, *Org. Lett.* **2019**, *21*, 4008.

[118] A. R. Becker, L. A. Sternson, *J. Org. Chem.* **1980**, *45*, 1708.

[119] S. S. Acharyya, S. Ghosh, R. Bal, *ACS Sustainable Chem. Eng.* **2014**, *2*, 584.

[120] S. P. Annen, H. Grützmacher, *Dalton Trans.* **2012**, *41*, 14137.

[121] Y.-F. Chen, J. Chen, L.-J. Lin, G. J. Chuang, *J. Org. Chem.* **2017**, *82*, 11626.

[122] Y. Nishiyama, A. Fujii, H. Mori, *React. Chem. Eng.* **2019**, *16*, 10456.

[123] K. Hertwig, L. Martens, C. Hamel, *Chemische Verfahrenstechnik. Berechnung, Auslegung, und Betrieb chemischer Reaktoren*, De Gruyter, Berlin, Boston, **2018**.

[124] F. Bergamelli, M. Iannelli, J. A. Marafie, J. D. Moseley, *Org. Process Res. Dev.* **2010**, *14*, 926.

[125] Dirk Thoenes, *Chemical Reactor Development*, Springer-Verlag, **2013**.

[126] F. Stoessel, *Thermal safety of chemical processes. Risk assessment and process design*, Wiley-VCH, Weinheim, **2009**.

[127] R. M. Felder, F. B. Hill, *Chem. Eng. Sci.* **1969**, *24*, 385.

[128] R. J. Willey, F. Rodrigues, S. Chippett, G. Melhem, S. K. Singh, *Proc. Safety Prog.* **2001**, *20*, 123.

[129] T.-C. Ho, Y.-S. Duh, J. R. Chen, *Proc. Safety Prog.* **1998**, *17*, 259.

[130] T. A. Kletz, *Proc. Safety Prog.* **1996**, *15*, 5.

[131] F. E. Powell, B. W. Brooks, *Chem. Eng. Sci.* **1995**, *50*, 837.

[132] G. Donati, *Catal. Today* **1999**, *52*, 183.

[133] S. Tapio, M. Jyri-Pekka, W. Johan, *Chemical Reaction Engineering and Reactor Technology*, Chapman and Hall/CRC, Boca Raton, FL : CRC Press, Taylor & Francis Group, 2019., **2019**.

[134] M. Giridhar, K. Krishnaiah, *Bioprocess Eng.* **1993**, *9*, 263.

[135] F. S. Mjalli, J. N. Subramanian, *Int. J. Chem. React. Eng.* **2008**, *6*.

[136] H. S. Sidhu, S. D. Watt, M. I. Nelson, A. K. Ray, *Int. J. Chem. React. Eng.* **2007**, *5*.

[137] J. Wegner, S. Ceylan, A. Kirschning, *Chem. Commun.* **2011**, *47*, 4583.

[138] D. Erickson, D. Sinton, D. Li, *Lab on a chip* **2003**, *3*, 141.

[139] D. Olivet, J. Valls, M. À. Gordillo, À. Freixó, A. Sánchez, *J. Chem. Technol. Biotechnol.* **2005**, *80*, 425.

[140] C. H. Bamford, C. F. H. Tipper, *Reactions of Non-metallic Inorganic Compounds (Comprehensive chemical kinetics ; v. 6)*, **1972**.

[141] O. Levenspiel, K. B. Bischoff, *Ind. Eng. Chem.* **1959**, *51*, 1431.

[142] A. N. Emery, J. P. Cardoso, *Biotechnol. Bioeng.* **1978**, *20*, 1903.

[143] H. Becker, *Talanta* **2002**, *56*, 267.

[144] C.-Y. Lee, C.-L. Chang, Y.-N. Wang, L.-M. Fu, *Int. J. Mol. Sci.* **2011**, *12*, 3263.

[145] T. J. Johnson, D. Ross, L. E. Locascio, *Anal. Chem.* **2002**, *74*, 45.

[146] a) J. C. McDonald, D. C. Duffy, J. R. Anderson, D. T. Chiu, H. Wu, O. J. A. Schueller, G. M. Whitesides, *Electrophoresis* **2000**, *21*, 27; b) S. K. Sia, G. M. Whitesides, *Electrophoresis* **2003**, *24*, 3563; c) J. C. McDonald, G. M. Whitesides, *Accounts of chemical research* **2002**, *35*, 491.

[147] J. N. Lee, C. Park, G. M. Whitesides, *Anal. Chem.* **2003**, *75*, 6544.

[148] a) C. M. B. Ho, S. H. Ng, K. H. H. Li, Y.-J. Yoon, *Lab on a chip* **2015**, *15*, 3627; b) N. Bhattacharjee, A. Urrios, S. Kang, A. Folch, *Lab on a chip* **2016**, *16*, 1720.

[149] a) D. J. Guckenberger, T. E. de Groot, A. M. D. Wan, D. J. Beebe, E. W. K. Young, *Lab on a chip* **2015**, *15*, 2364; b) Y.-S. Lin, C.-H. Yang, C.-Y. Wang, F.-R. Chang, K.-S. Huang, W.-C. Hsieh, *Sensors (Basel, Switzerland)* **2012**, *12*, 1455.

[150] J. V. Green, T. Kniazeva, M. Abedi, D. S. Sokhey, M. E. Taslim, S. K. Murthy, *Lab on a chip* **2009**, *9*, 677.

[151] L. Saias, J. Autebert, L. Malaquin, J.-L. Viovy, *Lab on a chip* **2011**, *11*, 822.

[152] J. Zhou, D. A. Khodakov, A. V. Ellis, N. H. Voelcker, *Electrophoresis* **2012**, *33*, 89.

[153] M. A. Holden, S.-Y. Jung, P. S. Cremer, *Anal. Chem.* **2004**, *76*, 1838.

[154] S. G. Newman, K. F. Jensen, *Green Chem.* **2013**, *15*, 1456.

[155] V. Franckevičius, K. Knudsen, M. Ladlow, D. Longbottom, S. Ley, *Synlett* **2006**, *2006*, 889.

[156] X. C. Cambeiro, R. Martín-Rapún, P. O. Miranda, S. Sayalero, E. Alza, P. Llanes, M. A. Pericàs, *Beilstein J. Org. Chem.* **2011**, *7*, 1486.

[157] P. Llanes, C. Rodríguez-Escrich, S. Sayalero, M. A. Pericàs, *Org. Lett.* **2016**, *18*, 6292.

[158] S. B. Ötvös, I. M. Mándity, F. Fülöp, *J. Catal.* **2012**, *295*, 179.

[159] a) F. G. Finelli, L. S. M. Miranda, R. O. M. A. de Souza, *Chem. Commun.* **2015**, *51*, 3708; b) I. Atodiresei, C. Vila, M. Rueping, *ACS Catal.* **2015**, *5*, 1972; c) R. Porta, M. Benaglia, A. Puglisi, *Org. Process Res. Dev.* **2016**, *20*, 2.

[160] A. Odedra, P. H. Seeberger, *Angew. Chem. Int. Ed. Engl.* **2009**, *48*, 2699.

[161] T. Majima, W. Schnabel, W. Weber, *Makromol. Chem.* **1991**, *192*, 2307.

[162] B. D. Fairbanks, M. P. Schwartz, C. N. Bowman, K. S. Anseth, *Biomaterials* **2009**, *30*, 6702.

[163] T. E. Kristensen, K. Vestli, K. A. Fredriksen, F. K. Hansen, T. Hansen, *Org. Lett.* **2009**, *11*, 2968.

[164] J. Pícha, V. Vaněk, M. Buděšínský, J. Mládková, T. A. Garrow, J. Jiráček, *Eur. J. Med. Chem.* **2013**, *65*, 256.

[165] B. Neises, W. Steglich, *Angew. Chem. Int. Ed. Engl.* **1978**, *17*, 522.

[166] G. Han, M. Tamaki, V. J. Hruby, *The journal of peptide research* **2001**, *58*, 338.

[167] B. Priewisch, K. Rück-Braun, *J. Org. Chem.* **2005**, *70*, 2350.

[168] a) T. Gong, B. J. Adzima, C. N. Bowman, *Chem. Commun.* **2013**, *49*, 7950; b) R. A. Dilla, C. M. M Motta, S. R. Snyder, J. A. Wilson, C. Wesdemiotis, M. L. Becker, *ACS Macro Lett.* **2018**, *7*, 1254.

[169] X. Yu, UB-PAD - Paderborn University Library, **2018**.

[170] F. Pirani, N. Sharma, A. Moreno-Cencerrado, S. Fossati, C. Petri, E. Descrovi, J. L. Toca-Herrera, U. Jonas, J. Dostalek, *Macromol. Chem. Phys.* **2017**, *218*, 1600400.

[171] V. Trujillo, J. Kim, R. C. Hayward, *Soft matter* **2008**, *4*, 564.

[172] A. Nyberg, A. Usano, P. Pihko, *Synlett* **2004**, *2004*, 1891.

[173] P. M. Pihko, K. M. Laurikainen, A. Usano, A. I. Nyberg, J. A. Kaavi, *Tetrahedron* **2006**, *62*, 317.

[174] S. Saha, J. N. Moorthy, *Tetrahedron Lett.* **2010**, *51*, 912.

[175] Z. Tang, F. Jiang, L.-T. Yu, X. Cui, L.-Z. Gong, A.-Q. Mi, Y.-Z. Jiang, Y.-D. Wu, *J. Am. Chem. Soc.* **2003**, *125*, 5262.

[176] F. Giacalone, M. Gruttadauria, P. Agrigento, P. Lo Meo, R. Noto, *Eur. J. Org. Chem.* **2010**, *2010*, 5696.

[177] A. A. Elmekawy, J. B. Sweeney, D. R. Brown, *Catal. Sci. Technol.* **2015**, *5*, 690.

[178] B. Altava, M. I. Burguete, E. García-Verdugo, S. V. Luis, *Chem. Soc. rev.* **2018**, *47*, 2722.

[179] K. G. Orrell, V. Šik, D. Stephenson, *Magn. Reson. Chem.* **1987**, *25*, 1007.

[180] D. Beaudoin, J. D. Wuest, *Chem. Rev.* **2016**, *116*, 258.

[181] S. P. González Martínez, S. Bernès, *Acta Crystallogr E Struct Rep Online* **2007**, *63*, o3639-o3639.

[182] D. B. Ramachary, C. F. Barbas, *Org. Lett.* **2005**, *7*, 1577.

[183] Y. Hayashi, J. Yamaguchi, T. Sumiya, M. Shoji, *Angew. Chem. Int. Ed. Engl.* **2004**, *43*, 1112.

[184] Z. Liu, Y. Huang, Q. Xiao, H. Zhu, *Green Chem.* **2016**, *18*, 817.

[185] a) S. Ghosh, S. S. Acharyya, T. Sasaki, R. Bal, *Green Chem.* **2015**, *17*, 1867; b) B. Paul, S. K. Sharma, S. Adak, R. Khatun, G. Singh, D. Das, V. Joshi, S. Bhandari, S. S. Dhar, R. Bal, *New J. Chem.* **2019**, *43*, 8911.

[186] M. Rueping, A. Kuenkel, F. Tato, J. W. Bats, *Angew. Chem.* **2009**, *121*, 3754.

14 Appendix

Crystal data of the single crystals obtained

Crystal data of 1,2-Bis(4-chlorophenyl)diazene oxide

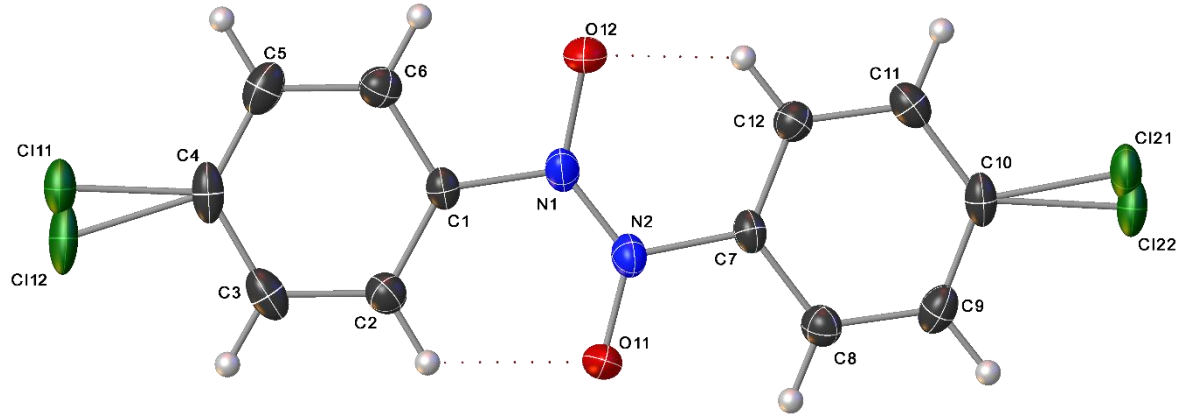

Identification code	cs_0112n_0m_a_pl	
Empirical formula	C12 H8 Cl2 N2 O	
Formula weight	267.10	
Temperature	120(2) K	
Wavelength	0.71073 Å	
Crystal system	Triclinic	
Space group	P-1	
Unit cell dimensions	a = 7.221(2) Å	α= 99.413(12)°.
	b = 7.244(2) Å	β= 97.835(15)°.
	c = 12.011(3) Å	γ = 110.843(12)°.
Volume	566.2(3) $Å^3$	
Z	2	
Density (calculated)	1.567 Mg/m^3	
Absorption coefficient	0.555 mm^{-1}	
F(000)	272	
Crystal size	0.26 x 0.10 x 0.08 mm^3	
Theta range for data collection	3.088 to 33.265°.	
Index ranges	-11<=h<=11, -11<=k<=11, -18<=l<=18	
Reflections collected	89991	
Independent reflections	4323 [R(int) = 0.0509]	
Completeness to theta = 25.242°	99.8 %	
Absorption correction	Semi-empirical from equivalents	
Refinement method	Full-matrix least-squares on F^2	

Data / restraints / parameters	4323 / 2 / 184
Goodness-of-fit on F^2	1.084
Final R indices [I>2sigma(I)]	R1 = 0.0399, wR2 = 0.1040
R indices (all data)	R1 = 0.0503, wR2 = 0.1164
Extinction coefficient	n/a
Largest diff. peak and hole	0.644 and -0.449 e.Å^{-3}

Crystal data of 1,2-Bis(4-bromoophenyl)diazene oxide

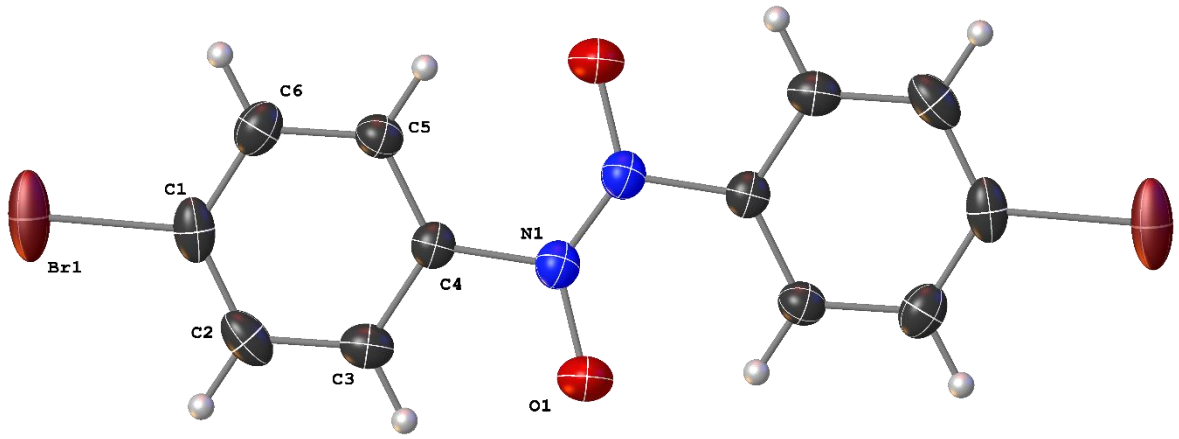

Identification code	CS_0103n_0m_a	
Empirical formula	C12 H8 Br2 N2 O	
Formula weight	356.02	
Temperature	124(2) K	
Wavelength	0.71073 Å	
Crystal system	Monoclinic	
Space group	$P2_1/c$	
Unit cell dimensions	a = 3.9033(3) Å	α= 90°.
	b = 5.9819(4) Å	β= 90.288(2)°.
	c = 25.0625(18) Å	γ = 90°.
Volume	585.18(7) Å^3	
Z	2	
Density (calculated)	2.021 Mg/m^3	
Absorption coefficient	6.909 mm^{-1}	
F(000)	344	
Crystal size	0.280 x 0.040 x 0.040 mm^3	
Theta range for data collection	3.251 to 32.047°.	
Index ranges	-5<=h<=5, -8<=k<=8, -37<=l<=37	
Reflections collected	20792	

Independent reflections	2033 [R(int) = 0.0359]
Completeness to theta = 25.242°	99.6 %
Absorption correction	Semi-empirical from equivalents
Refinement method	Full-matrix least-squares on F^2
Data / restraints / parameters	2033 / 0 / 82
Goodness-of-fit on F^2	1.126
Final R indices [I>2sigma(I)]	R1 = 0.0553, wR2 = 0.1005
R indices (all data)	R1 = 0.0625, wR2 = 0.1040
Extinction coefficient	n/a
Largest diff. peak and hole	1.644 and -2.290 e.$Å^{-3}$

Mechanistic Studies of the Reductive Dimerization of Nitrosoarenes

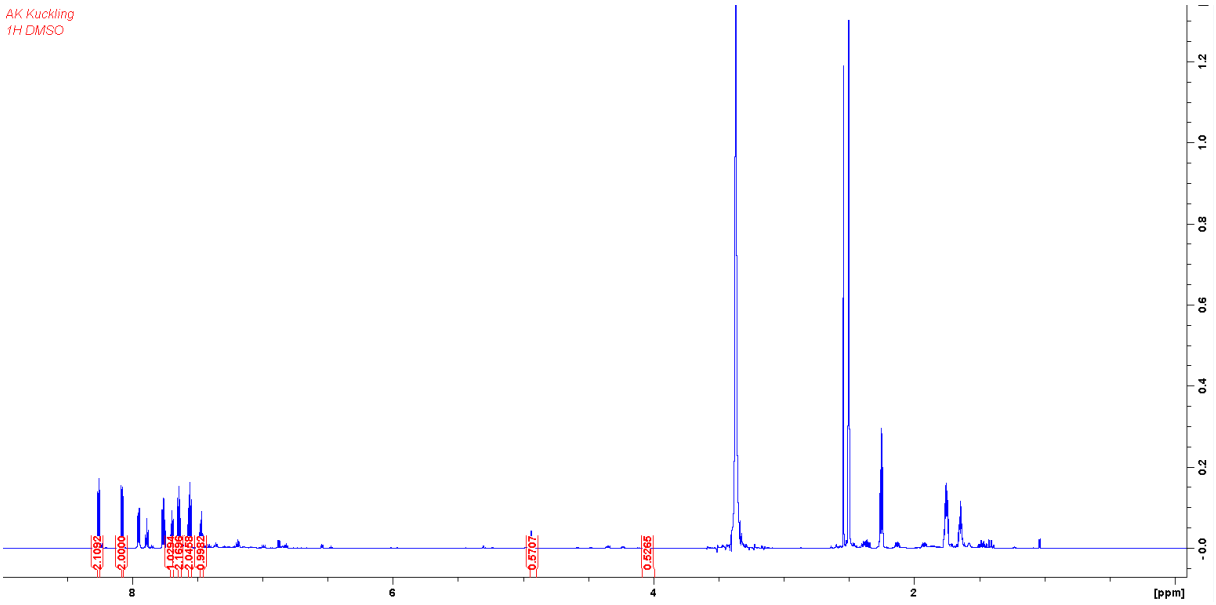

Figure A1: Crude ^{1}H-NMR of reaction mixture of 0.05 M nitrosobenzene (1 eq) and cyclohexanone (0.5 eq), respectively.

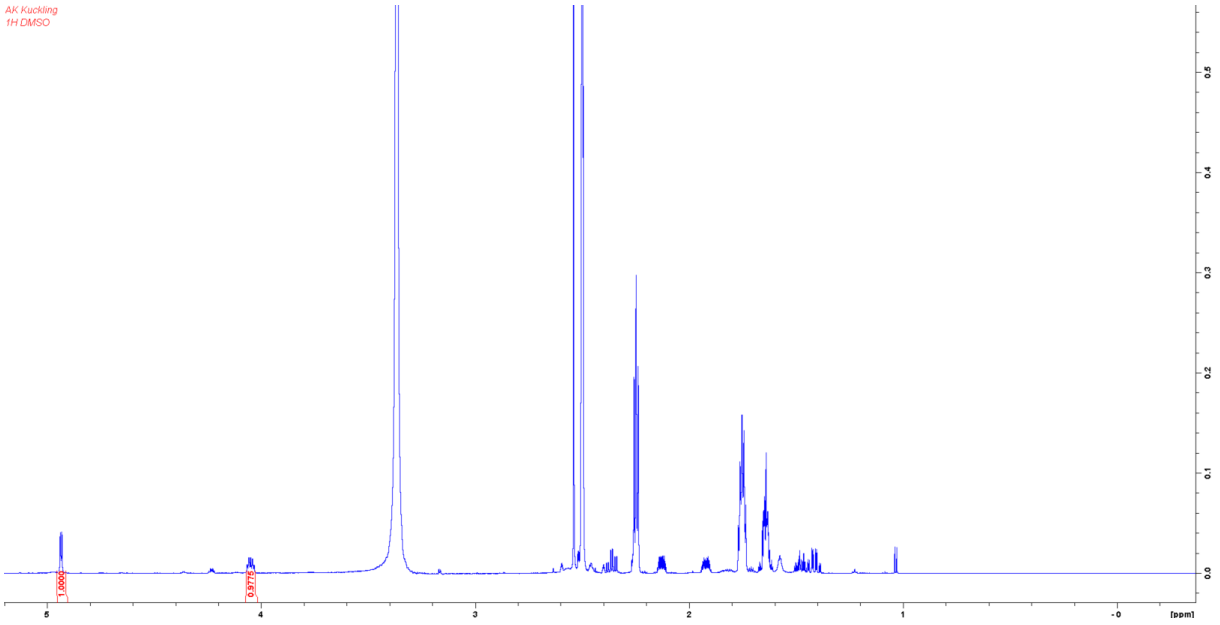

Figure A2: Crude ^{1}H-NMR of reaction mixture of 0.05 M nitrosobenzene (1 eq) and cyclohexanone (0.5 eq), respectively.

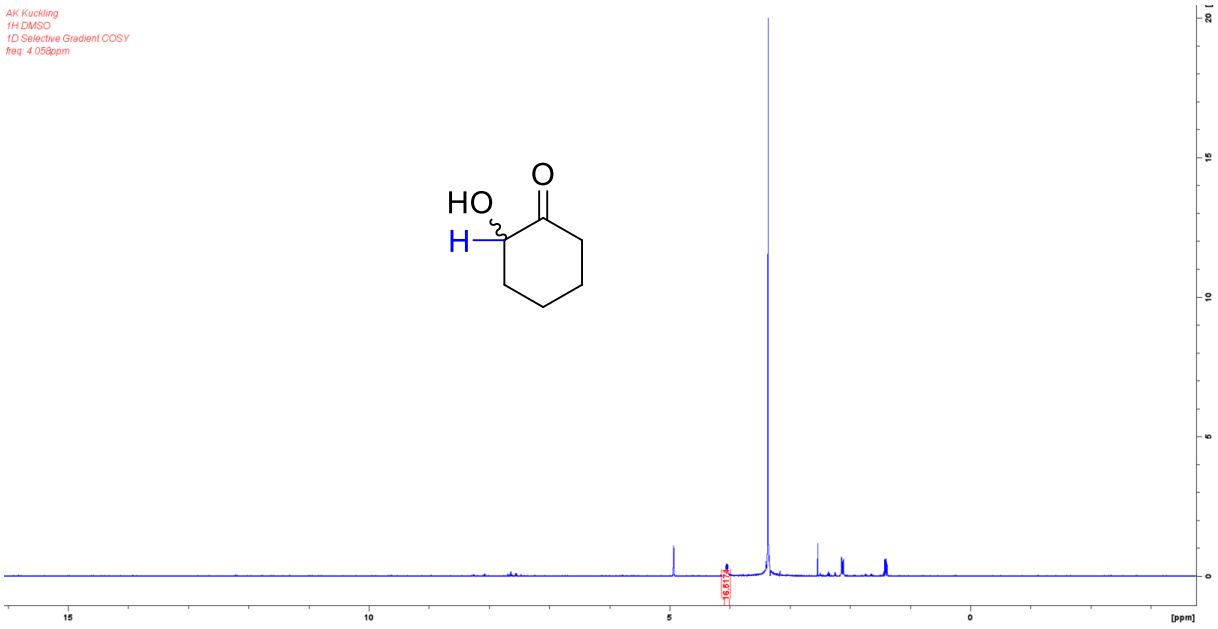

Figure A3: 1D selective gradient COSY of the same sample. (freq.: 4.058 ppm).

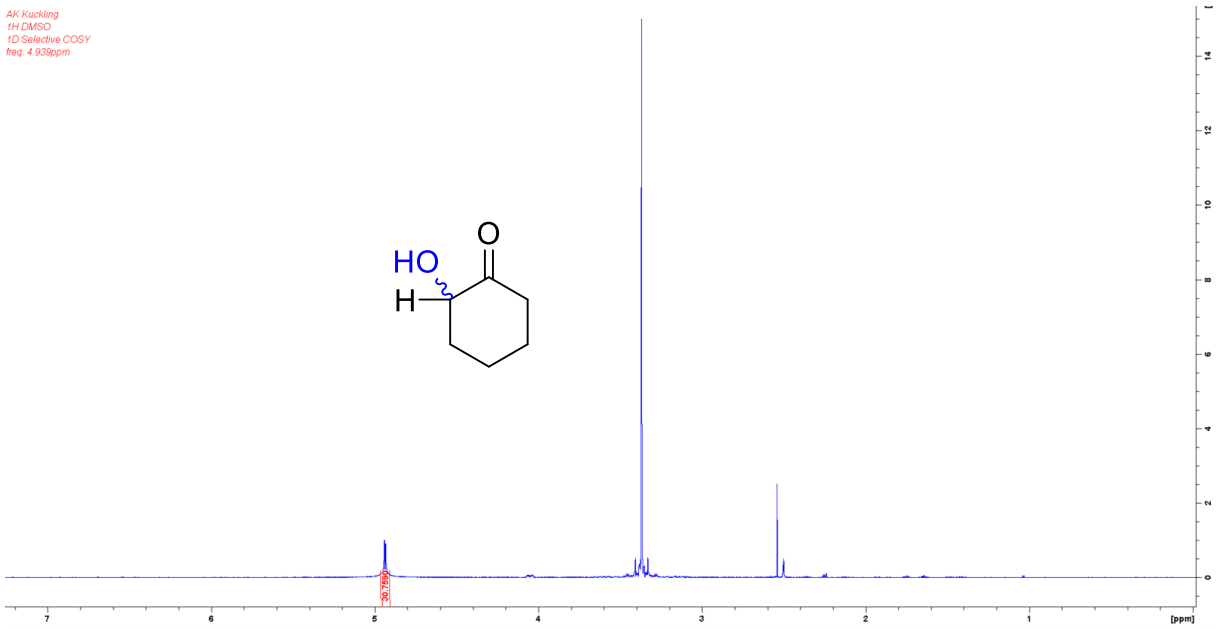

Figure A4: 1D selective gradient COSY of the same sample. (freq.: 4.939 ppm).